The Role of TGF-β-Responsive Myeloid Cells in Tumor-Induced Bone Disease

By

Denise Buenrostro

Dissertation

Submitted to the Faculty of the

Graduate School of Vanderbilt University

in partial fulfillment of the requirements

for the degree of

DOCTOR OF PHILOSOPHY

in

Cancer Biology

May 31, 2018

Nashville, Tennessee

Approved:

Harold L. Moses, M.D

Albert B. Reynolds, Ph.D.

Linda J. Sealy, Ph.D.

Scott A. Guelcher, Ph.D.

Julie A. Sterling, Ph.D.

I dedicate this work to all of my fellow cancer survivors who do not allow their lives to be defined by their disease but instead continuously fight every day to move forward. I also dedicate this work to my family, who has never been anything but supportive during some of the toughest years of my life. It is because of their sacrifice that I am here.

ACKNOWLEGEMENTS

This work would not possible without the following financial support: VA Merit Award 1I01BX001957 (J.A.S), NIH grant R01 CA163499 (J.A.S), DOD funding W81XWH-15-1-0622 (J.A.S), core funding 1S10RR027027631 (μCT). Initiative to Maximize Student Diversity (IMSD) Award 5R25GM062459 (D.B, K.A.K), Cellular, Biochemical and Molecular Sciences Training Program 5T32GM008554 (D.B), Microenvironmental Influences in Cancer Training Program 2T32CA009592 (K.A.K), NIAID 1 F31 AI133926 (N.E.P), NIAID grant K08 AI113107 (J.E.C) and internal funding from the Vanderbilt-Ingram Cancer Center. Flow Cytometry experiments were performed in the VMC Flow Cytometry Shared Resource. The VMC Flow Cytometry Shared Resource is supported by the Vanderbilt Ingram Cancer Center (P30 CA68485) and the Vanderbilt Digestive Disease Research Center (DK058404). I would like to recognize my PI, Julie Sterling, for continuously choosing to ride the roller coaster that is graduate school with me. My success at Vanderbilt would not have been possible without the support of Linda Sealy, an amazing scientist and mentor who never wavered in her belief in me, even when I felt like a failure and an imposter. I thank her for her honesty and forever will be grateful for the significant role she played in my graduate career. I would like to recognize the numerous people who helped me excel in my graduate studies, both directly and indirectly, by answering questions (even simple silly ones), giving advice (career and/or personal), donating materials and supplies (mice, protocols, etc.) and also training on equipment and techniques. The last people I would like acknowledge are my fabulous friends. These amazing bad ass women have been so supportive and encouraging through some of my toughest moments at Vanderbilt. My “sisterwives,” Shellese Cannonier and Ushashi Dadwal, have been so vital to my success at Vanderbilt (GFP!). They have been instrumental in my personal growth and success as a scientist and I always be grateful to them. I would also like to thank the following people for making me a more well-rounded and grounded individual; Leslie Roteta (Yoga dates/feeding me/honest advice and perceptive), Megan Culbreth (Venting/ranting/unwavering love+ support), Holli Loomans (Scientific role model/random hugs/our shared dark & twisty humor), Kirsten Diggins (Listening/feeding me/walking dead marathons) and Megan Shuey (for being my person/family).

TABLE OF CONTENTS

Page

LIST OF TABLES

Page

LIST OF FIGURES

Page

Chapter I.

INTRODUCTION

Breast Cancer

Molecular subtypes of breast cancer and diagnosis. Breast cancer is the most common cancer diagnosed in women. In 2017, it is estimated that invasive breast cancer will be diagnosed in about 252,710 women and 2,470 men in the United States with an estimated 41,070 deaths due to breast cancer [1]. Mutations in the BRCA1 and BRCA2 genes increase the lifetime risk of developing breast cancer to 75% and increase susceptibility to other cancer types [2].

Currently research studies divide breast cancer into four molecular subtypes, 1) Luminal A, 2) Luminal B, 3) Triple negative or basal-like, and 4) HER2 type [3].

Luminal tumor cells originate from the inner cells lining the mammary ducts and tend to be Estrogen receptor-positive (ER-positive), and either HER2 receptor-negative or HER2 receptor-positive (HER2-negative or HER2-positive) [4]. Compared to the other four molecular subtypes, luminal A tumors are most commonly diagnosed as low-grade tumors and encompass about 30-70% of breast cancers and have fairly high survival rates and low recurrence rates. Luminal B tumors tend to have a poorer prognosis due to tumor grade, tumor size and lymph node-positivity. Despite these factors, luminal B tumors tend to have fairly high survival rates and make up about 10-20% of diagnosed breast cancers. While the majority of HER2 type tumors are HER2-positive, about 30% are HER2-negative and are for the most part ER-negative, progesterone receptor-negative (PR-negative), lymph node positive, and higher tumor grade [4-6]. About 5-15% of breast cancers are subtyped as HER2 type. Triple negative/basal-like breast cancers (TNBC) are composed of several subsets, but the major division is whether tumor cells resemble basal-like cells or not. Basal-like tumor cells resemble the outer cells surrounding the mammary ducts. Nonetheless, it is important to note that not all triple negative breast cancers contain basal-like cells and not all basal-like tumors are triple negative. TNBC are ER-negative, PR-negative and HER2-negative and compose about 15-20% of breast cancers. TNBC often occur in younger women, tend to be aggressive and have the worst prognosis as compared to the luminal tumors [3-6].

However, these molecular subtypes are currently not used to diagnosis or treat breast cancer in the clinical setting.

Prognosis and treatment decisions are guided mainly by tumor stage, tumor grade, hormone receptor status and HER2 status. Currently the TMN system of staging is used to classify breast cancer stage and is based on the pathological study of tumor tissue and/or lymph nodes removed during surgery [7]. TMN classifies tumors based on tumor size (T), the number and location lymph nodes with cancer (N), and whether there is evidence of metastases (M). The stages of breast cancer range from 0 to IV, where a stage 0 diagnosis indicates ductal carcinoma in situ and a stage IV diagnosis signifies invasive metastatic breast cancer [7, 8].

Metastatic breast cancer. The definition of metastatic breast cancer is when breast cancer cells are no longer contained to the primary site, but have colonized and established in other organs [9]. In order for cancer cells to metastasize to other organs they have undergo a process called the metastatic cascade. The metastatic cascade describes the mechanism in which cancer cells have to disseminate from the primary tumor to the lymph nodes or blood during the early stages of tumor growth, and how these disseminated cancer cells proliferate and form solid metastases in the lymph nodes and/or distant sites [9-11]. In regards to breast cancer, this cancer preferentially metastasizes to lung, liver, brain and bone [12]. Metastatic breast cancer often leads to skeletal complications including but not limited to, bone metastases, bone pain, hypercalcemia and spinal compression [13]. Specifically, in the case of breast cancer metastasizes to bone, 70-79% patients with metastatic breast cancer at autopsy present with evidence of bone metastases [11]. Many investigators have studied whether a specific gene signature could predict clinical outcomes for breast cancer patients, specifically in the context of breast cancer metastases to bone, a bone metastasis gene expression signature was identified by Massagué's group in 2003 [14]. This genetic signature included factors such as CXCR4, CTGF, IL-11 and Osteopontin (OPN) that were identified through a microarray analysis. These factors are involved in processes that include homing to the bone marrow, invasion, angiogenesis and osteoclastogenesis [14]. This work has been instrumental in understanding the complexity of the bone microenvironment and how cancer cells can change phenotypically and genetically in accordance with the corresponding microenvironment.

Breast cancer treatments. Currently there are various treatment options for breast cancer, including surgery, radiation, chemotherapy, hormone therapy and targeted therapy [15-17].

However, treatment options are dependent on a combination of factors including but not limited to, tumor stage, tumor grade, hormone receptor status, HER2 status, medical history and age [16, 17].

For example, a hormone receptor (HR) positive breast cancer diagnosis indicates that cancer cells contain hormone surface receptors that bind hormones (i.e. estrogen and progesterone) and promote the progression of breast cancer. These cancers are treated with hormone therapy, which prevent the production of hormones or interfere with the effect of hormones on cancer cells. Therapies for inhibiting hormone production consist of aromatase inhibitors and ovarian suppression drugs, while selective estrogen receptor modulators (SERMs) and anti-estrogen drugs interfere with hormone binding to the receptor [15]. Targeted therapies are also used in the treatment of breast cancer including, monoclonal antibodies, tyrosine kinase inhibitors (TKIs), mammalian target of rapamycin (mTOR) inhibitors and PARP inhibitors. Trastuzumab (monoclonal antibody), lapatinib, (TKI), everolimus (mTOR inhibitor) palbociclib, (cyclin-dependent kinase inhibitor), are a few of the targeted therapies used to treat HER2 positive breast cancer [16, 18-20]. PARP inhibitors are currently in clinical trials for the treatment of patients with TNBC with germ-line BRCA1 and BRCA2 mutations [15, 21].

The challenge of treating and potentially curing breast cancer has been the identification of a therapeutic window for treatment. This has proven to exceptionally difficult in the prevention and treatment of patients with cancer induced bone disease. Currently patients with evidence of bone metastases are treated with anti-resorptive therapies such as bisphosphonates or monoclonal antibodies such as denosumab, which prevent bone loss and skeletal-related events (SREs) [17]. While these therapies have proven to be successful in preventing further bone loss, they have no therapeutic effect on tumor burden in bone. Breast cancer can be cured if diagnosed and treated early, but once it has metastasized, it can no longer be cured only treated.

Bone Biology

Physiological bone remodeling. Bone modeling and remolding is a dynamic and continuous process that is necessary to maintain the skeletal system. This includes skeletal size, shape, structural integrity and regulation of mineral homeostasis [22].

Bone modeling and remolding is a tightly regulated process that is coordinated by many different cellular processes to ensure that bone resorption and formation occur in the same anatomical location to conserve bone homeostasis [22]. The two main cell types that are involved in maintaining bone homeostasis are the osteoclasts and osteoblasts. Osteoclasts are bone resorbing cells that are derived from the hematopoietic stem cell lineage while osteoblasts are bone forming cells that are derived from mesenchymal stem cells. While these cells have opposing functions, they are part of a tightly regulated feedback loop [23].

Osteoblastogenesis occurs in three stages; proliferation, matrix maturation and mineralization and is dependent on two transcription factors, Runx2 and Osx [24-27]. Osteoblast differentiation is defined by the temporal expression of certain genes markers, such as alkaline phosphatase (ALP) in the early phase of osteoblast development, and osteocalcin and osteopontin at the late stages of differentiation [25]. Osteoblast can further differentiate into osteocytes, cells that are contained within the mineralized bone, and have mechanosensory and metabolic functions that regulate bone remolding [28-31].

Osteoblasts express two necessary cytokines required for osteoclast precursors (OCPs) differentiation; receptor activator of NF-κB ligand (RANKL) and macrophage-colony stimulating factor (M-CSF). M-CSF binds to its receptor on OCPs and activates signaling via the MAP kinase and ERK pathways during the early phase of OCP differentiation [32, 33]. RANKL binds to its receptor, RANK, on the surface of OCPs activating signaling through several factors including NF-κB to promote differentiation of OCPs into osteoclasts [32, 33]. Differentiated osteoclasts are multinucleated that secrete metalloproteinase enzymes that are tartrate resistant, therefore osteoclasts known as tartrate resistant acid phosphatase (TRAP) positive cells. Differentiated and functional osteoclasts include a sealing zone where the plasma membrane of the cell adheres to the bone surface through the use of integrin mediated podosomes and a resorption pit. The ruffled border of an osteoclast is necessary to increase the surface area of the cell that can directly contact the bone and allow for the release of proteins such as Cathepsin K, a protease known to break down collagen [22, 23]. Together, TRAP, Cathepsin K, the acidic gradient produced in the resorption pit, and other secreted enzymes degrade of the extracellular matrix (ECM) of bone [34]. This osteoclast-mediated bone resorption releases a substantial amount of growth factors and cytokines that would normally be sequestered in bone ECM.

These released signaling factors have several cellular effects including supporting osteoblastogenesis and promoting osteoprotegerin (OPG) expression. OPG is recognized as a decoy receptor for RANKL because of its ability to bind free RANKL and thus preventing RANK/RANKL binding, inhibiting additional osteoclastogenesis [35]. Osteoblastogenesis and osteoclastogenesis is a tightly regulated coupled process that is essential to maintain the balance of bone remolding in which bone is resorbed at the same rate as it is formed.

Tumor-induced bone disease (TIBD). Several cancers have the potential to metastasize to bone, where tumors in bone disrupt normal bone remolding and cause TIBD [36]. Patients with TIBD often suffer from bone pain, hypercalcemia, pathological fractures and have reduced bone mass and bone metastases [37]. Many cancers, including breast, prostate, and lung cancer metastasize to bone through the circulatory system, while head and neck cancers can invade directly into bone due to proximity. Primary bone tumors, including osteosarcoma and multiple myeloma, also have the potential to cause TIBD. Specifically, in breast cancer, TIBD is regulated by a process called the "The Vicious Cycle" [38]. The vicious cycle describes the process in which tumors arrive and respond to environmental signal propagated by the bone microenvironment. This includes cytokine and chemokines, such as transforming factor beta (TGF-β), that are abundantly present as a result of normal bone remolding and can stimulate tumor cells [39, 40]. Complex cell interactions between tumor and bone marrow residing cells play an essential role in remodeling the bone microenvironment into a pro-tumorigenic place for tumor establishment and progression. Furthermore, our group has demonstrated that the rigidity of the bone matrix can stimulate the development of TIBD via mechanotransduction signaling pathways [41]. While the vicious cycle can propagate TIBD through several different mechanisms, the consequences of this multifaceted illness among different tumor types are similar, deregulation of normal bone remolding and abnormal skeletal changes due to excessive bone resorption and/or bone formation.

TGF-β Signaling

Canonical TGF-β signaling. Transforming growth factor beta (TGF-β) is a part of the TGF-β superfamily and is a multifaceted cytokine that has effects on cellular behavior and growth inhibition.

TGF-β and other members of the superfamily control many essential aspects of development such as cell proliferation, differentiation, migration, wound healing, apoptosis and organ homeostasis [42, 43]. Activation of canonical TGF-β signaling begins with the binding of the TGF-β ligand to transforming growth factor beta receptor 2 (TGF-βRII) inducing the formation of a serine/threonine kinase complex composed of transforming TGF-βRII and transforming growth factor beta receptor 1 (TGF-βRI) [44]. Once this heterotetrameric complex is formed, the TGF-βRII kinase phosphorylates a regulatory region called the GS domain within TGF-βRI causing kinase activation of the receptor. TGF-βRI specifically recognizes and phosphorylates the receptor-regulated SMAD proteins (R-SMADs), SMAD2 and SMAD3. Specifically, SMAD2/3 can basally bind several proteins, including SMAD anchor for receptor activation (SARA) which retains these SMADs in the cytoplasm. Upon activation of the TGF-β receptor complex and phosphorylation of the R-SMADs, the binding affinity of SARA is reduced and once released SMAD2/3 can interact with SMAD4. The SMAD2/3-SMAD4 complex is translocated to the nucleus where these activated SMADs can directly recognize and bind target genes that contain SMAD binding elements regulating transcription [42, 44]. An additional effect of TGF-β stimulation is the activation of a negative feedback loop that utilizes proteins that recognize the activated receptor complex and mediate its ubiquitination and internalization leading to the termination of TGF-β signaling. Once TGF-β stimulation ends, SMADs are dephosphorylated and are shuttled back into the cytoplasm. Transcription of TGF-β target genes can also be executed in a SMAD-independent manner known as non-canonical TGF-β signaling that involves cross-talk with other fundamental signaling pathway including MAPK, PP2A, RhoA and TAK1/MEKK1 [42].

TGF-β and bone. Bone is the largest source of TGF-β. Upon bone resorption, latent TGF-β is released from the bone ECM and activated by proteolysis by several cell types, such as macrophages, mesenchymal cells, osteoclasts, osteoblasts and endothelial cells [34]. TGF-β is an important regulator of both osteoclast and osteoblast activity by coupling both bone formation and resorption. TGF-β can both facilitate and suppress osteoclast formation, first by antagonizing inflammatory signaling, therefore rendering osteoclast precursors resistant to anti-osteoclastic signals. TGF-β can suppress osteoclast formation by indirectly decreasing the availability of osteoblastic NF-kappa B ligand (RANKL)[34].

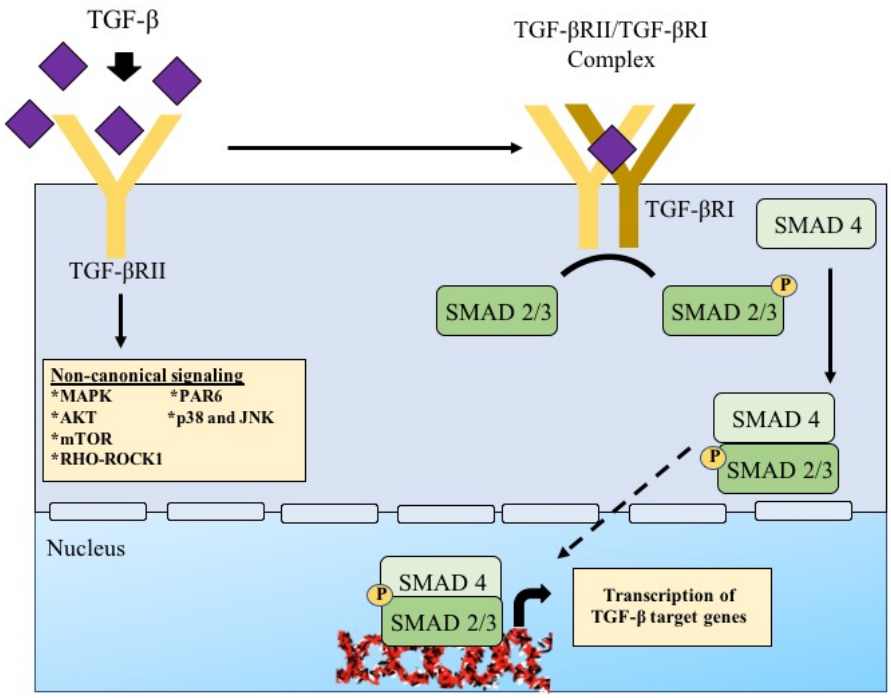

Figure 1: Canonical and non-canonical TGF-β signaling. The TGF-β ligand binds to the TGF-βRII to activate downstream transcriptional targets. Canonical signaling involves phosphorylation of TGF-βRI to induce nuclear localization and transcriptional activity of SMADs. Non-canonical signaling occurs independently of SMADs and includes activation of several signaling pathways including and but not limited to RHOA, AKT and MAPK pathways.

The effect of TGF-β on osteoblastic cells are context, time, and dose dependent [45]. Most studies suggest that TGF-β can promote osteoblast proliferation, early differentiation of progenitor cells and matrix production while inhibiting differentiation and matrix mineralization as well [46-49]. Additionally, TGF-β can activate a negative feedback loop to inhibit its own signaling via Runx2 to decrease TGF-βRI leading to a reduction in TGF-β responsiveness [50]. The use of mouse models targeting TGF-β signaling have further shown the complexity surrounding the role of TGF-β on osteoblast differentiation and osteogenesis. For example, TGF-$\beta1^{-/-}$ mice do not have mature osteoblasts and display a decrease in ALP activity but contain normal osteoclast activity and number [51], while mice overexpressing a dominant negative TGF-βRII have an increase in bone mass and a reduction in osteoclast activity [52].

Furthermore, TGF-β plays a complex role in osteoclastogenesis as well, including lineage commitment and the ability to stimulate and inhibit bone resorption.

Osteoclasts are derived from a monocytic lineage, and lineage commitment is dependent on environmental signals, for example, TGF-β is necessary to prime non-committed progenitor cells for RANKL/TNF-α induced osteoclast formation, while inflammatory cytokines, including IL-10, IL-4 and IFN-γ, commit the same progenitor cells for macrophage differentiation in the presence of TNF-α [34]. Once progenitors have committed to a specific lineage (i.e. Osteoclast vs. macrophage), opposing cytokine stimulus have no effect. TGF-β may regulate lineage commitment and switching by inhibiting activation of the JAK/STAT (Janus kinase/signal transducer and activator of transcription) signaling pathway, a pathway utilized by several inflammatory cytokines [53]. Published studies have shown that TGF-β can induce SOCS expression (suppressors of cytokine signaling), a family of STAT-induced factors that inhibit STAT activation and prevent over-stimulation by subsequently shut down further JAK/STAT signaling. Osteoclast have been shown to express several of these negative feedback regulators, and specifically SOCS3 has been found to be critical for RANKL and TNF-α induced osteoclast formation [54-56]. Osteoclast number and resorptive activity is indirectly regulated by TGF-β via regulation of osteoblastic RANKL/OPG, since osteoclast differentiation is dependent on a balance between RANKL and OPG [57-60]. TGF-β can simultaneously increase OPG production and inhibit RANKL expression, thus decreasing osteoblastic stimulus resorption [57-60].

This alteration of the RANKL/OPG ratio attenuates the stimulus provided by osteoblasts and leads to a reduction of osteoclast differentiation.

Published literature has shown that the effect of TGF-β on bone homeostasis is highly regulated and any perturbation can lead to the development of various bone diseases.

TGF-β and cancer. Over the years many studies have identified mutations within the TGF-β signaling pathway that are associated with the development of human cancer and progression[61, 62]. For example, overexpression of the TGF-β1 isoform has been correlated with several types of cancer including breast, colon, lung, and pancreatic cancer [62].

The role that TGF-β signaling plays in regulating cancer is both cell and context specific, where in the earlier stages of tumorigenesis, TGF-β is a tumor suppressor, while in the late stages TGF-β can act as a tumor promotor [63]. As tumors progress, tumor cells may lose their growth-inhibitory response to TGF-β stimulation and instead initiate epithelial-mesenchymal transition (EMT), promoting tumor cell migration [63]. Insights into the role of TGF-β in tumorigenesis have come from the use of mouse models with manipulations within the TGF-β signaling pathway. Experimental data from these studies supports the notion that both loss and gain of TGF-β can be pro-tumorigenic, as both overexpression of TGF-β and inhibition of TGF-β signaling increased metastasis [63-65]. These studies conceptualize the idea that the effects of TGF-β extend beyond the tumor itself and into the tumor microenvironment. In regards to the effect of TGF-β on the tumor microenvironment, every TGF-β-responsive cell behaves differently and the diversity of these responses affect tumor progression. For example, mammary fibroblast that specifically lacked TGF-βRII transplanted with mammary carcinoma cells promote growth and invasion of tumor cells [66], while mice with myeloid cells that lack TGF-βRII had a reduction in tumor growth [67].

TGF-β and The Vicious Cycle. The bone matrix contains an abundant amount of growth factors including but not limited to TGF-β, insulin-like growth factor I and II (IGF-1/IGF-2), fibroblast growth factor (FGF), platelet-derived growth factors (PDGF) and bone morphogenetic proteins (BMPs) [68]. While all of these growth factors play important roles in bone resorption, TGF-β specifically promotes a feed-forward cycle responsible for tumor progression known as the Vicious Cycle [39]. TGF-β is released and activated from the mineralized bone matrix by osteoclastic resorption and further promotes tumor progression and production of osteolytic factors, such as Parathyroid hormone-related protein (PTHrP) and IL-11 [40]. PTHrP secretion in human breast cancer cells can be induced by either canonical and non-canonical TGF-β signaling [69]. Studies have elucidated that PTHrP is a critical mediator of TGF-β induced bone metastases as mice treated with PTHrP neutralizing antibody have no evidence of breast cancer induced bone metastases [70]. Specifically, PTHrP has been found to be an important mediator of osteolytic lesions due to its increased expression in human breast cancer bone metastases [71].

PTHrP can stimulate RANK ligand and inhibit OPG production by osteoblasts, thus supporting osteoclastogenesis [72]. Therefore, TGF-β is considered an important proponent of the Vicious Cycle.

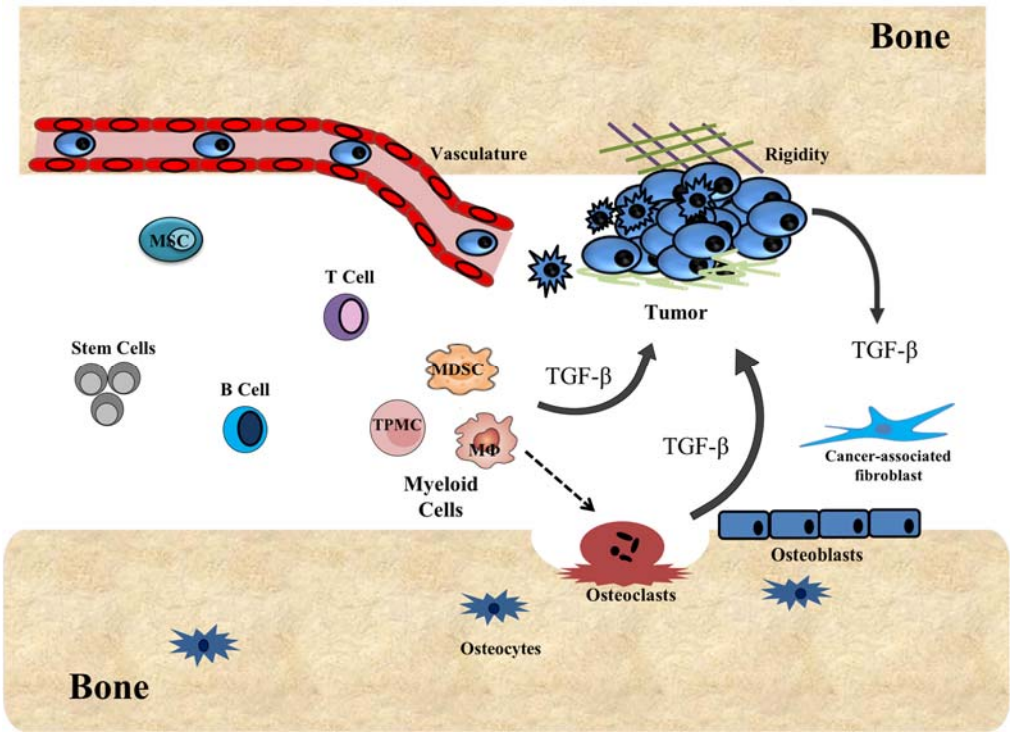

Figure 2: The tumor-bone microenvironment. The bone-marrow environment includes many different cell types including progenitors and mature cells that can be circumvented to assist tumor progression. Tumors in bone can secrete factors that indirectly increase osteoclast resorption and lead to the release of TGF-β into the environment and feed-forward the vicious cycle. Other cell types found in the environment, such as myeloid cells, can also secrete and express TGF-β, thus, propagating tumor growth and progression.

The Immune System and TIBD

Myeloid cells, cancer and TIBD. Myeloid cells originate from the hematopoietic stem cell lineage and encompass many different cell subsets, including progenitor and terminally differentiated mature cells. Myeloid-derived suppressor cells (MDSCs) are heterogeneous cell population that include immature macrophages, dendritic cells, granulocytes and other myeloid progenitor cells [73, 74].

MDSCs can be further stratified into two separate populations, one that is phenotypically and morphologically similar to monocytes (M-MDSCs), and the other compromised polymorphonuclear (PMN) cells that are similar to neutrophils (PMN-MDSCs) [75]. Immune-suppressive activity is a hallmark characteristic of MDSC, and due to the heterogeneity of these cells, the lack of unique phenotypic markers has it made it difficult for the field to come to a consensus about the characterization of MDSCs if immune-suppressive activity was not detected [76]. Several factors have been found to be involved in MDSC-mediated immune suppression including arginase (ARG1), inducible nitric oxide synthase (iNOS), TGF-β, IL-10, sequestration of cysteine, decreased expression of L-selectin by T cells, and induction of T regulatory cells (Tregs) [75, 77-79]. Additionally, MDSCs have been demonstrated to aid tumor growth and progression through four different methods [75]:

1. Decreasing immune surveillance through their suppressive function

2. Remolding of the tumor microenvironment

3. Establishment of a pre-metastatic niche

4. Promoting the EMT in tumor cells

In regard to bone metastases, MDSCs have been found to play an important role in both breast and prostate cancer induced bone metastases. In a mouse model of prostate cancer, tumor-derived PTHrP indirectly increased MDSC's angiogenesis potential, leading to tumor growth in bone [80]. Danilin and colleagues published that MDSCs contributed to bone destruction by activating expression of Gli2 and PTHrP in breast cancer model of metastatic bone disease [81]. Our group and others have shown that MDSCs isolated from tumor-bearing mice have the potential to differentiate into osteoclast, therefore contributing to the bone resorption seen during breast cancer metastasis to bone [81, 82].

Macrophages, a mature myeloid cell subset, are antigen presenting cells that have roles in promoting wound healing, regulating adaptive immunity and eliminating infectious agents [74]. These cells play active roles in initiation, promotion and progression of several tumor types including breast, lung and colon tumors [83-85].

Macrophages are plastic cells and their phenotype is constantly modulated by the local microenvironment, a characteristic that is often exploited by cancer cells. Cells that are activated by factors such as interferon-gamma (IFN-γ) have anti-tumor properties and are considered classically activated macrophages or "M1-like" macrophages; verses cells activated by factors such as IL-4 are considered tumor promoting and are referred to as alternatively activated macrophages or "M2-like macrophages [86, 87].

Since macrophages can be modulated by their environment, several distinct cell subsets such as tumor-associated macrophages (TAMs) and metastasis-associated macrophages (MAMs) express a mixed phenotype of both M1 and M2 markers, therefore making it difficult to target and classify these cells exclusively by their subtype [87]. Specifically, macrophage inhabiting the bone marrow can differentiate into osteoclast with the correct environmental signals, however their exclusive role in TIBD is still unknown [88]. Published work has identified a novel resident macrophage population that is $F4/80^+$ and tartrate-resident acid phosphatase (TRAP) negative in bone called osteomacs [89]. Investigations focusing on osteomacs have shown that they different functions than osteoclasts and are important for osteoblast maintenance and functional activity [88-90]. Nevertheless, these studies focused on the osteomac's role in bone marrow homeostasis and bone healing, as their role in TIBD has yet to be examined.

T and B cells, cancer and TIBD. T cells and B cells play crucial roles in adaptive immunity and have been shown the have conflicting roles in cancer progression [91]. These cells types are composed of several cell subsets that have diverse biological functions including both anti-tumor and pro-tumor properties. For instance, $CD8^+$ T cells are widely recognized as effector or cytotoxic cells that are responsible for the majority of tumor killing by several mechanisms including but not limited to apoptosis and target cell cytotoxicity [92]. Tregs, for example, have been involved in contributing to tumor growth and progression [93]. In regards to B cells, mature B cells can differentiate into plasma cells and release antibodies specific for tumor antigens causing an immune response that targets the tumor [91, 94]. These cells, however, can also accumulate at tumor sites and secrete immunosuppressive cytokines, such as IL-10, assisting in tumor progression [95]. Publications have surfaced describing the T cell-dependent mechanisms that promote TIBD. A study investigating the role of T cells found that T cell stimulation in a tumor-bearing mouse decreased overall tumor growth in bone [96].

However, T cells have been implicated in secreting RANK ligand and inducing osteoclastogenesis, leading to bone destruction prior to tumor establishment in bone [97]. Collectively these finding suggest that T cells may have opposing roles in TIBD, one that is anti-tumor and the other that stimulates tumor progression. Although it is important to recognize that the majority of published studies have utilized T cell-deficient mice, it is evident that T cells are not required for tumor cell growth and metastases to bone [74].

All of this together suggests that TIBD is a complex and multifaceted illness that involves several factors that include the bone and its microenvironment.

Chapter II.

EARLY TGF-β INHIBITION IN MICE REDUCES THE INCIDENCE OF BREAST CANCER INDUCED BONE DISEASE IN A MYELOID DEPENDENT MANNER

*This chapter is adapted from a published manuscript in Bone 2018

Introduction

Breast cancer is the second leading cause of death among women [98], and up to 80% of metastatic breast cancer patients will develop bone metastases [13].Once established in bone, tumors can induce bone destruction, increase fracture, and hypercalcemia, all factors associated with high morbidity and mortality rates [13]. While current therapies, including bisphosphonates and denosumab, targeting osteoclast-mediated bone destruction have successfully improved patient morbidity and time to skeletal-related events, they have limited effect on tumor growth and patient survival [13]. Thus, therapies that reduce tumor growth and extend survival are needed to help improve patient outcomes.

Once tumors have established in bone they secrete factors (e.g. parathyroid hormone-related protein (PTHrP)) that stimulate osteoclast-mediated bone resorption. Previous work has established transforming growth factor beta (TGF-β) as a regulator of PTHrP expression, and our lab and others have shown that when you inhibit TGF-β systemically or within tumor cells, tumor burden and tumor-induced bone disease (TIBD) is reduced [99-102]. While this has been a promising target, tumors have not been completely eliminated when treated with TGF-β inhibitors, especially in models where tumors were allowed to establish first [101, 103, 104]. This observation is supported by computational modeling for the treatment of prostate cancer metastases that suggested a minimal effect on tumor growth when using TGF-β inhibitors after the establishment of tumors in bone [105]. Several studies have proposed that in the context of TIBD, adjuvant TGF-β inhibition may be advantageous over treatment of active disease [101, 103, 105].

However, the mechanisms of how TGF-β inhibition reduces TIBD, remains unclear.

Work from our group and others has established the $CD11b^{+}$ $Gr\text{-}1^{+}$ myeloid cells as contributors to TIBD through their expression of TGF-β [81, 82, 106].

Outside of the bone, myeloid cells have been implicated in the expression and secretion of TGF-β and regulation of tumorigenesis [83, 107]. Since myeloid cells abundantly express and secrete TGF-β, investigators have focused on targeting TGF-β receptor II (TGF-βRII), which when removed in myeloid cells reduces primary tumor growth, lung metastases and osteolytic lesions as compared to control mice [67, 108, 109]. Past publications have focused on the role of myeloid cells in the primary tumor microenvironment [67, 84, 110-112] and it is only recently that investigators have started to explore the role of myeloid cells in the context of TIBD [80, 81, 106, 113].

Since previous work has provided evidence of interactions between tumors and the bone microenvironment that can drive TIBD[80, 81, 106, 113], we hypothesized that pre-treatment with TGF-β inhibitors would reduce myeloid expansion, tumor burden in bone, and osteoclast-mediated bone destruction. In this study, we show that early pharmacological or genetic TGF-β inhibition remodels the bone microenvironment by altering myeloid populations and pro-tumorigenic factors leading to a decrease in osteolytic lesions and tumor burden in bone.

Materials and Methods

Cell lines and reagents. Bone metastatic clones of the human breast cancer cell line MDA-MB-231 and mouse mammary carcinoma cell line 4T1 were used in these experiments as previously described by our laboratory [81, 114]. A bone metastatic clone of 4T1 cells was stably transduced with GFP. Mouse 4T1 cells were purchased from ATCC and a bone metastatic variant was stably transduced with GFP. Viral plasmid was constructed using the MultiSite Gateway on the pLenti6.2/V5-DEST backbone (Life Technologies, V36820). Viral particles were produced in LentiX 293T cells (Clontech, 632180) with ViraPower Packaging Mix (Life Technologies, K497500). The cells were stably transduced with 1 mL pRBow-mTagGFP2 for 72 hrs in the presence of 8ug/mL Polybrene. Cells were expanded and selected with 2.5 ug/mL Blasticidin. GFP expression was confirmed by fluorescent microscopy and flow cytometry. MDA-MB-231 cells-GFP were maintained in DMEM (Corning, 10-013-CV) supplemented with 10% fetal bovine serum (FBS, Peak Serum PS-500A) and 1% penicillin/streptomycin (Corning, 30-002-CI). 4T1-GFP cells were maintained in RPMI 1640 (Corning, 10-041-CV) supplemented with 10% FBS and 1% penicillin/streptomycin.

The MMTV-PyMT cells were generously provided by Harold Moses (Vanderbilt University) and derived as described previously [115, 116]. Prior to experimentation, the MMTV-PyMT cells were injected into the tibia of wild-type 6-week-old female FVB mice. These cells were harvested and expanded once mice developed bone lesions as observed though x-ray analysis. This bone-derived MMTV-PyMT variant cell line was maintained in DMEM/F12 (Corning, 10-092-CV) with 5% adult bovine serum (ABS, HyClone Laboratories SH30075) and 1% penicillin/streptomycin. Cells were cultured in a 37°C atmosphere with 5% CO_2. The TGF-β neutralizing antibody (1D11) and its isotype control (13C4) were generously provided by SANOFI. TGF-β was purchased from R&D systems (240-B).

Animal Studies. All procedures were performed with the approval of the Vanderbilt University Institutional Animal Care and Use Committee and in accordance with Federal guidelines. For bone metastasis experiments, n=12 mice per group, and tumorigenicity (intratibial) experiments, n=8 mice per group, were calculated by a power analysis using a probability of type I error ± 0.05; probability of type II error ± 0.20 based on previous data obtained in our laboratory. Female 4-5-week-old athymic nude and BALB/c mice were purchased from Envigo. Mice were inoculated with 10mg/kg of a TGF-β neutralizing antibody (1D11) or the isotype control antibody (13C4) by intraperitoneal injection seven days prior to tumor inoculation and were treated continuously 3 times per week until sacrifice. After 7 days of treatment, 6-7-week-old athymic nude mice were injected with MDA-MB-231-GFP cells and BALB/c mice were injected with 4T1-GFP cells by intracardiac injection. Mice were imaged weekly by x-ray and sacrificed at three separate time points post tumor inoculation (athymic: 10, 14, 32 days, BALB/c: 7, 10, 14 days). Female mice were specific pathogen free and housed 4-5 per cage, and female athymic nude mice were housed in sterile cages, also 4-5 per cage. Mice were fed an irradiated laboratory rodent diet (Lab Diet, 5LOD). TGF-βRII^{MyeWT} (WT) and TGF-βRII^{MyeKO} mice were generously provided by Harold Moses (Vanderbilt University). To generate these mice, LysM-Cre mice were crossed with TGFβRII floxed mice which were established and maintained as described [117-119]. These mice are on a pure FVB background. Female 5-6-week-old FVB TGF-βRII^{MyeWT} (WT) and TGF-βRII^{MyeKO} mice (6-8 per group) were injected with MMTV-PyMT tumor cells by intratibial injection. Mice were imaged weekly by x-ray and sacrificed at 10, 14, 28 days post tumor inoculation.

Intracardiac injections. MDA-MB-231-GFP cells and 4T1-GFP cells were trypsinized, washed and resuspended in ice-cold PBS at a final concentration of 1×10^6 cells/mL. Female, 6-7 week old mice (12 per group) were anesthetized and inoculated as previously described [120]. Each mouse received 1×10^5 cells in a 100 μL volume or PBS as a control.

Intratibial Injections. The bone-derived MMTV-PyMT cell line was trypsinized, washed and resuspended in ice-cold PBS at a final concentration of 1×10^5 cells/10 μl. Female 5-6 week old FVB TGF-βRII^{MyeWT} (WT) and TGF-βRII^{MyeKO} mice (6-8 per group) were injected with tumor cells as previously described [120]. Each mouse received 1×10^5 cells/10 μl or PBS as a control.

Western Blot. Briefly, spleens from naïve BALB/c treated with 1D11 or 13C4 were homogenized in Complete Lysis-M (Roche) as per manufacturer's instructions. Total protein concentrations of the resulting cell lysates were quantified using the BCA Protein Assay Kit (Pierce). 20 μg of protein was loaded per well and SDS-PAGE was performed using Bio-Rad supplies prior to being transferred to PVDF membranes (EMD Millipore). Membranes were then blocked in 5% w/v BSA, 1X TBS, 0.1% Tween 20 at room temperature with gentle shaking for 1 hour. Primary antibodies (Phospho-Smad2/Smad3 and Smad2/3) (Cell Signaling) were incubated overnight at 4°C under gentle agitation and the secondary antibody (Anti-Rabbit IgG HRP-linked) (Cell Signaling) was incubated for 1 hour at room temperature with gentle shaking. Membranes were exposed using Western Lightning Plus-ECL (Perkin Elmer) and read on a ChemiDoc Imaging System (BioRad).

Bone marrow derived macrophages (BMDM). Bone marrow was harvested from 6 week and younger female BALB/ mice. Bone marrow was flushed from the tibia and femur of the mice and resuspended in PBS. Cell were incubated in red blood cell lysis buffer for 5 mins on ice. After two PBS washes, cells were resuspended in RPMI 1640 media (Corning, 10-041-CV) supplemented with 10% FBS, 1% penicillin/streptomycin, and 20 ng/ml of recombinant macrophage colony stimulating factor (M-CSF, Sigma M6518) for 7 days on 150mm dishes (Corning, 353025) [121]. On the 7th day, BMDM were plated in 6-well plates at a concentration of $8x10^5$ cells/well in low serum RPMI (RPMI 1640 media supplemented with 1% FBS, 1% penicillin/streptomycin) and used for subsequent experiments.

In vitro experiments. For *in vitro* macrophage expression experiments, $8x10^5$ BMDM/well were kept in a naïve state or stimulated with mouse IL-4 (40ng/ml, Sigma-Aldrich SRP3211), IFN-γ + LPS (each at 50ng/ml, Sigma-Aldrich SRP3058), tumor-conditioned media (TCM) collected from 4T1 cells, for 24 hrs. After 24 hrs of stimulation, BMDM derived from BALB/c mice were treated with 1D11 or 13C4 (20μg/ml) +/- TGF-β (5ng/ml, R&D systems 240-B) for 24 hours. 4T1 cells were plated at $2x10^5$ cells/well and treated with 1D11 or 13C4 (20μg/ml) +/- TGF-β (5ng/ml, R&D systems 240-B) for 24 hours. Supernatants were then collected and cells were harvested and used for subsequent experiments.

Protein cytokine and chemokine array. BALB/c femurs were flash frozen at the time of sacrifice for all stages of TIBD (early, middle and late disease) and stored at -80°C. BMDM and 4T1 cell supernatants were obtained as previously described above and stored at -20°C. Femurs and cell supernatants were assessed using Milliplex® MAP multiplex magnetic bead-based antibody detection kits (EMD Millipore, Billerica, MA) according to the manufacturer's protocols. Bones were thawed and each femur was homogenized in CelLytic™ Buffer MT Cell Lysis Reagent (Sigma, Saint Louis, MO) in a RNase-free NAVY Bullet Blender Bead Lysis Tubes, using the Bullet Blender Storm (Next Advance, Inc., Averill Park, NY) at 4°C. Cytokine and chemokine quantification from bone homogenate and cell culture supernatants were performed in triplicate (3-4 femora per group, 3 independent *in vitro* experiments) using a 32 analyte (32-plex) Luminex assay kit on the FLEXMAP 3D instrument. Two analytes (Eotaxin, MIG) failed to fall within the range of the quality controls and these were excluded from analysis.

Histomorphometry. Mouse hind limbs were excised at death; soft tissues were removed from the tibias and femurs; and tibias were fixed for 48 h in 10% neutral-buffered formalin. Fixed bones were decalcified in a 20% ethylenediaminetetraacetic acid (EDTA) solution for 4 days at room temperature with one solution change after 48 hours. The samples were then processed and embedded in paraffin. Serial sections (thickness, 4 μm) were stained with either hematoxylin and eosin to define the region of interest (ROI) and the bone surface, tartrate resistant acid phosphatase (TRAP) to measure osteoclast number, or toluidine blue to measure osteoblast number [122]. Osteoclast and osteoblast number and size were assessed using the Osteomeasure imaging software (OsteoMetrics, Decatur, GA). Tibal sections were analyzed for osteoclasts by counting TRAP positive cells with 3 or more nuclei along the bone surface.

Sections were counterstained with hematoxylin. Osteoblasts were counted based on morphology, contact with bone tissue, and a series of at least 3 similar cells. Presence of tumors was confirmed by histology and images were captured by an Olympus BX41 microscope at a magnification of 4x and 10x.Percent tumor burden analysis was performed by a defining region of interest (ROI) per total area using Metamorph Microscopy Automation and Image Analysis Software (Metamorph, Molecuar Devices, Inc.).

Quantitative PCR (qPCR). Cells were harvested by direct lysis using RNeasy Mini Kit (Qiagen), per manufactor's instructions. cDNA was synthesized using qScript cDNA Supermix (Quanta Biosciences, 95048-500) for reverse-transcriptase PCR. cDNA was serially diluted to create a standard curve, and combined with TaqMan Universal PCR Master Mix (Applied Biosystems, 4304437) and Taqman primers: TaqMan Euk 18S rRNA (4333760F), Arginase (Arg-1, Mm00475988), LIF (Mm00434762), G-CSF (CSF3, Mm00438334) and VEGF-α (Mm00437306). Samples were loaded onto an optically clear 96- well plate and performed under the following cycling conditions: 50℃ for 2 minutes, 95℃ for 10 minutes, (95℃ for 15 seconds, 60℃ for 1 minute) x40 cycles on the 7500 Real-Time PCR System (Applied Biosystems) [81]. Quantification was performed using the absolute quantitative for human cells method using 18S as an internal control.

Flow Cytometry. Bone marrow was flushed from the femurs of BALB/c and WT/TGF-βRII^{MyeKO} and resuspended in PBS [81]. Cells were stained with the following antibodies purchased from Miltenyi Biotec (with the exception of F4/80 pacific blue (AbD Serotec) and propidium iodide (Life Technologies); anti-GR-1 PE, CD11b APC, Ly6C PE-Vio770, Ly6G VioBlue, F4/80 PE. Flow Cytometry experiments were performed on a BD LSRII instrument. Analysis was performed using Flowjo Software v.10.1 (Tree Star, Inc).

X-ray Imagining and Analysis. Mice were sedated using isoflurane vaporizer (2.5% Isoflurane: 2-3 L/min O_2) and x-ray images were taken at 35 kVp for 8 seconds using a digital radiography system (Faxitron LX-60). Mice were monitored by x-ray imaging and three stages of disease were established: early, middle and late disease. Images were saved and lesion numbers were determined using MetaMorph Microscopy Automation and Image Analysis Software (Metamorph, Molecuar Devices, Inc.). Lesion number was calculated as total number of tibial lesions per mouse.

Micro-computed X-ray Tomography (μCT). μCT analysis was performed in the Vanderbilt Institute of Small Animal Imaging. The long axis of each specimen was aligned with the scanning axis. One hundred slices from the proximal tibia were scanned at a 12-μm resolution (μCT Scanco Medical, Switerland). The region of interest was trabeculae within the proximal metaphysis of the tibia below the growth plate. Images were acquired using 55 kV, 114 μA, 300-ms integration and 500 projections per 180° rotation [81]. Images were analyzed using the Scanco Medical Imaging software to determine the bone volume/total volume (BV/TV), trabecular number and thickness, and tissue mineral density.

Osteoclast Resorption Assays. Bone marrow was harvested from the hindlimbs of 5-6-week-old BALB/c, WT and TGF-βRII^{MyeKO} mice and plated in MEMα (Corning, 10-022-CV) supplemented with 10% FBS and 1% penicillin/streptomycin for 2 hours. After 2 hours incubation, the non-adherent cells were plated at a concentration of $2x10^6$ cells/well on a dentin disc in a 24-well plate. $2x10^3$ 4T1 tumor cells or 10 nM Vitamin D3 were added to stimulate osteoclast differentiation. For systemic TGF-β inhibition experiments, cells were treated with 10 μg/mL 1D11 or 13C4. Resorption pit analysis and TRAP staining were performed after 28 days in culture. For resorption pit analysis, dentin discs were fixed in 1M NH_4OH overnight and sonicated for 2 minutes to rid of any cells, then stained with 0.5% Toluidine Blue and allowed to air dry. Images were taken at 2.5x and 8x magnification using a Leica S8 APO stereoscope and percent resorption area per total area was measured using MetaMorph. Cells were fixed and stained for TRAP using an Acid Phosphatase Leukocyte kit (Sigma-Aldrich, 387A-1KT) following manufacturer's instructions. Representative images (n=3) were taken on an Olympus BX43 microscope.

Statistics and Replicates. All data are presented as means ± the standard error mean (SEM). All *in vitro* experiments were done in triplicate with a minimum of three independent replicates. For experiments comparing two groups, a standard two-tailed unpaired student's *t* test was used unless otherwise stated in the figure legend. For experiments comparing more than 2 groups, one-way ANOVA was used with a Tukey's post-hoc test unless specifically stated in the figure legend. For all tests, a *p* value less than .05 was considered significant. All statistical analyses were done using GraphPad Prism 7.01 (GraphPad Software, La Jolla, CA). n.s, not significant.

Results

Inhibition of TGF-β alters expansion of different myeloid subpopulations throughout the progression of tumor-induced bone disease (TIBD). 5-6-week-old female athymic nude and BALB/c mice were pre-treated with either the TGF-β neutralizing antibody, 1D11, or its isotype control, 13C4, beginning seven days prior to tumor inoculation by intracardiac injection (athymic: MDA-MB-231-GFP, BALB/c: 4T1-GFP) and continuously treated until sacrifice (Figure 3A). To determine the direct role for TGF-β in myeloid cells, we injected bone-derived MMTV-PyMT cells directly into the tibia of genetically modified mice that lacked the transforming growth factor beta receptor II (TGF-βRII) specifically in myeloid cells (TGF-βRII^{MyeKO}) and its wild-type control (TGF-βRII^{MyeWT}, called from here on WT) (Figure 3B). The mice were monitored by x-ray imaging and three stages of disease were established based on the appearance of bone lesions: early, middle and late disease. Specifically, early disease was defined as no evidence of bone loss, middle disease as minor to moderate bone loss, and late disease as extensive bone loss (Figure 3C-3E).

In order to determine how TGF-β inhibition alters myeloid cell expansion in bone, flow cytometry analysis was performed at each stage of TIBD, defined by the degree of bone loss, on bone marrow from both tumor bearing and non-tumor bearing BALB/c mice treated with 1D11 or 13C4 or the WT/TGF-βRII^{MyeKO} mice. Gating strategy for all flow cytometry analysis can be found in Supplementary figure 2A. When TGF-β was systemically inhibited with 1D11 before tumor inoculation, monocytic immature cells (CD11b$^+$ CD11c$^-$ Ly6G$^-$ Ly6C$^+$) significantly decreased by 6% and the granulocytic immature cells (CD11b$^+$ CD11c$^-$ Ly6C$^-$ Ly6G$^+$) significantly increased by 14% (Figure 4A-4B).

As TIBD progressed, specifically in this model, there were no significant expansion changes in either monocytic or granulocytic immature myeloid cells while there was a significant decrease (4%) in mature myeloid cells (CD11b$^+$ F4/80$^+$, Figure 4C) at middle disease.

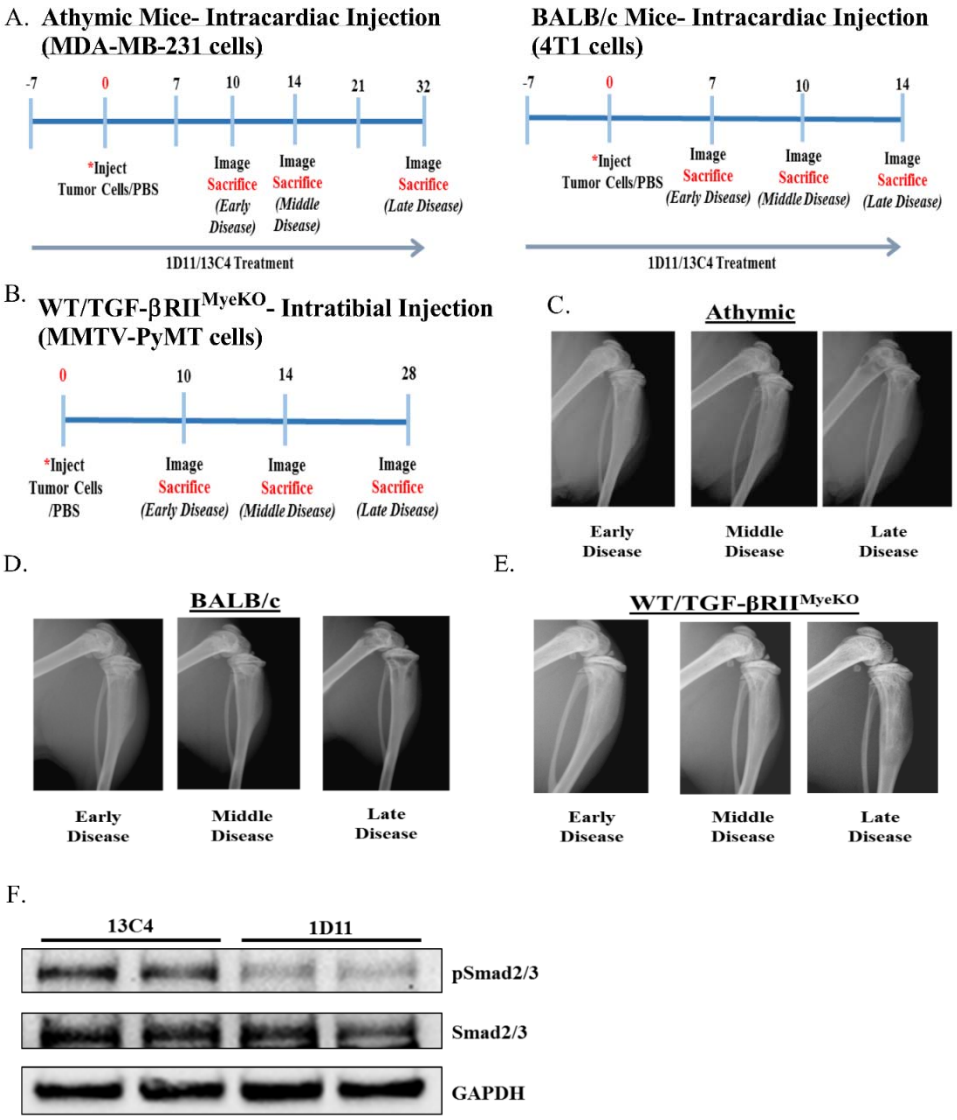

Figure 3: Mouse models utilized for TGF-β inhibition studies. **A**. Experimental outline for 1D11 experiments, athymic (left), BALB/c (right). **B.** Experimental outline for WT/ TGF-βRII^{MyeKO} mice. **C.** Representative athymic x-ray images of early, middle and late disease. **D.** Representative BALB/c x-ray images of early, middle and late disease. **E.** Representative x-ray images of early, middle and late disease for WT/ TGF-βRII^{MyeKO} mice. **F.** Western blot analysis from naïve BALB/c mice treated with 13C4 or 1D11. Spleen lysate from a mouse treated with 1D11 demonstrates a decrease in p-Smad 2/3 levels.

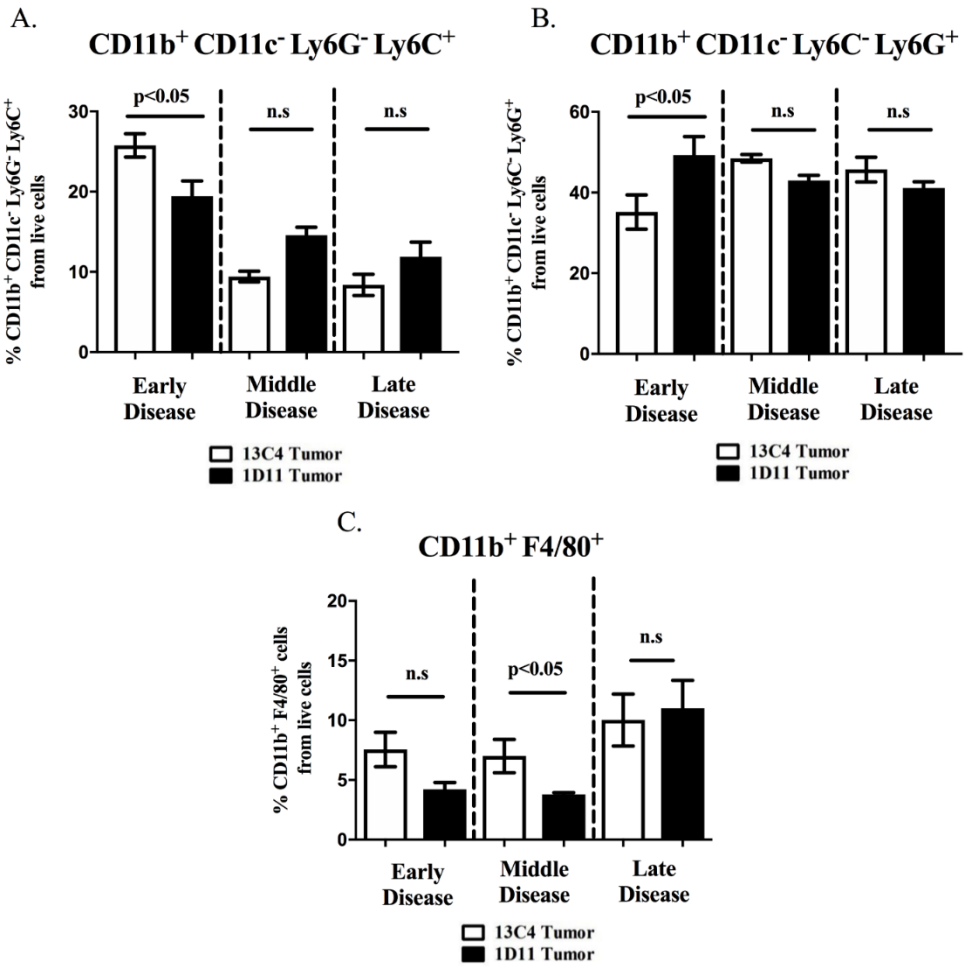

Figure 4: Early TGF-β inhibition alters immature myeloid cell expansion at early disease and mature myeloid cells at middle disease in tumor-bearing BALB/c. Bone marrow was harvested and prepared for flow cytometry as described in the methods section. **A.** Tumor-bearing BALB/c mice treated with 1D11 have a cell percentage decrease in the monocytic immature myeloid cells ($CD11b^+$ $CD11c^-$ $Ly6G^-$ $Ly6C^+$) at early disease.
B. Granulocytic immature myeloid cells ($CD11b^+$ $CD11c^-$ $Ly6C^-$ $Ly6G^+$) from tumor-bearing BALB/c mice treated with 1D11 have an increase in their expansion at early disease. **C.** Mature myeloid cells ($CD11b^+$ $F4/80^+$) decrease at middle disease when TGF-β is inhibited. (5-6 mice per group).

In regards to the genetically modified model, there were no significant expansion changes in either monocytic or granulocytic immature myeloid cell ($CD11b^+$ $CD11c^-$ $Ly6G^-$ $Ly6C^+$, $CD11b^+$ $CD11c^-$ $Ly6C^-$ $Ly6G^+$) expansion between tumor-bearing WT and TGF-βRII^{MyeKO} at any stage of TIBD (Figure 5A-5B). In contrast, mature myeloid cells ($CD11b^+$ $F4/80^+$) increased by 4% in tumor-bearing TGF-βRII^{MyeKO} mice as TIBD progressed to the middle disease state (Figure 5C).

Considering that there were no significant changes in myeloid cell expansion at late disease for either model of TGF-β inhibition (systemic and genetically modified, Figure 4A-4C, Figure 5A-5C), these studies suggest that TGF-β signaling may play an important role in regulating myeloid cell expansion in the earlier stages of disease, but not when extensive bone loss is present in our models of TIBD.

TGF-β inhibition modulates expression and secretion of factors associated with tumor progression and immune suppression. Since changes in myeloid expansion were observed when TGF-β signaling was inhibited and TGF-β itself can stimulate the production of pro-tumorigenic factors that can expand myeloid cells, we investigated whether systemic TGF-β inhibition alters pro-tumorigenic factors in whole bone from PBS and tumor-bearing BALB/c 13C4/1D11 treated mice at all stages of TIBD (i.e. early, middle and late disease). Femurs were subjected to a cytokine and chemokine analysis using a multiplex assay system and results are outlined in Supplementary table 1A-1I. Analyses indicated that significant protein changes in femurs only occurred at late disease (Supplementary table 1C), thus, emphasis was only placed on significant differences observed between cytokine and chemokines at late disease. Compared to control femurs, two factors significantly increased in femurs from tumor-bearing mice; granulocyte colony-stimulating factor (G-CSF) and leukemia inhibitory factor (LIF); but only G-CSF significantly decreased with TGF-β inhibition (Figure 6A). Unexpectedly, the pro-tumorigenic factor, vascular endothelial growth factor (VEGF) was significantly increased in femurs from 1D11 treated tumor-bearing mice (Figure 6C). This data demonstrates that pre-treatment with a TGF-β inhibitor can both reduce and increase pro-tumorigenic proteins in bone at the late disease state, suggesting multiple mechanisms are at play.

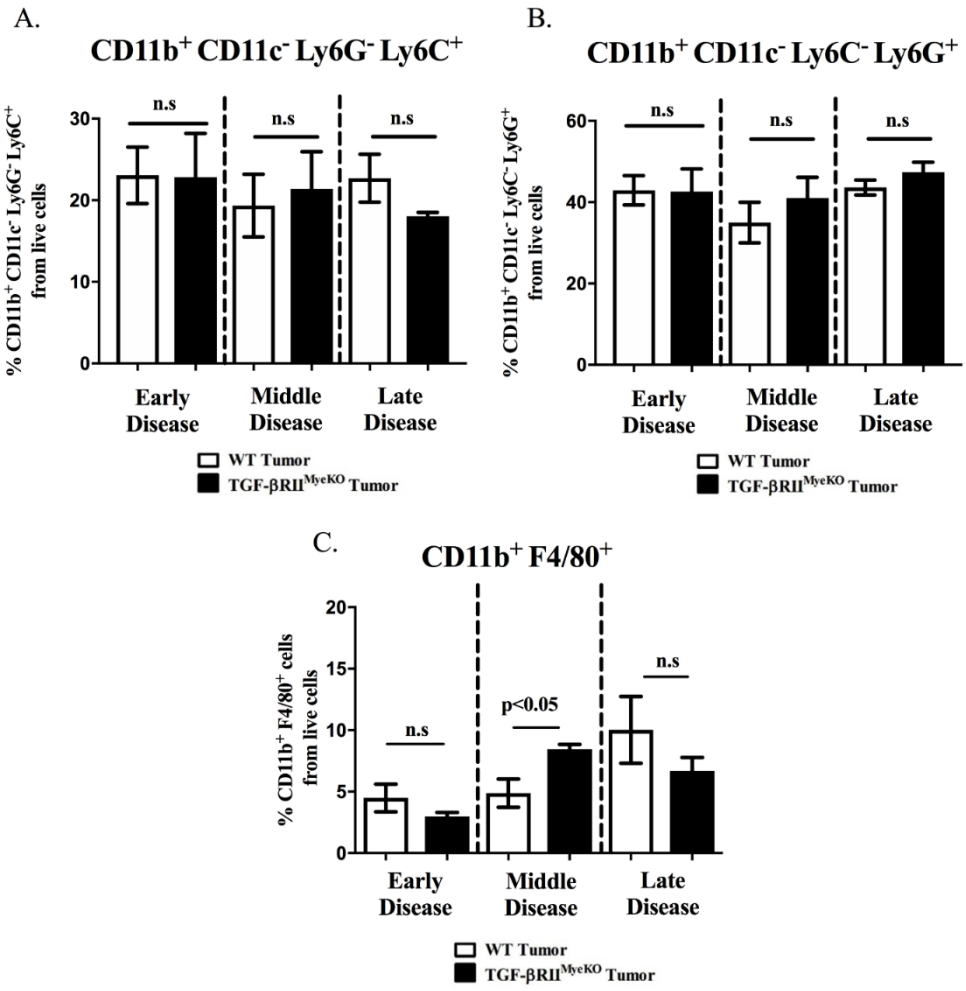

Figure 5. Early TGF-β inhibition alters mature myeloid expression at middle disease for tumor-bearing TGF-βRII^{MyeKO} mice. Bone marrow was harvested and prepared for flow cytometry as described in the methods section. **A.** No significant expansion differences in monocytic immature myeloid cells (CD11b$^+$ CD11c$^-$ Ly6G$^-$ Ly6C$^+$)) between tumor-bearing WT and TGF-βRII^{MyeKO} mice. **B.** No significant expansion differences in granulocytic immature myeloid cells (CD11b$^+$ CD11c$^-$ Ly6C$^-$ Ly6G$^+$) between tumor-bearing WT and TGF-βRII^{MyeKO} mice. **C.** Mature myeloid cells (CD11b$^+$ F4/80$^+$) from tumor-bearing TGF-βRII^{MyeKO} mice increase in cell percentage at middle disease. (5-6 mice per group).

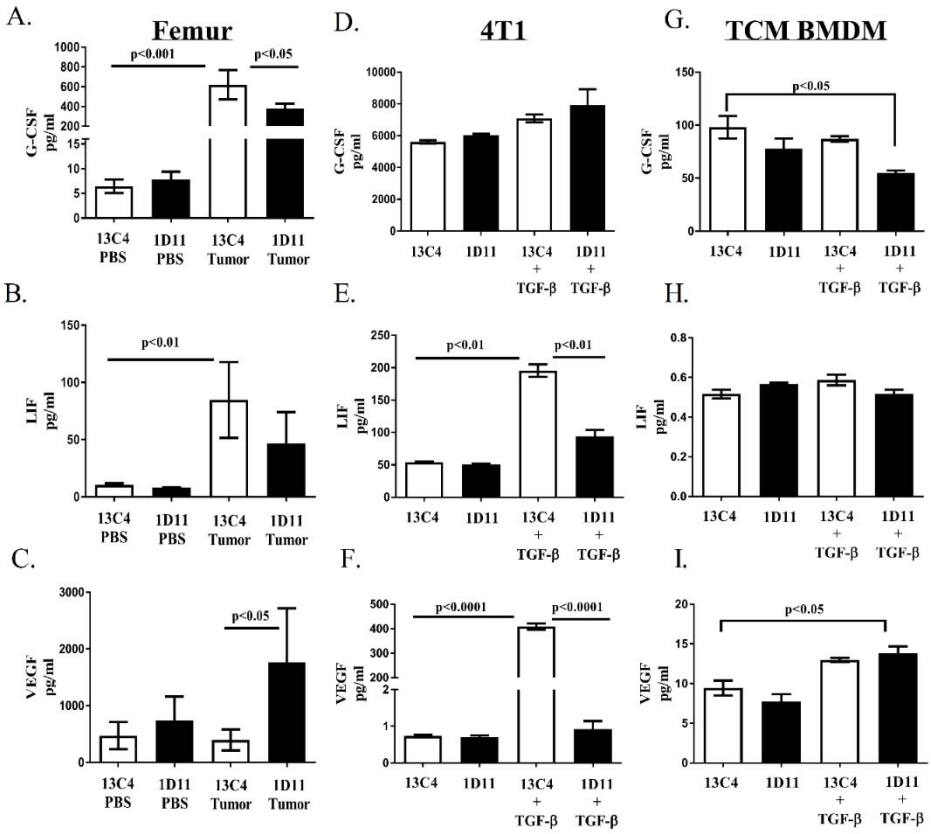

Figure 6. TGF-β inhibition modulates secretion of factors associated with tumor promotion. BALB/c femurs and cell supernatants were collected and prepared for the protein cytokine/chemokine array as described in the methods section. **A.** G-CSF protein levels increase in femur homogenates from tumor-bearing mice and levels decrease when tumor-bearing mice were treated with 1D11 at late disease. **B.** LIF protein levels increase in femur homogenates from tumor- bearing mice at late disease. **C.** VEGF protein levels increase in femur homogenates from 1D11 treated tumor- bearing mice at late disease. **D.** G-CSF proteins levels do not change when TGF-β is inhibited in 4T1 cells. **E.** LIF protein levels increase with TGF-β stimulation and decrease when 4T1 cells are treated with 1D11. **F.** VEGF protein levels increase with TGF-β stimulation and decrease when 4T1 cells are treated with 1D11. **G.** G-CSF levels decrease when TGF-β is inhibited in TCM stimulated BMDM. **H.** Treatment with 1D11 does not change LIF protein levels in TCM stimulated BMDM. **I.** VEGF protein levels increase with TGF-β stimulation in TCM stimulated BMDM. Protein cytokine/chemokine array data was analyzed using a two-way ANOVA with a Tukey's post-hoc test (3-4 femurs per group, 3 independent *in vitro* cell supernatants per group).

Since TGF-β inhibition affects the cytokine and chemokine profile within bone and TGFβ-responsive tumor and myeloid cell populations reside in the tumor-bearing femurs that were analyzed, these two cell subsets were further evaluated *in vitro*.

To further investigate the cytokine and chemokine profile of tumor and myeloid cells in response to TGF-β inhibition, 4T1 tumor cells and differentially polarized bone marrow derived macrophages (BMDM) were stimulated and simultaneously inhibited for TGF-β for 24 hours, followed by a chemokine/cytokine analysis performed on all cell supernatants (Supplementary table 1D-1I). TGF-β stimulation increases protein levels of LIF and VEGF, while inhibition of TGF-β with 1D11 reduces these cytokines significantly in 4T1 tumor cells (Figure 6E, 6F). Likewise, G-CSF levels were reduced while VEGF protein levels were increased in tumor-conditioned media (TCM) stimulated BMDM under TGF-β inhibitory conditions (Figure 6G, 6I). Thus, this *in vitro* data supports the notion that the changes in G-CSF and VEGF observed in bone may be myeloid-dependent.

Since arginase has been implicated in promoting immune suppression in cancer [107, 108, 123, 124], we investigated the effect of TGF-β inhibition on arginase expression in differentially polarized BMDMs. Arginase, a marker of immune suppression, was decreased significantly in IL-4 stimulated macrophages (Supplementary figure 3B), and while TCM stimulated macrophages responded similarly, their decrease in arginase expression was not statistically significant (Supplementary figure 3C). Interestingly, all BMDM independent of their stimulation profile had a statistically significant increase in arginase expression after TGF-β stimulation (Supplementary figure 3A-3D). While publications have addressed the link between arginase expression and TGF-β stimulation [123, 124], our findings suggest that TGF-β may promote immune suppression in bone, a microenvironment that contains an abundant amount of TGF-β when tumor is present [39].

TGF-β inhibition decreases osteoclast function. Published work by our group and others has demonstrated that myeloid cells found in the bone marrow, such as macrophages and $CD11b^+$ $Gr\text{-}1^+$ cells, have the potential to differentiate into osteoclasts [81, 82, 106, 125]. Therefore, in order to explore if pre-treatment with a TGF-β inhibitor would alter osteoclast number and activity, histological analyses were performed on the tibias of tumor-bearing mice that were treated with 1D11.

These analyses indicated that although the number of $TRAP^+$ osteoclasts were decreased in both tumor-bearing athymic nude and BALB/c mice treated with 1D11, only athymic nude mice had a statistically significant decrease when TGF-β was inhibited at late stage disease (Figure 7A, 7B).

When osteoclast activity was examined *in vitro*, treatment with 1D11 decreased both the percent of resorption area and the number of resorption pits that were made by $TRAP^+$ osteoclasts derived from BALB/c bone marrow (Figure 7C, 7D). These data suggest that pre-treatment with TGF-β inhibitors can reduce osteoclast number and function.

Histological analyses of the WT/TGF-βRII^{MyeKO} tibiae indicated that there was no change in $TRAP^+$ osteoclasts between tumor-bearing TGF-βRII^{MyeKO} and WT mice (Figure 7E). Despite no significant changes in osteoclast number, TGF-βRII^{MyeKO} $TRAP^+$ osteoclasts have a significant decrease in percent resorption area *in vitro* (Figure 7H, 7I). Together this suggests that TGF-βRII^{MyeKO} specific osteoclasts may be impaired in their ability to resorb dentin, indicating a decrease in osteoclast function. While osteoclast number varies between the two models of TGF-β inhibition (systemic and genetic) through histological analysis, osteoclast activity is significantly reduced in both tumor-bearing 1D11 treated mice and TGF-βRII^{MyeKO} mice implying a reduction in overall TIBD.

Early TGF-β inhibition reduces osteolytic lesions and tumor burden in bone. Since TGF-β inhibition has an effect on the bone microenvironment once tumors are established, we hypothesized that TGF-β inhibition prior to tumor inoculation would decrease TIBD. By x-ray imaging, we identified that tumor-bearing athymic nude and BALB/c mice that were treated with 1D11 had reduced osteolytic lesions as compared to their isotype control, 13C4, at late disease (Figure 8A, 8C). While it has been previously published that 1D11 can increase overall bone volume in a naïve mouse model [126] and our studies recapitulate those results (Supplementary figure 5A-5C), we demonstrate that treatment with 1D11 increases overall bone volume in both mouse models of early systemic TGF-β inhibition at all stages of TIBD (Figure 8B and 8D). Additionally, mice treated with 1D11 (athymic and BALB/c mice) have an overall decrease in tumor burden (as determined by histomorphometry) compared to 13C4 treated mice at late stage disease (Figure 9A, 9B).

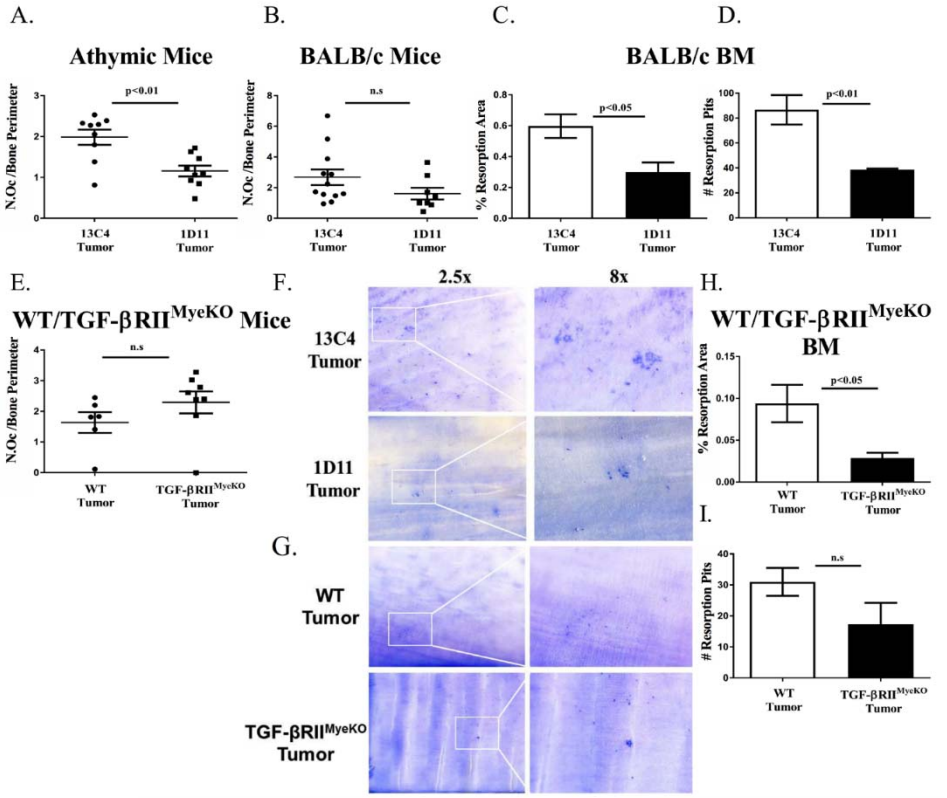

Figure 7. TGF-β inhibition decreases osteoclast activity in mouse models of TIBD. Tibial sections were stained with tartrate resistance acid phosphatase (TRAP) for osteoclast analyses and *in vitro* osteoclast resorption assays were performed as described in the methods section. **A&B.** Histological osteoclast analyses for tumor-bearing athymic and BALB/c mice at late disease. At late disease only tumor-bearing athymic mice that were treated with 1D11 have a significant reduction in their osteoclast number per bone perimeter (11-12 tibias per group). **C&D.** Quantification of osteoclast resorption area and resorption pits for systemic TGF-β inhibition experiments. Treatment with 1D11 significantly decreases osteoclast resorption area and resorption pits. **E.** At late disease, there is no significant difference in osteoclast number per bone perimeter between tumor-bearing WT and TGF-βRII^{MyeKO} mice (6-8 tibias per group). **F.** Representative images of dentin discs containing osteoclast resorption area and resorption pits for systemic TGF-β inhibition experiments. **G.** Representative images of dentin discs containing osteoclast resorption area and resorption pits for WT and TGF-βRII^{MyeKO} experiments. **H&I.** Quantification of osteoclast resorption area and resorption pits for WT and TGF-βRII^{MyeKO} experiments. TRAP^{+} osteoclasts derived from TGF-βRII^{MyeKO} bone marrow create a significantly smaller resorption area as compared to their WT control. **BM**, bone marrow.

Early TGF-β inhibition reduces osteolytic lesions and tumor burden in bone. Since TGF-β inhibition has an effect on the bone microenvironment once tumors are established, we hypothesized that TGF-β inhibition prior to tumor inoculation would decrease TIBD. By x-ray imaging, we identified that tumor-bearing athymic nude and BALB/c mice that were treated with 1D11 had reduced osteolytic lesions as compared to their isotype control, 13C4, at late disease (Figure 8A, 8C). While it has been previously published that 1D11 can increase overall bone volume in a naïve mouse model [126] and our studies recapitulate those results (Supplementary figure 5A-5C), we demonstrate that treatment with 1D11 increases overall bone volume in both mouse models of early systemic TGF-β inhibition at all stages of TIBD (Figure 8B and 8D). Additionally, mice treated with 1D11 (athymic and BALB/c mice) have an overall decrease in tumor burden (as determined by histomorphometry) compared to 13C4 treated mice at late stage disease (Figure 9A, 9B).

In the genetic TGF-β inhibition mouse model, tumor-bearing TGF-βRII^{MyeKO} mice had a significant decrease in the number of bone lesions at late disease (Figure 8E) while significant changes in overall bone volume between WT and TGF-βRII^{MyeKO} mice were only seen at early disease (Figure 8F). μCT analysis demonstrated that tumor-bearing TGF-βRII^{MyeKO} mice had a decrease in overall bone volume (BV/TV), trabecular spacing and trabecular number as compared to WT mice at early disease (Supplementary table 2). While significant changes in these bone parameters were only seen during early disease between tumor-bearing WT and TGF-βRII^{MyeKO} mice, changes in overall bone volume did not decrease as TIBD progressed in tumor-bearing TGF-βRII^{MyeKO} mice (Figure 8F). This may imply that loss of functional TGF-β signaling specifically in myeloid cells may stabilize bone loss in the presence of tumor. Analyses at late stage disease revealed that TGF-βRII^{MyeKO} mice had lower tumor burden than WT tumor-bearing mice (Figure 9C). Overall, this data suggests that early TGF-β inhibition prior to tumor inoculation can prevent TIBD by reducing osteolytic lesions and decreasing tumor burden in bone.

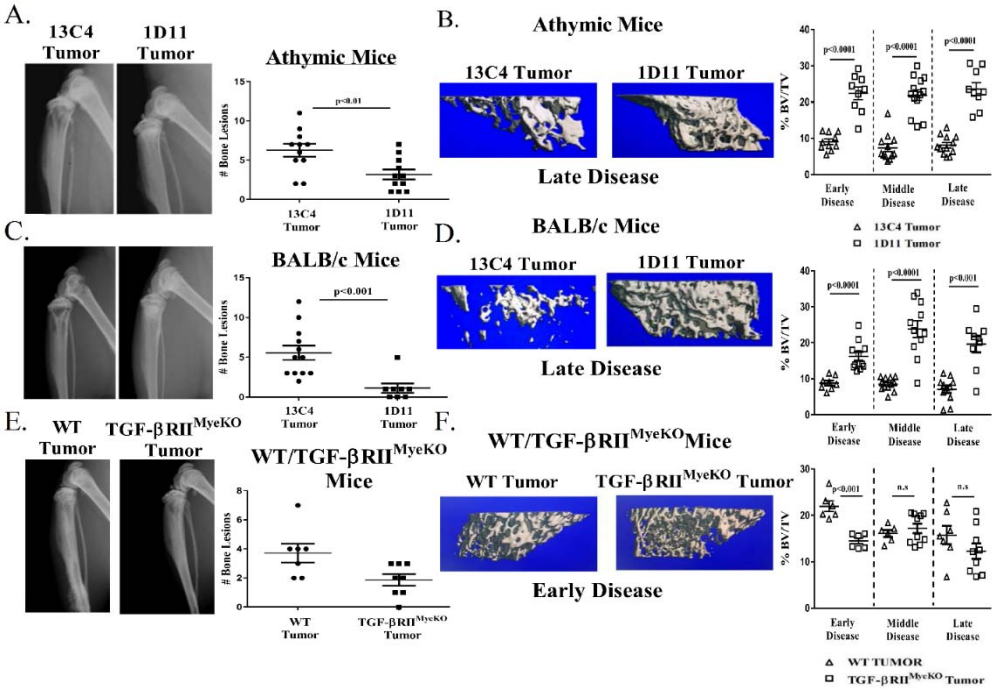

Figure 8: TGF-β inhibition reduces osteolytic lesions and improves overall bone volume. X-ray analysis of tumor-bearing mice at late stage disease prior to sacrifice. Representative images are from late stage disease. Formalin fixed tibias were scanned and analyzed by μCT as described in the methods section. Percent bone volume normalized to total volume (BV/TV) for each treatment group. **A.** Athymic mouse model: X-ray images, 13C4 treated (left), 1D11 treated (right) and quantification of bone lesions. Tumor-bearing athymic mice treated with 1D11 have less osteolytic lesions than isotype control. **B.** Left: three-dimensional (3D) rendered μCT images from two tumor-bearing athymic mice at late stage disease, 13C4 treated (left), 1D11 treated (right). Right: percent BV/TV over the course of tumor-induced bone disease (TIBD) in the athymic mouse model. Treatment with 1D11 increases overall bone volume over the course of TIBD. **C.** BALB/c mouse model: X-ray images, 13C4 treated (left), 1D11 treated (right) and quantification of bone lesions. Tumor-bearing BALB/c mice treated with 1D11 have less osteolytic lesions than isotype control. **D.** Left: 3D rendered μCT images from two tumor-bearing BALB/c mice at late stage disease, 13C4 treated (left), 1D11 treated (right). Right: percent BV/TV over the course of tumor-induced bone disease in the BALB/c mouse model. Treatment with 1D11 increases overall bone volume over the course of TIBD. **E.** WT/ TGF-βRII^{MyeKO} mice mouse model: X-ray images, WT tumor (left), TGF-βRII^{MyeKO} tumor (right) and quantification of bone erosions. Tumor-bearing TGF-βRII^{MyeKO} have a reduced incidence of bone lesions as compared to tumor-bearing WT mice. **F.** Left: 3D rendered μCT images from two tumor-bearing mice at early stage disease, WT (left), TGF-βRII^{MyeKO} (right). Right: percent BV/TV over the course of tumor-induced bone disease in the WT/ TGF-βRII^{MyeKO} mice mouse model. Tumor-bearing TGF-βRII^{MyeKO} mice only have a significant decrease in their overall bone volume at early disease. (9-13 tibias per group).

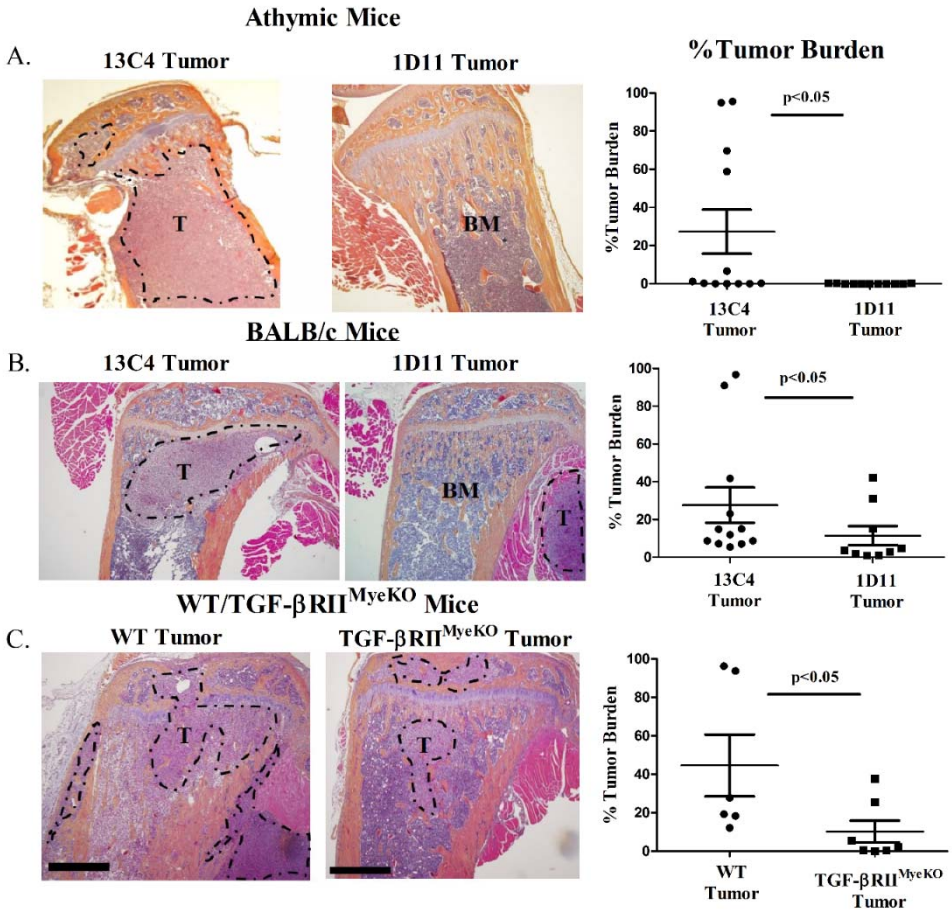

Figure 9: TGF-β inhibition reduces tumor burden at late stage disease in all three mouse models of TIBD. Tibal sections were stained with hematoxylin & eosin (H+E) for tumor burden analysis at late stage disease as described in the methods section. **A&B.** 4x magnification H+E sections from two tumor-bearing mice (athymic and BALB/c) at late stage disease, 13C4 treated (left), 1D11 treated (right) and quantification of percent tumor burden between treatment groups at late stage disease. Tumor-bearing mice (athymic and BALB/c) treated with 1D11 have a reduction in tumor burden as compared to isotype control. **C.** 4x magnification H+E sections from two tumor-bearing WT and TGF-βRII^{MyeKO} mice at late stage disease, WT (left), TGF-βRII^{MyeKO} (right) and quantification of percent tumor burden between mice at late stage disease. Tumor-bearing TGF- βRII^{MyeKO} mice have a reduction in tumor burden as compared to isotype control. **T**, Tumor. **BM**, Bone Marrow. Scale, 50 μm.

Discussion

This study illustrates that TGF-β inhibition alters myeloid expansion that leads to a reduction in tumor burden and bone destruction, and an increase in bone volume. Specifically, we show that early TGF-β inhibition alters the tumor-bone microenvironment by affecting expansion of myeloid cells that are at different stages of differentiation, modulating pro-tumorigenic factors and decreasing osteoclast function. Since systemic treatment with TGF-β inhibitors may alter other cell types, we utilized a conditional knock out mouse model that lacked TGF-βRII specifically in myeloid cells (TGF-βRII^{MyeKO}). In this model, mature myeloid cells expand in the presence of tumor but have less bone lesions, contain deficient osteoclasts and have a significant reduction in tumor burden in bone. Together these data strengthen the notion of the complexity of the tumor-bone microenvironment and that early TGF-β inhibition is a promising potential therapeutic target for reducing TIBD.

While it is well known that myeloid cells, specifically CD11b$^+$ Gr-1$^+$ cells, expand in the presence of a tumor, and that this expansion contributes to the production of pro-tumorigenic and immune suppressive factors that support tumor progression and metastasis [73, 81, 110, 116], the regulation and function of these cells in TIBD is still unclear. Since TGF-β has been shown to play an important role in myeloid differentiation, chemotaxis and polarization [83, 107, 123], we reasoned that inhibition of TGF-β signaling would decrease myeloid expansion in bone in the context of TIBD. Our data reveals that systemic TGF-β inhibition with 1D11 can both increase and decrease immature myeloid cells (decrease: CD11b$^+$ CD11c$^-$Ly6G$^-$ Ly6C$^+$, increase: CD11b$^+$ CD11c$^-$Ly6C$^-$ Ly6G$^+$) at early disease and reduce expansion of mature myeloid cells (CD11b$^+$ F4/80$^+$) at the middle disease state (Figure 4A-4C). However, loss of TGF-βRII in myeloid cells does not alter the expansion profile in either monocytic or granulocytic immature myeloid cells (CD11b$^+$ CD11c$^-$Ly6G$^-$ Ly6C$^+$, CD11b$^+$ CD11c$^-$Ly6C$^-$ Ly6G$^+$, Figure 5A-5B) at any stages of TIBD. On the other hand, CD11b$^+$ F4/80$^+$ myeloid cells from tumor-bearing TGF-βRII^{MyeKO} are increased as TIBD progresses to the middle disease state, where minor to moderate bone loss was detected by x-ray analysis (Figure 5C).

Since the strategies to neutralize TGF-β within our mouse models were different, one model was injected with a TGF-β neutralizing antibody that would affect all TGF-β responsive cells while the other model contained a genetic deletion of TGF-βRII in myeloid cells; it is not surprising that distinct myeloid expansion profiles are observed in our studies.

While it is possible that the changes in expansion are due to myeloid effects on other cell types, our findings imply that TGF-β signaling plays a role in regulating the expansion of immature and mature myeloid cells when tumors in bone are first developing. However, once these tumors become established in bone and begin promoting symptoms of TIBD (i.e. bone loss and overwhelming tumor burden), myeloid expansion may no longer be controlled by TGF-β signaling but by other mechanisms that regulate myeloid expansion [127].

Recent studies have focused on investigating the cross-talk between tumors and the immune system and how it contributes to immune suppression and evasion. Immune evasion is currently considered an emerging hallmark of cancer, and it involves the ability for tumors to evade immunological destruction by T and B cells, natural killer cells, and macrophages [128]. Specifically, in breast cancer, TGF-β has been shown to promote pro-tumorigenic and immunosuppressive factors [115, 116], therefore we expected a significant reduction in these factors when TGF-β was systemically inhibited in our BALB/c model of breast cancer metastasis to bone. Surprisingly, our femur analyses revealed that systemic TGF-β inhibition can both increase and decrease factors that contribute to tumor progression at late disease. For example, the pro-tumorigenic factor G-CSF is significantly reduced in femurs from tumor-bearing mice that were treated with the TGF-β inhibitor 1D11 (Figure 6A). G-CSF has been shown to contribute to chemoresistance, migration and expansion of myeloid cells, and is correlated with a reduced overall survival in patients [129-132]. Evidence from pre-clinical studies indicate that G-CSF can act directly on myeloid cells promoting their mobilization from the bone marrow to the peripheral circulation [133]. Reduction of G-CSF by 1D11 could imply that bone marrow residing myeloid cells are prevented from entering circulation and migrating to tertiary organs to set up the pre-metastatic niche, allowing for additional metastases to form.

Nonetheless, systemic TGF-β inhibition also increases VEGF and CCL4, factors known to support tumor progression in bone (Figure 6C, supplementary table 1C) [122, 134]. Since significant cytokine changes in bone were only observed at late disease, it suggests that these changes occur when severe symptoms of TIBD are present, including but not limited to tumor burden.

Considering that both myeloid cells and 4T1 tumor cells are TGF-β- responsive cells that reside in the tumor-bearing femurs that were analyzed, we wanted to investigate whether the changes observed in bone when TGF-β was inhibited were tumor or myeloid-dependent. Thus, these two distinct cell populations were evaluated for changes in their cytokine and chemokine profiles *in vitro*.

When TGF-β was inhibited, 4T1 tumor cells significantly decreased both VEGF and LIF protein levels (Figure 6E, 6F), while TCM stimulated BMDM reduced G-CSF but increased VEGF levels significantly (Figure 6G, 6I). This implies that both tumor cells and BMDM have contrasting responses to TGF-β inhibition, and that both of these cell types contribute differently to the changes in pro-tumorigenic factors we observe in bone. For example, the decrease in bone G-CSF when TGF-β is inhibited suggests that this decrease is mediated through a myeloid-dependent mechanism because a similar trend is seen in TCM-stimulated BMDM (Figure 6A, Figure 6G). The same rational can be applied to the changes in VEGF in bone, the increase in bone VEGF is also observed in TCM-stimulated BMDM, suggesting a myeloid-dependent mechanism. It is also reasonable that other cells of the bone microenvironment, such as osteoblasts, are contributing to the changes in factors we observe in bone. For example, osteoblasts produce an abundant amount of VEGF [122] and LIF [135, 136], and while the role of LIF in tumorigenesis is complex [137, 138], angiogenesis and osteogenesis has been established as a coupled process in normal bone remodeling [139]. Thus, the increased levels of VEGF in bone and TCM-stimulated BMDM in response to TGF-β inhibition may reflect the increase in bone volume seen with 1D11 treatment. Therefore, the increase in VEGF may be beneficial and this benefit may outweigh the consequences of an increased blood supply to the tumor.

Since our *in vitro* analyses only included 4T1 tumor cells and BMDM cells, we acknowledge that we may have missed important *in vivo* interactions and changes in other cell types due to TGF-β inhibition. Despite these limitations and the increase in pro-tumorigenic factors with TGF-β inhibition, there is an overall reduction in TIBD in our mouse model of breast cancer metastasis to bone. It is currently unknown the concentration of factors that are needed to promote a pro-tumorigenic environment.

We reason that perhaps it is a certain ratio of cytokines and chemokines that are needed to tip the scale between tumor promoting and cytotoxicity and that a combination of the right factors can determine which direction the scale tips.

TGF-β inhibitors are currently in clinical trials for the treatment of gliomas, metastatic breast cancer, non-small cell lung cancer, melanoma, mesothelioma and renal cell carcinoma [140-142]. While many of these clinical trials are still ongoing, evidence from preclinical studies indicate that TGF-β inhibitors, like the human monoclonal antibody fresolimumab, would be most effective if used in combination with chemotherapy and/or radiation [143-146]. A preclinical study using an orthotropic model of breast cancer demonstrated that 1D11 enhanced the effects of chemotherapy by normalizing the tumor stroma [145]. Similar observations are seen in our studies where pre-treatment with 1D11 remodels the bone-tumor microenvironment by regulating the expansion of the myeloid population, the ratio of pro-tumorigenic factors and decreasing the function of osteoclasts leading to an overall reduction in TIBD. While the combination of a TGF-β inhibitor and a chemotherapeutic are not yet the standard of care for metastatic breast cancer patients, it is worth exploring in preclinical setting in the context of TIBD. In conclusion, our work supports the notion that early TGF-β inhibition is a potential therapeutic approach for reducing TIBD.

Supplementary tables and figures

Supplementary table 1A. BALB/c early disease femurs

Analyte	13C4 PBS (pg/mg protein)	1D11 PBS (pg/mg protein)	13C4 Tumor (pg/mg protein)	1D11 Tumor (pg/mg protein)	*p* value 13C4 PBS vs. 13C4 Tumor	*p* value 13C4 Tumor vs. 1D11 Tumor
CCL2/MCP-1	18.3±3.1	13.1±5.8	4.8 ±1.6	13.2±7.7	0.9927	0.9982
CCL3/MIP-1α	17.0±3.6	12.6±2.1	16.1±3.7	19.6±4.6	0.9997	0.9833
CCL4/MIP-1β	12.2±5.5	6.3±1.6	7.5±3.8	6.1±2.9	0.7731	0.9908
CCL5/RANTES	20.1±2.9	11.9±1.5	14.2±2.8	11.3±2.9	0.2333	0.7703
CXCL1/KC	24.9±1.4	21.8±1.8	25.1±4.5	23.3±7.0	p>0.9999	p>0.9999
CXCL2/MIP-2	35.6±2.8	29.2±3.3	20.4±2.9	30.1±3.2	0.9997	0.9988
CXCL5/LIX	103.9±9.4	94.0±27.9	74.6±41.1	141.3±18.4	p>0.9999	0.9887
CXCL10/IP-10	85.9±1.1	70.8±9.9	72.8±7.8	70.9±16.2	0.9998	p>0.9999
G-CSF	5.1±1.1	4.0±1.2	32.8±26.4	57.5±28.2	0.9845	0.9889
GM-CSF	11.6±4.3	12.7±3.2	12.7±3.2	11.6±4.3	0.9988	0.9988
M-CSF	41.8±8.5	35.5±7.1	28.8±7.7	44.6±13.0	0.5179	0.3544
VEGF	47.7±8.5	41.6±12.5	74.1±38.3	57.8±10.8	p>0.9999	p>0.9999
IL-1α	37.3±3.2	41.2±4.5	40.7±4.3	43.0±4.1	0.9997	p>0.9999
IL-1β	9.8±0.3	8.7±1.0	15.6±3.0	16.5±2.8	0.9777	0.9999
IL-2	7.4±1.5	8.0±1.3	6.5±0.3	8.5±0.8	0.9962	0.9585
IL-3	1.4±0.0	1.2±0.1	1.1±0.2	1.4±0.1	0.8322	0.6992
IL-4	1.2±0.1	1.1±0.2	1.2±0.2	1.1±0.2	p>0.9999	0.9984
IL-5	2.1±0.2	4.4±2.0	1.5±0.4	2.2±0.7	0.9889	0.9766
IL-6	5.3±1.4	5.1±1.2	4.9±0.5	5.2±1.4	p>0.9999	p>0.9999
IL-7	1.0±0.3	1.6±0.7	0.5±0.1	0.9±0.2	0.8757	0.9449
IL-9	220.7±41.6	218.3±44.7	181.9±28.8	211.7±14.1	0.9984	0.9993
IL-10	9.9±0.8	8.0±1.0	7.5±0.7	11.3±1.4	0.9908	0.9649
IL-12p40	3.5±3.4	2.0±0.7	0.9±0.4	6.7±6.3	p>0.9999	0.9997
IL-12p70	2.2±0.7	2.2±0.3	1.2±0.2	3.3±0.5	0.7096	0.1088
IL-13	7.8±0.2	7.4±0.9	5.7±0.8	7.5±0.3	0.7152	0.8153
IL-15	7.6±1.9	9.5±2.9	8.2±1.0	6.1±1.1	0.9992	0.9550
IL-17	2.2±0.6	1.9±0.5	2.2±0.4	1.6±0.1	p>0.9999	0.8198
TNF-α	5.7±1.1	3.6±0.7	4.4±0.5	7.7±2.3	0.9791	0.7483
IFN-γ	1.3±0.4	1.2±0.3	1.2±0.3	1.8±0.3	p>0.9999	0.9965
LIF	21.4±2.0	13.1±2.3	12.8±1.0	11.9±2.1	0.9668	p>0.9999

Values represent the mean ± SEM of the cytokine/chemokine concentrations (pg cytokine/mg total protein) in the femur homogenates, measured by Luminex assay (pg cytokine/ml) and Bradford assay (mg protein/ml). Protein cytokine/chemokine array data was analyzed using a two-way ANOVA with a Tukey's post-hoc test. * indicates statistically significant change. (3-4 femurs per group)

Supplementary table 1B. BALB/c middle disease femurs

Analyte	13C4 PBS (pg/mg protein)	1D11 PBS (pg/mg protein)	13C4 Tumor (pg/mg protein)	1D11 Tumor (pg/mg protein)	*p* value 13C4 PBS vs. 13C4 Tumor	*p* value 13C4 Tumor vs. 1D11 Tumor
CCL2/MCP-1	38.7±17.7	43.5±12.9	66.4±30.0	100.6±41.6	0.9424	0.8983
CCL3/MIP-1α	33.4±11.8	26.5±7.5	23.4±5.1	23.5±4.6	0.7252	p>0.9999
CCL4/MIP-1β	12.2±5.5	6.3±1.6	7.5±3.8	6.1±2.9	0.8249	0.9906
CCL5/RANTES	19.7±2.0	15.6±1.0	19.1±2.2	16.2±4.1	0.9977	0.7657
CXCL1/KC	56.0±15.6	62.8±13.5	61.4±13.5	56.2±15.7	0.9999	p>0.9999
CXCL2/MIP-2	121.6±50.7	128.9±45.5	170.7±50.2	132.1±49.3	0.8767	0.9348
CXCL5/LIX	391.5±168.8	545.0±170.1	547.9±43.2	389.6±155.3	0.8786	0.8748
CXCL10/IP-10	357.7±156.1	394.1±108.3	377.5±116.0	349.4±140.3	0.9995	0.9985
G-CSF	5.4±1.4	6.2±1.5	46.0±36.5	40.7±23.0	0.9542	0.9999
GM-CSF	10.8±5.2	15.9±5.9	15.0±5.5	17.3±7.2	0.9378	0.9871
M-CSF	40.3±2.6	40.3±2.9	40.3±4.6	47.6±4.5	p>0.9999	0.8675
VEGF	516.7±248.0	444.9±160.2	644.8±330.5	532.5±256.3	0.9922	0.9947
IL-1α	37.3±3.2	41.2±4.5	40.7±4.3	43.0±4.1	p>0.9999	0.9987
IL-1β	51.7±14.9	43.1±10.4	42.6±13.1	34.2±10.5	0.9215	0.9393
IL-2	16.0±4.6	16.4±3.1	12.5±2.4	14.2±4.2	0.8215	0.9706
IL-3	0.2±0.1	0.1±0.0	0.2±0.1	0.4±0.4	p>0.9999	0.8211
IL-4	0.9±0.1	1.1±0.2	0.9±0.1	1.3±0.2	0.9995	0.6716
IL-5	1.9±0.4	2.6±1.3	2.2±1.0	3.6±1.8	0.9975	0.8702
IL-6	17.2±7.1	19.3±5.4	15.9±4.5	16.2±5.9	p>0.9999	p>0.9999
IL-7	1.8±0.5	1.9±0.4	1.9±0.4	1.8±0.5	0.9985	0.9981
IL-9	608.3±205.6	723.0±170.8	650.8±178.6	683.7±259.5	0.9979	0.9990
IL-10	16.1±5.9	23.6±4.6	21.8±6.2	24.7±8.1	0.8948	0.9833
IL-12p40	14.1±7.2	89.9±50.3	96.0±65.9	101.8±56.8	0.5855	0.9997
IL-12p70	1.2±0.3	1.5±0.9	1.1±0.3	2.0±0.6	0.9987	0.7390
IL-13	3.4±2.0	2.8±1.4	3.3±1.9	2.81.4	p>0.9999	0.9933
IL-15	13.7±2.4	13.4±2.6	13.4±2.6	13.1±2.9	p>0.9999	0.9998
IL-17	2.8±0.4	2.8±0.4	2.6±0.5	2.4±0.5	0.9878	0.9951
TNF-α	3.8±0.1	5.1±1.1	8.7±2.5	8.7±2.3	0.4589	p>0.9999
IFN-γ	6.5±3.1	6.8±2.3	4.5±2.7	7.2±3.4	0.8853	0.7577
LIF	9.5±0.8	6.6±0.9	11.8±0.6	6.9±0.7	0.9993	0.9995

Values represent the mean ± SEM of the cytokine/chemokine concentrations (pg cytokine/mg total protein) in the femur homogenates, measured by Luminex assay (pg cytokine/ml) and Bradford assay (mg protein/ml). Protein cytokine/chemokine array data was analyzed using a two-way ANOVA with a Tukey's post-hoc test. * indicates statistically significant change. (3-4 femurs per group)

Supplementary table 1C. BALB/c late disease femurs

Analyte	13C4 PBS (pg/mg protein)	1D11 PBS (pg/mg protein)	13C4 Tumor (pg/mg protein)	1D11 Tumor (pg/mg protein)	*p* value 13C4 PBS vs. 13C4 Tumor	*p* value 13C4 Tumor vs. 1D11 Tumor
CCL2/MCP-1	81.9±50.5	63.4±22.2	177±76.0	97.2±37.5	0.2369	0.3824
CCL3/MIP-1α	32.0±8.3	32.3±8.6	19.3±3.2	27.5±12.4	0.5510	0.8249
*CCL4/MIP-1β	20.9±1.3	14.5±0.8	9.5±1.5	25.3±10.5	0.1082	*0.0144*
*CCL5/RANTES	19.8±2.3	13.7±1.4	5.9±0.4	5.3±0.4	*0.0004*	0.9978
CXCL1/KC	61.3±16.7	65.3±12.0	112.8±45.2	268.2±221.5	0.9175	0.2332
CXCL2/MIP-2	143.8±57.7	135.6±42.0	166.1±38.8	194.7±113.4	0.9862	0.9721
CXCL5/LIX	518±245.3	698.8±200.2	530.5±145.9	301.7±145.9	p>0.9999	0.6999
CXCL10/IP-10	407.7±167.6	392.1±109.7	569.5±173.8	558.4±245.7	0.7969	p>0.9999
*G-CSF	6.4±1.4	7.8±1.6	620.7±149.7	378.7±50.1	*p<0.0001*	*0.0213*
GM-CSF	16.2±6.9	11.2±3.4	14.5±5.1	13.1±5.0	0.9950	0.9971
M-CSF	39.1±3.6	35.5±4.5	60.0±8.8	45.2±1.9	0.1416	0.4109
*VEGF	473.7±239.9	743.3±418.5	398.6±184.2	1761±958.2	0.9984	*0.0276*
IL-1α	130.2±39.7	136.7±30.7	67.4±17.1	85.1±40.2	0.3227	0.9611
IL-1β	43.8±14.4	55.1±13.3	12.2±4.0	35.5±17.2	0.1525	0.3919
IL-2	16.1±4.7	15.8±2.7	9.2±2.3	10.1±4.1	0.3433	0.9968
*IL-3	0.3±0.2	0.1±0.0	1.1±0.3	0.8±0.4	*0.0421*	0.6859
*IL-4	1.1±0.2	1.1±0.2	0.5±0.0	1.5±0.5	0.2144	*0.0159*
IL-5	3.2±1.4	3.1±1.1	6.0±2.0	2.1±0.8	0.4542	0.1886
IL-6	18.4±7.3	17.7±4.4	18.6±9.1	84.6±77.6	p>0.9999	0.0980
IL-7	1.8±0.5	2.4±0.7	1.9±0.4	1.7±0.6	0.9998	0.9942
IL-9	660.5±257.3	649.5±184	567.3±151.3	573±256	0.9792	p>0.9999
IL-10	25.1±11.8	19±5.4	32.7±7.7	24.4±4.6	0.7871	0.7403
IL-12p40	90.2±46.2	58.8±20	199.8±61.7	131.2±87.8	0.3375	0.7107
IL-12p70	1.9±0.3	1.4±0.6	3.3±1.0	2.1±0.8	0.3732	0.4742
IL-13	3.0±1.6	2.7±1.3	2.9±1.5	2.9±1.5	p>0.9999	p>0.9999
IL-15	13.2±2.8	12.4±3.6	12.5±3.5	11.2±4.8	0.9971	0.9891
IL-17	2.6±0.5	2.7±0.6	1.0±0.2	1.5±0.6	0.9922	0.8958
*TNF-α	4.6±0.9	7.1±1.1	30.0±4.7	24.7±4.4	*0.0004*	0.9978
IFN-γ	3.6±1.6	3.3±1.3	2.0±1.3	5.4±2.7	0.9276	0.5886
*LIF	10.6±1.31	8.2±0.2	84.7±33.1	46.7±27.4	*0.0022*	0.1965

Values represent the mean ± SEM of the cytokine/chemokine concentrations (pg cytokine/mg total protein) in the femur homogenates, measured by Luminex assay (pg cytokine/ml) and Bradford assay (mg protein/ml). Protein cytokine/chemokine array data was analyzed using a two-way ANOVA with a Tukey's post-hoc test. * indicates statistically significant change. (3-4 femurs per group)

Supplementary table 1D. Naïve BMDM

Analyte	13C4 (pg/mg protein)	1D11 (pg/mg protein)	13C4 + TGF-β (pg/mg protein)	1D11 + TGF-β (pg/mg protein)	*p* value 13C4 vs. 13C4 + TGF-β	*p* value 13C4 +TGF-β vs. 1D11+ TGF-β
CCL2/MCP-1	117.4±18.1	191.2±9.3	174.4±99.0	104.5±4.3	0.8231	0.7237
CCL3/MIP-1α	371.1±85.0	1037.0±40.7	221.2±11.3	314.2±10.8	0.2760	0.6171
CCL4/MIP-1β	609.2±92.4	2008±131.4	270±33.4	298.3±8.2	0.1381	0.9960
CCL5/RANTES	4.5±0.8	9.7±0.5	15.6±11.3	7.2±0.3	0.5633	0.7426
CXCL1/KC	43.1±2.0	128.0±13.4	30.1±5.7	62.2±3.2	0.7115	0.1280
*CXCL2/MIP-2	194.7±12.6	554.1±30.1	100±12.0	213.8±7.7	*0.0469*	*0.0214*
CXCL5/LIX	4.3±1.1	7.9±4.7	4.0±0.8	3.7±0.5	0.9998	0.9998
*CXCL10/IP-10	3.8±0.7	13.9±1.1	15.9±2.6	17.6±1.3	*0.0100*	0.8969
G-CSF	2.4±0.1	15.9±1.5	1.8±1.0	1.3±0.1	0.9549	0.9799
GM-CSF	1.7±0.8	2.8±0.8	1.6±0.5	1.9±0.7	p>0.9999	0.9941
M-CSF	0.8±0.0	0.8±0.0	0.8±0.0	0.8±0.0	p>0.9999	p>0.9999
*VEGF	2.8±0.5	3.7±0.5	10.3±1.2	13.5±0.5	*0.0030*	0.1193
IL-1α	1.0±0.2	2.8±0.4	3.1±0.6	3.5±0.9	0.1901	0.9651
IL-1β	3.2±0.0	3.2±0.0	3.9±0.7	4.0±0.8	0.8197	0.9995
IL-2	0.3±0.0	0.3±0.0	0.4±0.0	0.3±0.1	0.8709	0.9938
IL-3	0.2±0.0	0.2±0.0	0.2±0.0	0.2±0.0	p>0.9999	0.7931
IL-4	0.6±0.0	0.6±0.0	0.6±0.0	0.6±0.0	p>0.9999	p>0.9999
IL-5	0.7±0.0	1.0±0.4	1.0±0.4	0.7±0.1	0.6413	0.6678
IL-6	1.1±0.3	3.4±0.5	1.8±0.7	2.6±0.1	0.6805	0.4704
IL-7	0.7±0.0	0.7±0.0	0.7±0.0	0.7±0.0	p>0.9999	p>0.9999
IL-9	6.2±2.2	5.2±0.9	15.8±5.6	7.9±3.0	0.2416	0.3743
IL-10	0.7±0.0	1.1±0.1	0.9±0.2	0.7±0.0	0.6161	0.7535
IL-12p40	0.8±0.0	0.8±0.0	0.8±0.0	0.8±0.0	p>0.9999	p>0.9999
IL-12p70	0.5±0.0	0.7±0.1	0.5±0.1	0.7±0.2	0.9983	0.8588
IL-13	0.6±0.0	0.6±0.0	0.7±0.0	0.6±0.0	0.3029	0.3029
IL-15	0.7±0.0	3.9±1.0	0.9±0.2	1.3±0.4	0.9962	0.9437
IL-17	0.7±0.1	2.1±0.1	0.5±0.0	0.4±0.0	0.4734	0.9941
TNF-α	3.8±0.3	8.5±0.8	3.8±0.4	4.8±0.4	0.9999	0.6067
IFN-γ	0.4±0.0	0.5±0.0	0.4±0.0	0.4±0.0	0.9107	0.9107
LIF	0.6±0.0	0.6±0.0	0.8±0.1	0.7±0.1	0.1675	0.8255

Values represent the mean ± SEM of the cytokine/chemokine concentrations (pg cytokine/mg total protein) in naïve BMDM supernatants, measured by Luminex assay (pg cytokine/ml) and Bradford assay (mg protein/ml). Protein cytokine/chemokine array data was analyzed using a two-way ANOVA with a Tukey's post-hoc test. * indicates statistically significant change. (n=3)

Supplementary table 1E. IL-4 stimulated BMDM

Analyte	13C4 (pg/mg protein)	1D11 (pg/mg protein)	13C4 + TGF-β (pg/mg protein)	1D11 + TGF-β (pg/mg protein)	***p* value** 13C4 vs. 13C4 + TGF-β	***p* value** 13C4 +TGF-β vs. 1D11+ TGF-β
*CCL2/MCP-1	1032±41.1	1057±25.9	521.1±7.1	645.2±38.7	*0.0001*	0.1116
*CCL3/MIP-1α	247.2±11.2	373.1±6.3	40.5±1.1	69.6±7.1	*p<0.0001*	0.1107
*CCL4/MIP-1β	698.1±33.9	1052±27.7	127.4±1.3	184.3±8.1	*p<0.0001*	0.3743
*CCL5/RANTES	11.7±0.6	11.9±0.1	8.5±0.2	9.3±0.7	*0.0175*	0.6943
*CXCL1/KC	50.9±2.0	74.6±3.0	14.5±0.6	24.5±2.2	*p<0.0001*	*0.0276*
*CXCL2/MIP-2	201±5.2	314.7±5.5	38.9±2.7	66.3±7.3	*p<0.0001*	0.0543
*CXCL5/LIX	112.5±2.7	105.9±3.7	38.0±2.3	36.5±3.6	*p<0.0001*	0.9859
CXCL10/IP-10	2.7±0.4	3.7±0.2	1.9±0.2	2.5±0.3	0.1580	0.2954
*G-CSF	2.6±0.1	3.7±0.3	0.6±0.0	1.0±0.2	*0.0015*	0.5573
*GM-CSF	3.0±0.2	2.1±0.4	1.6±0.4	1.6±0.6	0.1000	p>0.9999
M-CSF	0.8±0.0	0.8±0.0	0.8±0.0	0.8±0.0	p>0.9999	p>0.9999
*VEGF	2.3±0.2	2.1±0.1	7.8±0.2	6.2±0.7	*0.0002*	0.0772
*IL-1α	3.7±0.5	1.9±0.6	1.3±0.2	1.3±0.4	*0.0428*	p>0.9999
IL-1β	3.3±0.1	3.6±0.1	3.2±0.0	3.2±0.0	0.5398	p>0.9999
*IL-2	0.4±0.0	0.4±0.0	0.3±0.0	0.3±0.0	*0.0237*	0.9992
IL-3	0.3±0.0	0.2±0.0	0.2±0.0	0.2±0.0	0.2473	0.8908
*IL-4	630.1±30.6	619.6±16.6	142.9±5.0	128.7±4.9	p<0.0001	0.9342
*IL-5	4.5±0.3	4.1±0.3	2.2±0.3	2.9±0.4	*0.0135*	0.5722
*IL-6	1.0±0.1	1.2±0.1	0.6±0.1	0.4±0.1	*0.0359*	0.4696
IL-7	0.7±0.0	0.7±0.0	0.7±0.0	0.7±0.0	p>0.9999	p>0.9999
IL-9	23.1±4.9	16.4±0.3	12.6±2.5	4.8±1.4	0.1446	0.3198
IL-10	1.0±0.1	1.1±0.1	0.8±0.1	0.7±0.0	0.3188	0.5859
IL-12p40	0.8±0.0	0.8±0.0	0.8±0.0	0.8±0.0	p>0.9999	p>0.9999
IL-12p70	0.9±0.2	0.5±0.0	0.5±0.0	0.6±0.1	0.0798	0.8976
IL-13	0.8±0.0	0.7±0.0	0.6±0.0	0.7±0.1	0.0613	0.4997
IL-15	1.4±0.8	0.7±0.0	0.7±0.0	0.7±0.0	0.5541	p>0.9999
*IL-17	0.9±0.1	1.1±0.0	0.4±0.0	0.4±0.0	*0.0017*	p>0.9999
*TNF-α	5.9±0.1	6.4±0.1	2.9±0.3	3.6±0.1	*p<0.0001*	0.0597
IFN-γ	0.4±0.0	0.4±0.0	0.4±0.0	0.4±0.0	0.9738	0.9885
LIF	0.6±0.0	0.6±0.0	0.6±0.0	0.6±0.0	p>0.9999	p>0.9999

Values represent the mean ± SEM of the cytokine/chemokine concentrations (pg cytokine/mg total protein) in IL-4 stimulated BMDM supernatants, measured by Luminex assay (pg cytokine/ml) and Bradford assay (mg protein/ml). Protein cytokine/chemokine array data was analyzed using a two-way ANOVA with a Tukey's post-hoc test. * indicates statistically significant change. (n=3)

Supplementary table 1F. IFN-γ+LPS stimulated BMDM

Analyte	13C4 (pg/mg protein)	1D11 (pg/mg protein)	13C4 + TGF-β (pg/mg protein)	1D11 + TGF-β (pg/mg protein)	***p* value** 13C4 vs. 13C4 + TGF-β	***p* value** 13C4 +TGF-β vs. 1D11+ TGF-β
*CCL2/MCP-1	127.6±7.7	173.7±1.9	77.8±0.8	93.3±0.7	*0.0008*	0.1567
*CCL3/MIP-1α	220.8±4.9	474.1±4.5	44.4±1.8	62.8±1.9	*p<0.0001*	*0.0293*
*CCL4/MIP-1β	432.5±4.3	952.8±18.0	93.6±1.0	121.9±0.1	*p<0.0001*	0.2636
*CCL5/RANTES	11.6±0.7	18.9±0.4	14.5±0.1	14.8±0.3	*0.0215*	0.9701
*CXCL1/KC	56.0±2.4	109.5±0.3	32.7±0.3	44.5±1.7	*0.0003*	0.0118
*CXCL2/MIP-2	239.1±0.9	488.7±9.0	116.4±2.4	144.5±1.1	*p<0.0001*	0.0210
CXCL5/LIX	5.2±2.0	9.1±0.0	9.1±0.0	9.1±0.0	0.1057	p>0.9999
*CXCL10/IP-10	4.2±0.4	6.7±0.2	2.2±0.2	2.9±0.1	*0.0034*	0.2023
G-CSF	5.4±0.7	15.3±0.7	3.4±0.4	10.1±6.5	0.9701	0.5218
GM-CSF	1.4±0.8	3.1±0.0	3.1±0.0	3.1±0.0	0.1057	p>0.9999
M-CSF	0.7±0.1	0.5±0.0	0.5±0.0	0.5±0.0	0.1057	p>0.9999
*VEGF	5.3±0.4	5.6±0.2	10.6±0.3	9.1±0.2	*p<0.0001*	*0.0252*
IL-1α	1.4±0.5	4.2±0.7	2.2±0.3	2.0±0.4	0.7327	0.9929
IL-1β	2.3±0.9	0.7±0.5	0.5±0.3	1.8±1.1	0.5598	0.7709
IL-2	0.3±0.0	0.4±0.1	0.2±0.0	0.3±0.1	0.9665	0.7886
IL-3	0.3±0.0	0.2±0.0	0.2±0.0	0.2±0.0	0.5734	0.9999
IL-4	0.5±0.0	0.5±0.0	0.5±0.0	0.5±0.0	p>0.9999	p>0.9999
IL-5	0.7±0.1	0.9±0.0	0.5±0.1	0.4±0.1	0.2532	0.9575
IL-6	4.1±0.9	11.0±0.3	2.8±0.1	3.2±0.3	0.4221	0.9473
IL-7	0.6±0.0	0.6±0.0	0.6±0.0	0.6±0.0	0.1057	p>0.9999
IL-9	7.0±2.4	11.6±0.0	11.8±0.1	11.6±0.0	0.1217	0.9999
IL-10	0.8±0.1	1.6±0.1	0.6±0.1	0.7±0.0	0.5613	0.8213
IL-12p40	0.8±0.0	0.8±0.0	0.8±0.0	0.8±0.0	p>0.9999	p>0.9999
IL-12p70	0.4±0.1	0.4±0.2	0.3±0.0	0.4±0.1	0.7849	0.9049
*IL-13	0.6±0.0	0.4±0.0	0.4±0.0	0.4±0.0	*0.0005*	p>0.9999
IL-15	1.0±0.3	1.6±0.0	1.6±0.0	1.6±0.0	0.1057	p>0.9999
*IL-17	0.5±0.1	1.0±0.1	0.2±0.0	0.3±0.0	*0.0486*	0.8027
*TNF-α	2.9±0.3	6.0±0.1	1.7±0.1	1.9±0.1	*0.0131*	0.7332
*IFN-γ	0.4±0.0	0.3±0.0	0.3±0.0	0.3±0.0	*0.0016*	p>0.9999
LIF	0.5±0.1	0.3±0.0	0.3±0.0	0.3±0.0	0.1057	p>0.9999

Values represent the mean ± SEM of the cytokine/chemokine concentrations (pg cytokine/mg total protein) in IFN-γ + LPS stimulated BMDM supernatants, measured by Luminex assay (pg cytokine/ml) and Bradford assay (mg protein/ml). Protein cytokine/chemokine array data was analyzed using a two-way ANOVA with a Tukey's post-hoc test. * indicates statistically significant change. (n=3)

Supplementary table 1G. TCM stimulated BMDM

Analyte	13C4 (pg/mg protein)	1D11 (pg/mg protein)	13C4 + TGF-β (pg/mg protein)	1D11 + TGF-β (pg/mg protein)	*p* value 13C4 vs. 13C4 + TGF-β	*p* value 13C4 +TGF-β vs. 1D11+ TGF-β
*CCL2/MCP-1	437.3±24.5	352±13.3	148.1±1.5	299.9±6.0	*p<0.0001*	*0.0017*
*CCL3/MIP-1α	505.8±22.1	707±38.9	23.4±2.4	74.2	*p<0.0001*	0.5096
*CCL4/MIP-1β	846.2±33.7	1173±83.1	57.4±0.8	130.1±2.0	*0.0001*	0.7190
*CCL5/RANTES	3.1±0.3	3.7±0.2	1.5±0.0	2.8±0.1	*0.0034*	*0.0099*
*CXCL1/KC	191.1±19.9	258.4±21.9	64.8±1.5	80.3±4.3	*0.0082*	0.9167
*CXCL2/MIP-2	532.2±25.6	820.7±35.9	42.4±1.9	106.4±2.9	*p<0.0001*	0.2860
CXCL5/LIX	3.7±0.5	12±3.7	3.2±0.0	4.0±0.8	0.9975	0.9907
*CXCL10/IP-10	5.3±0.9	5.6±0.5	0.9±0.2	1.7±0.2	*0.0083*	0.7667
G-CSF	98.1±10.7	77.8±9.7	87.1±2.8	55.3±2.1	0.7969	0.1304
GM-CSF	1.4±0.5	1.8±0.1	0.6±0.0	0.8±0.1	0.1002	0.8543
M-CSF	0.8±0.0	0.8±0.0	0.8±0.0	0.8±0.0	p>0.9999	p>0.9999
VEGF	9.5±0.9	7.7±0.9	13.0±0.3	13.8±0.9	0.1089	0.9009
IL-1α	1.4±0.4	1.4±0.3	0.9±0.0	0.9±0.1	0.4460	0.9966
IL-1β	3.2±0.0	3.2±0.0	3.2±0.0	3.2±0.0	p>0.9999	p>0.9999
IL-2	0.3±0.0	0.3±0.0	0.3±0.0	0.3±0.0	p>0.9999	p>0.9999
IL-3	0.2±0.0	0.2±0.0	0.2±0.0	0.2±0.0	p>0.9999	p>0.9999
IL-4	0.6±0.0	0.6±0.0	0.6±0.0	0.6±0.0	p>0.9999	p>0.9999
*IL-5	2.2±0.0	1.9±0.3	0.8±0.0	1.5±0.3	*0.0100*	0.1327
IL-6	6.4±1.8	8.8±1.2	1.6±0.1	2.3±0.3	0.1217	0.9774
IL-7	0.7±0.0	0.7±0.0	0.7±0.0	0.7±0.0	p>0.9999	p>0.9999
IL-9	7.6±2.5	10.0±2.3	3.4±0.0	8.1±2.9	0.6707	0.5950
IL-10	0.7±0.0	0.7±0.1	0.7±0.0	0.7±0.0	p>0.9999	p>0.9999
IL-12p40	0.8±0.0	0.8±0.0	0.8±0.0	0.8±0.0	p>0.9999	p>0.9999
IL-12p70	0.5±0.0	0.5±0.0	0.5±0.0	0.5±0.0	p>0.9999	p>0.9999
IL-13	0.6±0.0	0.6±0.0	0.6±0.0	0.6±0.0	p>0.9999	p>0.9999
IL-15	1.9±1.2	1.2±0.5	0.7±0.0	0.7±0.0	0.6327	p>0.9999
*IL-17	0.7±0.1	1.2±0.1	0.4±0.0	0.4±0.0	*0.0242*	p>0.9999
*TNF-α	7.7±0.7	11.9±0.7	1.5±0.1	2.5±0.3	*0.0012*	0.6359
IFN-γ	0.4±0.0	0.4±0.0	0.4±0.0	0.4±0.0	p>0.9999	p>0.9999
LIF	0.6±0.0	0.6±0.0	0.6±0.0	0.6±0.0	p>0.9999	p>0.9999

Values represent the mean ± SEM of the cytokine/chemokine concentrations (pg cytokine/mg total protein) in tumor-conditioned media (TCM) stimulated BMDM supernatants, measured by Luminex assay (pg cytokine/ml) and Bradford assay (mg protein/ml). Protein cytokine/chemokine array data was analyzed using a two-way ANOVA with a Tukey's post-hoc test. * indicates statistically significant change. (n=3)

Supplementary table 1H. 4T1 tumor cells

Analyte	13C4 (pg/mg protein)	1D11 (pg/mg protein)	13C4 + TGF-β (pg/mg protein)	1D11 + TGF-β (pg/mg protein)	***p* value** 13C4 vs. 13C4 + TGF-β	***p* value** 13C4 +TGF-β vs. 1D11+ TGF-β
*CCL2/MCP-1	234.9±2.3	237.4±3.2	82.5±6.0	183.4±4.0	*0.0006*	*0.0018*
CCL3/MIP-1α	9.9±0.0	9.9±0.0	9.9±0.0	9.9±0.0	p>0.9999	p>0.9999
CCL4/MIP-1β	1.0±0.6	0.6±0.4	0.2±0.0	0.2±0.0	0.4743	p>0.9999
CCL5/RANTES	38.9±1.1	37.7±0.2	56.5±4.8	47.9±1.2	0.0534	0.2752
*CXCL1/KC	3725±39.0	3909±21.0	824±34.2	1887±96.5	*0.0001*	*0.0039*
CXCL2/MIP-2	13.8±6.8	7.0±0.0	25.5±0.7	17.2±10.2	0.5083	0.7137
*CXCL5/LIX	358.9±12.9	395.7±0.4	53.2±0.1	75.1±0.8	*0.0001*	0.2706
*CXCL10/IP-10	40.8±1.2	40.7±0.0	72.0±9.0	45.9±1.4	*0.0375*	0.0607
G-CSF	5614±99.5	6046±78	7094±244	7913±1011	0.3994	0.7504
GM-CSF	8.2±0.6	6.8±0.3	30.9±2.7	20.9±5.7	0.0599	0.3565
M-CSF	2.1±0.0	1.3±0.1	2.8±0.2	2.0±1.0	0.8207	0.7811
*VEGF	0.8±0.0	0.7±0.1	409.1±12.6	0.9±0.2	*p<0.0001*	*p<0.0001*
IL-1α	11.2±1.4	12.3±1.2	9.2±0.6	7.4±2.1	0.7692	0.7924
IL-1β	0.9±0.2	0.5±0.3	3.1±0.5	1.4±1.2	0.2919	0.4279
IL-2	0.5±0.0	0.7±0.0	1.1±0.2	0.8±0.3	0.3397	0.7795
IL-3	0.2±0.0	0.2±0.0	0.2±0.0	0.2±0.0	0.6470	0.4691
IL-4	0.5±0.0	0.5±0.0	0.5±0.0	0.5±0.0	p>0.9999	p>0.9999
IL-5	1.2±0.2	0.7±0.1	0.4±0.1	0.6±0.2	0.0511	0.7026
*IL-6	0.4±0.0	0.4±0.0	2.9±0.3	0.4±0.0	*0.0042*	*0.0042*
IL-7	0.6±0.0	0.6±0.0	0.6±0.0	0.6±0.0	p>0.9999	p>0.9999
IL-9	18.5±1.9	13.2±1.6	50.2±11.7	21.9±8.1	0.1018	0.1329
IL-10	0.7±0.1	0.6±0.1	0.8±0.1	0.5±0.0	0.9296	0.2299
IL-12p40	1.6±0.3	0.8±0.0	0.8±0.0	0.8±0.0	0.0636	p>0.9999
IL-12p70	0.3±0.0	0.3±0.0	0.4±0.1	0.3±0.0	0.5317	0.5317
IL-13	19.9±0.0	18.3±1.2	15.8±0.1	14.5±1.9	0.2723	0.8791
IL-15	1.6±0.0	1.6±0.0	1.6±0.0	1.6±0.0	p>0.9999	p>0.9999
IL-17	0.3±0.0	0.2±0.0	0.2±0.0	0.2±0.1	0.6238	0.8896
TNF-α	0.8±0.1	0.7±0.1	1.0±0.1	0.6±0.0	0.3967	0.1388
IFN-γ	0.3±0.0	0.3±0.0	0.3±0.0	0.3±0.0	p>0.9999	p>0.9999
*LIF	54.1±0.6	50.8±0.8	195.4±9.6	93.9±10.1	*0.0035*	*0.0091*

Values represent the mean ± SEM of the cytokine/chemokine concentrations (pg cytokine/mg total protein) in 4T1 tumor supernatants, measured by Luminex assay (pg cytokine/ml) and Bradford assay (mg protein/ml). Protein cytokine/chemokine array data was analyzed using a two-way ANOVA with a Tukey's post-hoc test. * indicates statistically significant change. (n=3)

Supplementary table 1I. IL-4 stimulated 4T1 tumor cells

Analyte	13C4 (pg/mg protein)	1D11 (pg/mg protein)	13C4 + TGF-β (pg/mg protein)	1D11 + TGF-β (pg/mg protein)	***p* value** 13C4 vs. 13C4 + TGF-β	***p* value** 13C4 +TGF-β vs. 1D11+ TGF-β
*CCL2/MCP-1	497.7±53.3	384.2±21.6	176.5±0.9	391.4±13.2	*0.0168*	0.0506
CCL3/MIP-1α	9.9±0.0	9.9±0.0	9.9±0.0	9.9±0.0	p>0.9999	p>0.9999
CCL4/MIP-1β	0.2±0.0	0.2±0.0	0.5±0.2	0.2±0.0	0.5686	0.5686
CCL5/RANTES	126.9±16.2	83.8±3.3	117.4±2.3	116.8±3.7	0.8704	p>0.9999
*CXCL1/KC	5321±645.5	4587±129	1037±54.5	3317±114.5	*0.0098*	0.0563
CXCL2/MIP-2	27.3±3.9	19.1±1.5	15.2±8.2	18.0±5.4	0.5300	0.9823
*CXCL5/LIX	450.2±13.0	467±29.8	63.2±0.8	144.4±9.6	*0.0024*	0.1660
CXCL10/IP-10	121.4±26.1	73.2±2.5	174.3±16.5	116.9±1.2	0.3263	0.2814
G-CSF	9997±812	7359±24	10285±313.5	13007±375	0.9721	0.0846
*GM-CSF	13.9±2.3	6.3±1.9	36.4±3.8	32.2±0.3	*0.0258*	0.6854
M-CSF	3.4±1.1	2.5±0.6	3.2±0.2	2.8±0.4	0.9971	0.9636
*VEGF	0.8±0.0	0.7±0.0	365.8±48.4	0.7±0.1	*0.0054*	*0.0054*
IL-1α	16.3±2.4	11.6±0.3	12.4±1.9	7.7±1.3	0.5422	0.4231
IL-1β	1.2±0.4	0.3±0.1	2.0±0.1	1.7±1.4	0.8307	0.9940
IL-2	0.8±0.2	0.6±0.0	1.2±0.0	0.6±0.1	0.1192	0.0501
IL-3	0.2±0.0	0.2±0.0	0.2±0.0	0.2±0.0	0.9128	p>0.9999
IL-4	90.4±8.7	74.0±4.8	84.4±9.7	109.4±1.2	0.9443	0.2939
IL-5	1.6±0.2	1.4±0.1	0.6±0.1	1.1±0.0	0.0505	0.3176
*IL-6	0.4±0.0	0.4±0.0	2.9±0.2	0.4±0.0	*0.0012*	*0.0012*
IL-7	0.6±0.0	0.6±0.0	0.6±0.0	0.6±0.0	p>0.9999	p>0.9999
*IL-9	20.4±5.7	12.3±0.6	46.1±4.7	14.1±2.5	0.0731	*0.0411*
*IL-10	0.9±0.0	0.5±0.0	1.4±0.1	0.6±0.0	*0.0022*	*0.0006*
IL-12p40	1.4±0.3	0.9±0.2	0.8±0.0	0.8±0.1	0.2661	0.9939
IL-12p70	0.3±0.0	0.3±0.0	0.3±0.0	0.3±0.0	0.8232	0.8232
IL-13	18.1±0.8	18.2±0.0	16.7±0.9	16.8±0.0	0.3530	0.9991
IL-15	1.6±0.0	1.6±0.0	1.6±0.0	1.6±0.0	p>0.9999	p>0.9999
IL-17	0.2±0.0	0.2±0.0	0.2±0.0	0.2±0.0	0.2658	p>0.9999
TNF-α	0.3±0.0	0.3±0.0	0.3±0.0	0.3±0.0	p>0.9999	p>0.9999
IFN-γ	0.3±0.0	0.3±0.0	0.3±0.0	0.3±0.0	p>0.9999	p>0.9999
*LIF	104.3±17.5	58.8±2.8	210.6±3.2	134.8±5.4	*0.0135*	*0.0349*

Values represent the mean ± SEM of the cytokine/chemokine concentrations (pg cytokine/mg total protein) in IL-4 stimulated 4T1 tumor supernatants, measured by Luminex assay (pg cytokine/ml) and Bradford assay (mg protein/ml). Protein cytokine/chemokine array data was analyzed using a two-way ANOVA with a Tukey's post-hoc test. * indicates statistically significant change. (n=3).

Supplementary table 2. Bone parameters for all stages of disease.

	Early Disease			Middle Disease			Late Disease		
Athymic mice	13C4	1D11	P value	13C4	1D11	P value	13C4	1D11	P value
Percent Bone Volume/Total Volume (BV/TV)	9.1±0.7	22.4±1.7	p<0.0001	7.5±1.1	22.0±1.5	p<0.0001	8.2±0.8	23.6±1.8	p<0.0001
Trabecular Spacing	0.3±0.0	0.2±0.0	p<0.001	0.3±0.0	0.2±0.0	p<0.0001	0.4±0.0	0.2±0.3	p<0.0001
Trabecular Number	3.5±0.2	5.4±0.3	p<0.0001	3.1±0.3	5.6±0.3	p<0.0001	2.8±0.1	5.2±0.3	p<0.0001
Tissue Mineral Density	999.1±9.2	999.8±4.2	n.s	980.0±7.3	987.0±3.8	n.s			n.s

	Early Disease			Middle Disease			Late Disease		
BALB/c mice	13C4	1D11	P value	13C4	1D11	P value	13C4	1D11	P value
Percent Bone Volume/Total Volume (BV/TV)	8.8±0.7	16.3±1.2	p<0.001	8.5±0.5	23.8±2.3	p<0.0001	7.1±1.0	19.6±2.2	p<0.0001
Trabecular Spacing	0.3±0.0	0.2±0.0	p<0.001	0.3±0.0	0.2±0.0	p<0.001	0.4±0.0	0.2±0.0	p<0.05
Trabecular Number	3.6±0.1	4.7±0.2	p<0.0001	3.5±0.2	5.5±0.3	p<0.0001	3.2±0.3	5.2±0.4	p<0.001
Tissue Mineral Density	937.6±6.4	939.1±5.4	n.s	980.7±5.3	971.1±4.9	n.s	991.0±9.7	968.5±3.6	n.s

	Early Disease			Middle Disease			Late Disease		
WT/TGF-βRII^{MyeKO} mice	WT	TGF-βRII^{MyeKO}	P value	WT	TGF-βRII^{MyeKO}	P value	WT	TGF-βRII^{MyeKO}	P value
Percent Bone Volume/Total Volume (BV/TV)	22.0±1.1	14.5±0.6	p<0.001	16.1±0.7	17.2±1.0	n.s	15.8±2.0	12.3±1.7	n.s
Trabecular Spacing	0.1±0.0	0.2±0.0	p<0.01	0.2±0.0	0.2±0.0	n.s	0.2±0.0	0.2±0.0	n.s
Trabecular Number	6.3±0.1	5.2±0.2	p<0.01	5.6±0.1	5.6±0.2	n.s	5.1±0.5	4.3±0.4	n.s
Tissue Mineral Density	940.8±6.2	938.4±4.1	n.s	946.0±4.9	952.2±4.6	n.s	946.4±11.7	949.2±8.5	n.s

Supplementary table 2: Bone parameters for all stages of disease. Bone parameters obtained from μCT analyses for all stages of disease (early/middle/late) in mouse models utilized in our studies. Values represent the mean ± SEM for specific bone parameter. Bone parameters include: BV/TV, trabecular spacing, trabecular number and tissue mineral density. *p* value is based on comparisons between tumor-bearing experimental and control mice (13C4 vs 1D11, WT and TGF-βRII^{MyeKO}). n.s, not significant.

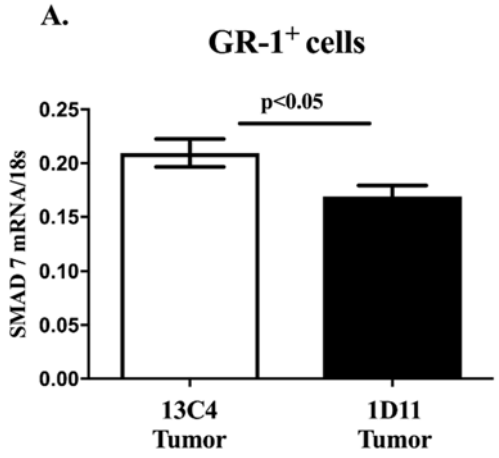

Supplementary figure 1: SMAD7 expression in Gr-1$^+$ sorted myeloid cells.
A. SMAD 7 expression is decreased in sorted Gr-1$^+$ myeloid cells from tumor-bearing BALB/c treated with 1D11. (3 mice per group).

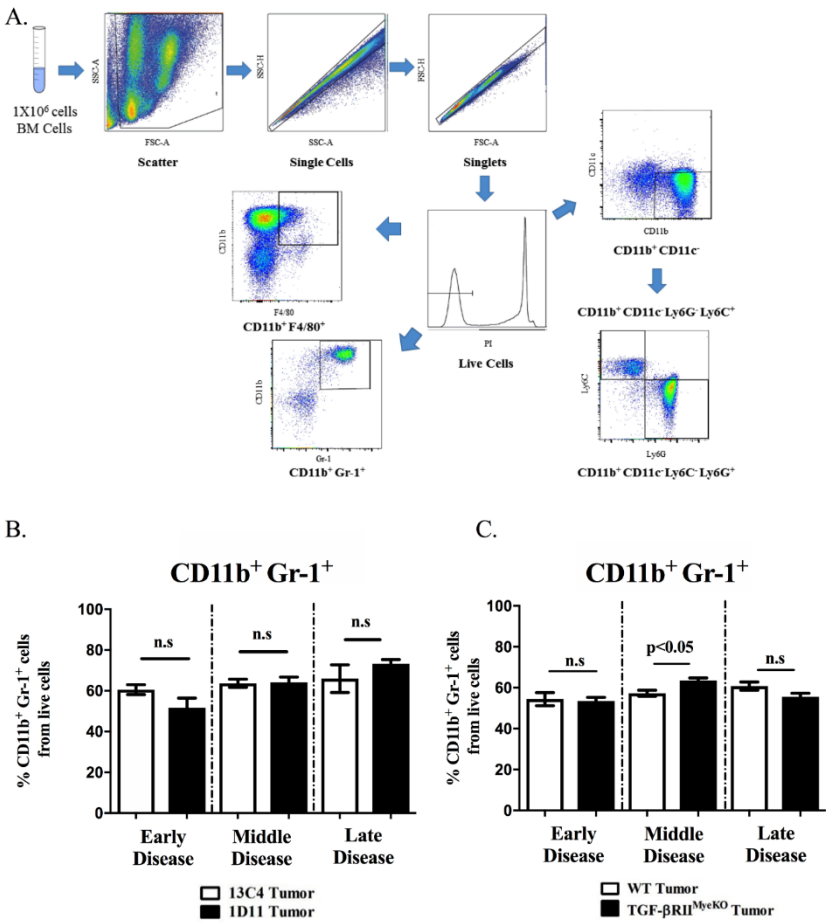

Supplementary figure 2: Flow cytometry gating strategy and effect of TGF-β inhibition on CD11b$^+$ Gr-1$^+$ cells. A. Flow cytometry gating strategy for all myeloid subsets. **B.** No significant expansion changes in CD11b$^+$ Gr-1$^+$ cells when TGF-β was inhibited in tumor-bearing mice. **C.** CD11b$^+$ Gr-1$^+$ cells increase in tumor-bearing TGF-βRII^{MyeKO} at the middle disease state. (4-6 mice per group).

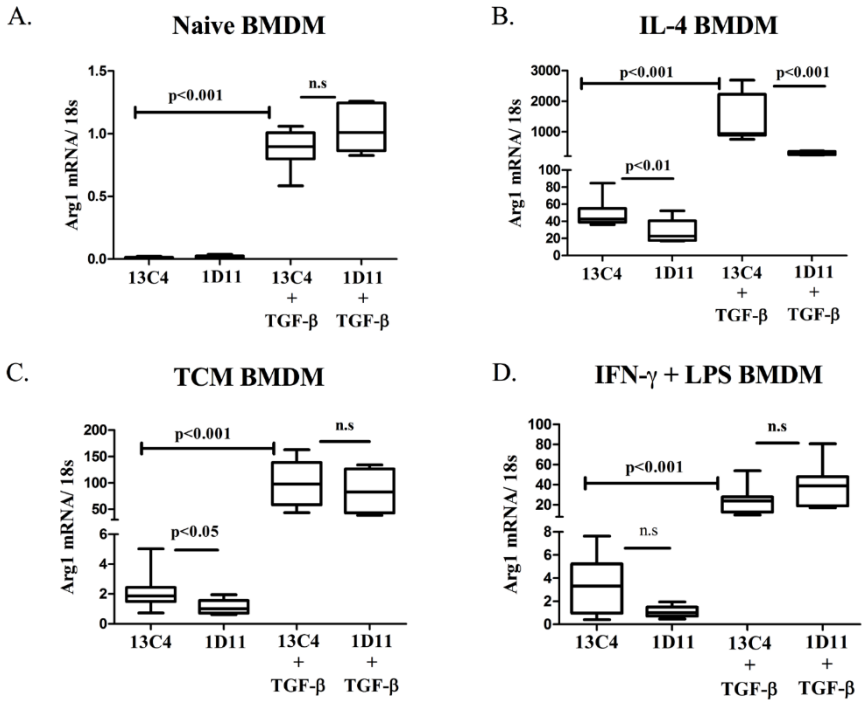

Supplementary figure 3. TGF-β increases arginase mRNA expression in BMDM.
BMDM were differentiated, TGF-β stimulated and inhibited for 24 hours then analyzed by qPCR as described in the methods section. **A-D.** Arginase mRNA increases with TGF-β stimulation in BMDM despite their stimulation profile. **B.** Arginase mRNA increases with TGF-β stimulation and significantly decreases with 1D11 treatment in IL-4 stimulated BMDM.

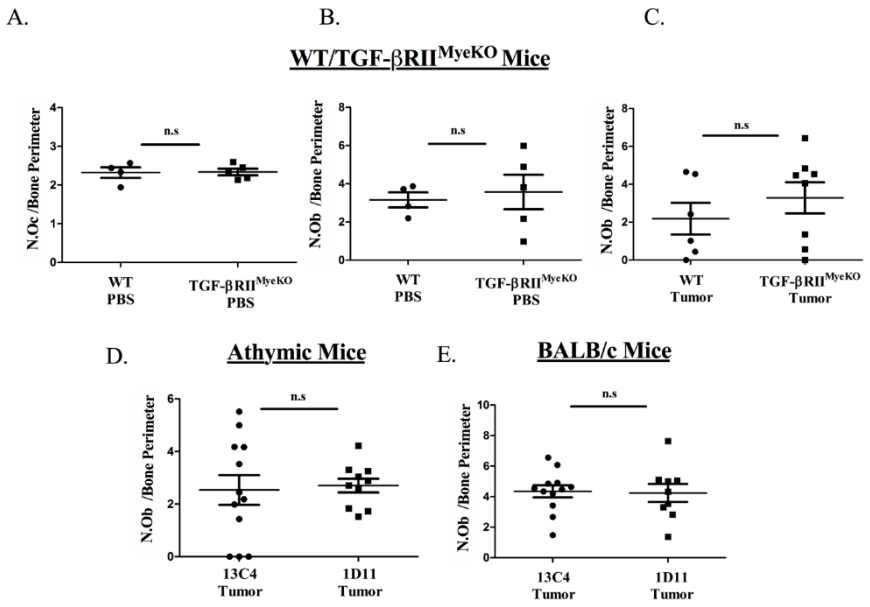

Supplementary Figure 4: The effect of TGF-β inhibition on osteoclast and osteoblast number. A. No difference in osteoclast number per bone perimeter between naïve WT and TGF-βRII^{MyeKO} mice at day 28. **B.** No difference in osteoblast number per bone parameter between naïve WT and TGF-βRII^{MyeKO} mice at day 28. **C.** No difference in osteoblast number per bone parameter between tumor-bearing WT and TGF-βRII^{MyeKO} mice at late disease. **D&E.** No difference in osteoblast number per bone parameter between tumor-bearing 13C4 and 1D11 treated mice (athymic and BALB/c) at late disease.

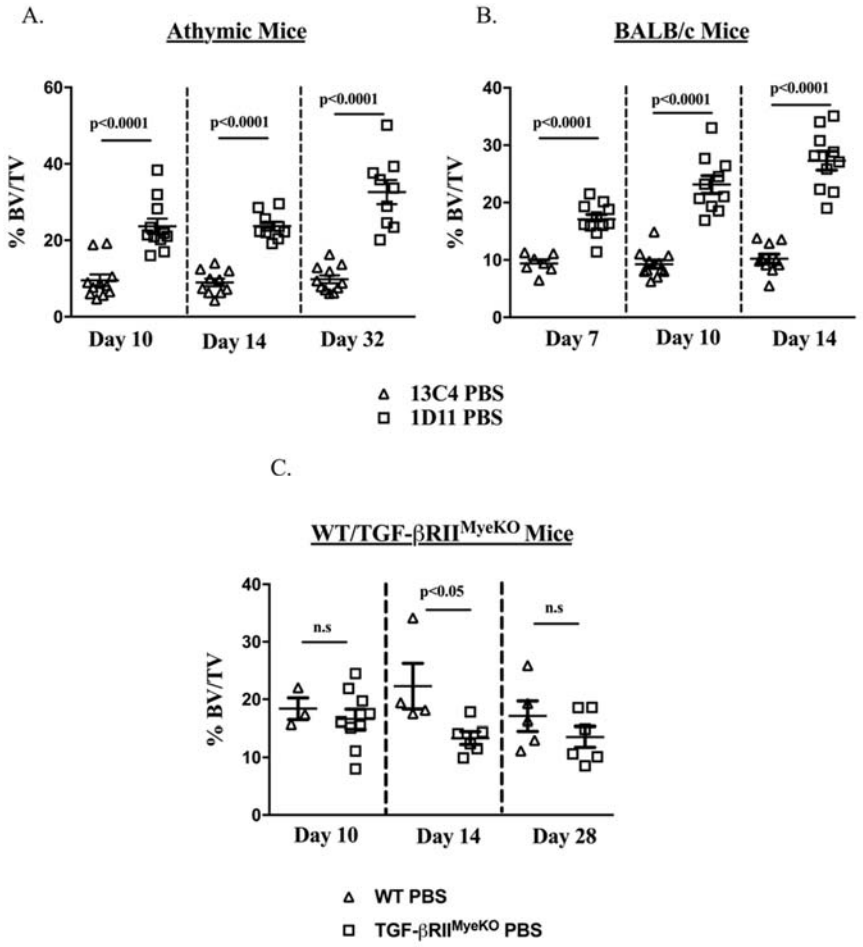

Supplementary Figure 5: TGF-β inhibition improves overall bone volume in systemic inhibition PBS experiments. Percent bone volume normalized to total volume (BV/TV) for each treatment group. **A.** Athymic mouse model: naïve athymic mice treated with 1D11 have an increased percent BV/TV at day 10, day 14 and day 32. **B.** BALB/c mouse model: naïve BALB/c mice treated with 1D11 have an increased percent BV/TV at day 7, day 10 and day 14. **C.** WT/TGF-βRII^{MyeKO} mouse model: naïve TGF-βRII^{MyeKO} have a decrease BV/TV at day 14.

Manuscript acknowledgements

We would like to acknowledge the following people for their generosity and support of this manuscript: Dr. Linda Sealy, Dr. Scott Guelcher, Dr. Rachelle Johnson, Dr. Harold Moses, Dr. Philip Owens, Dr. Ushashi Dadwal, Dr. Shellese Cannonier, Anna Chytil, Ryan Murray, David Florian, Vera Mayhew and SANOFI for the 1D11.

Authors' roles: Study design: D.B, A.R.M, K.AK, J.A.S. Study conduct, data analysis and collection: D.B, A.R.M, K.AK, N.E.P, J.R.J., J.E.C. Data interpretation: D.B, J.A.S, A.R.M, K.A.K, N.E.P. Drafting and revising manuscript: D.B, A.R.M, J.A.S, K.A.K, J.E.C, J.R.J, N.E.P. Approval of final version of manuscript: D.B and J.A.S.

Chapter III.

THE ROLE OF STING IN BONE MARROW DERIVED MACROPHAGES (BMDM)

Introduction

Stimulator of interferon genes (STING) is predominantly an endoplasmic reticulum (ER) protein that mediates the type I interferon production in response to intracellular DNA, and various intracellular viruses, bacteria and parasites [147]. The intracellular/cytosolic recognition of double-stranded (ds) DNA through the cyclic GMP-AMP synthase (cGAS)-STING signaling pathway is essential for identification of various pathogens and cancers [147]. Upon recognition and binding of cytosolic ds DNA, cGAS induces the synthesis of cyclic GMP-Amp (2'3'-cGAMP), which then interacts with STING. Once activated, STING recruits TANK binding kinase (TBK1) that in turn, phosphorylates STING allowing for the STING-IRF-3 (Interferon regulatory factor 3) interaction to occur [148]. Dissociation of IRF-3 from STING results in its translocation into the nucleus regulating gene expression. This coordinated activation of transcription factors promotes the induction of the several different genes, including the IFN family members [149]. Additionally, the STING pathway is associated with production of many proinflammatory cytokines and chemokines.

In the context of cancer, STING can both enhance tumor development and have anti-tumor effects on cancer development. Chronic inflammatory signaling, for instance, can contribute to the onset of cancer through several different mechanisms, including but not limited to, angiogenesis and cellular proliferation and survival [150, 151]. For example, the well-studied carcinogen, polyaromatic hydrocarbon 7,12-dimethylbenz[α]anthracene (DMBA), is known to induce development of cutaneous skin tumors by promoting pro-inflammatory cytokine production and triggering immune cell infiltration [152, 153]. A study investigating the development of skin carcinoma identified that DMBA initiated DNA damage lead to nucleosome leakage into the cytosol and triggered STING dependent cytokine production by self-DNA [154]. It was hypothesized that infiltrating immune cell were phagocytosing dying or damaged cells and subsequent release of cellular DNA was activating STING signaling, further propagating production of pro-inflammatory cytokines [155].

The use of STING deficient mice ($STING^{-/-}$) showed that $STING^{-/-}$ mice are protected against DMBA induced skin tumors, thus establishing a role for STING signaling in the promotion of DMBA induced tumorigenesis [154].

However, the anti-tumorigenic properties of the STING pathway have also been recognized. For example, it has been demonstrated that STING activation in damaged intestinal cells stimulated type I interferons (IFN), which play a critical role in priming anti-tumor T cells [156-158]. Recent studies have shown that the STING pathway is vital for radiation induced anti-tumor T cell responses, and $STING^{-/-}$ mice are unable to generate efficient T cell responses and inhibit melanoma tumor growth [159, 160]. This anti-tumor response has sparked interest in investigating whether STING agonists could be used to treat cancer. The STING activator 5,6-dimethyl- xanthenone-4-acetic acid (DMXAA) has been shown to have anti-tumor properties in mouse models but failed to stimulate human STING in clinical trials [161]. Alternatively, published papers have reported that cyclic dinucleotides (CDNs) bind human STING and exert anti-tumor effects in several mouse models[162]. The natural occurring CDN, 2'3'-cGAMP, has shown promise as an anti-tumor therapeutic by repolarizing the pro-tumorigenic "M2-like" macrophages towards a "M1-like" phenotype, thus potentially reducing the expression and secretion of tumor promoting factors [163]. Nonetheless, an effective route of delivery for CDNs has been difficult to obtain due to low cellular uptake, lysosomal degradation, endosomal recycling and inefficient delivery to cytosolic STING [164].

Therefore, in collaboration with John Wilson's group at Vanderbilt University, we hypothesized that macrophages would be the perfect candidate for CDN delivery because of their phagocytic activity. The barrier to delivery of CDNs would be circumvented by packaging 2'3'-cGAMP into polymer vesicles with potent endosomal escape activity, resulting in enhanced STING activation. We hypothesized that IL-4 stimulated macrophages, a pro-tumorigenic phenotype, treated *in vitro* with nanoparticle encapsulated 2'3'-cGAMP would express anti-tumorigenic factors due to repolarization towards a "M1-like" anti-tumor phenotype.

Material and Method

Bone marrow derived macrophages (BMDM). Bone marrow was harvested from 6 week and younger female BALB/ mice. Bone marrow was flushed from the tibia and femur of the mice and resuspended in PBS. Cell were incubated in red blood cell lysis buffer for 5 mins on ice.

After two PBS washes, cells were resuspended in DMEM media containing 4.5 g/L with L-glutamine and sodium pyruvate and supplemented with 10% FBS, 1% penicillin/streptomycin, 10% L929 supernatant, 5% heat inactivated horse serum and 1% nonessential amino acids as previously published [165]. Cells were incubated with conditioning media containing M-CSF for 6 days on 150mm dishes (Corning, 353025), harvested on day 7 by scraping and subsequently plated in low serum DMEM (1% FBS, 1% penicillin/streptomycin) in 6-well plates at a concentration of $2x10^6$ cells/well in triplicate.

Polymer nanoparticle and treatment regimen. 2'3'-cGAMP was encapsulated in a polymer-based nanoparticle as previously described (STING particle) [164]. Plated differentiated BMDM were stimulated with 40 ng/ml of IL-4 for 48 hrs. After the 48hr stimulation, cells were washed with 1x PBS and treated with the following conditions in low serum DMEM media for 24 hrs in triplicate:

a. DMXAA @ 20μg/ml (positive control)

b. DMSO @ 20μg/ml (control)

c. Empty Particle @ 100ng/ml (control)

d. STING Particle @ 100ng/ml (experimental treatment)

After 24 hrs of treatment, cells were harvested by direct lysis using RNeasy Mini Kit (Qiagen), per manufactor's instructions.

Quantitative PCR (qPCR). cDNA was synthesized using qScript cDNA Supermix (Quanta Biosciences, 95048-500) for reverse-transcriptase PCR. cDNA was serially diluted to create a standard curve and combined with TaqMan Universal PCR Master Mix (Applied Biosystems, 4304437) and Taqman primers: TaqMan Euk 18S rRNA (4333760F), Arginase (Arg-1, Mm00475988), VEGF-α (Mm00437306), MMP9 (Mm00442991), TGF-β (Mm01178820), IFN-β (Mm00439552), TNF-α (Mm00443258). Samples were loaded onto an optically clear 96- well plate and performed under the following cycling conditions: 50℃ for 2 minutes, 95℃ for 10 minutes, (95℃ for 15 seconds, 60℃ for 1 minute) x40 cycles on the 7500 Real-Time PCR System (Applied Biosystems) [81]. Quantification was performed using the absolute quantitative for human cells method using 18S as an internal control.

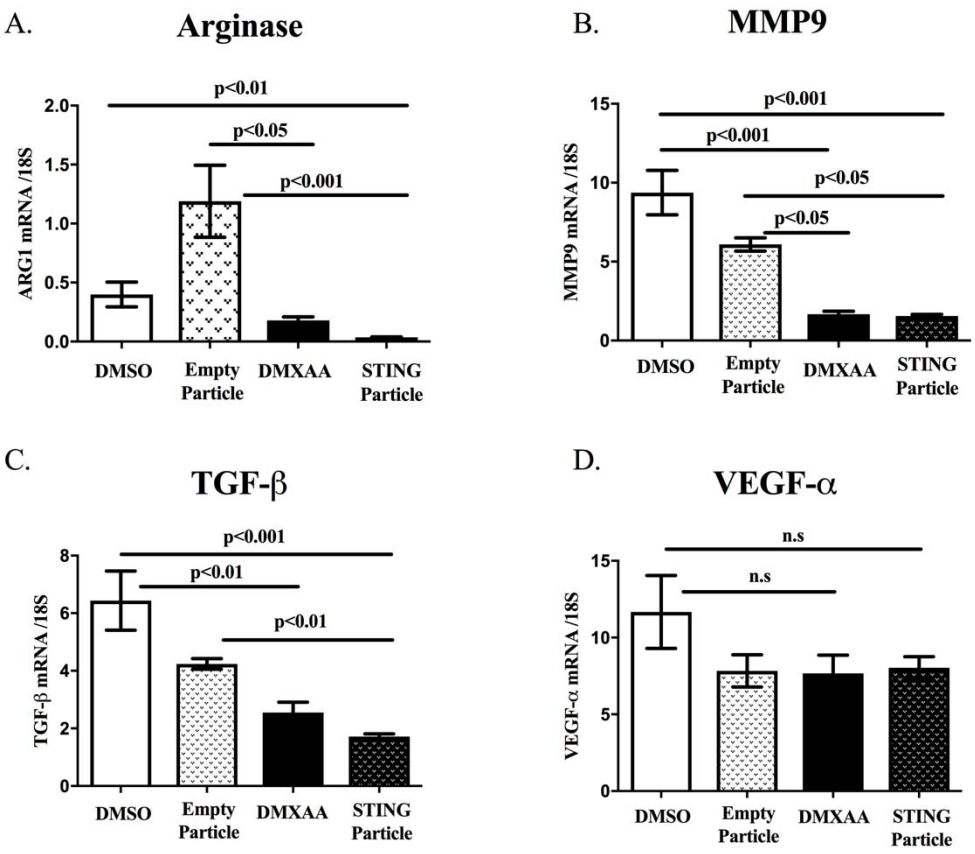

Figure 10: IL-4 stimulated BMDM treated with STING particle have a decrease in expression of pro-tumorigenic factors. A. Arginase expression is significantly decreased with STING particle treatment. **B.** MMP9 expression is significantly decreased with STING particle treatment. **C.** TGF-β expression is significantly decreased with STING particle treatment. **D.** VEGF-α expression is not affected by STING particle treatment. All data are presented as means± the standard error mean (SEM). All *in vitro* experiments were done in triplicate with a minimum of three independent replicates. Data was analyzed using a one one-way ANOVA with a Tukey's post-hoc test.

Results

IL-4 was used to polarize bone marrow derived macrophages (BMDM) towards a pro-tumorigenic phenotype and accesses whether treatment with an encapsulated nanoparticle could change their expression profile.

After 24 hours of STING particle treatment, IL-4 stimulated BMDM decreased expression of arginase, Matrix metallopeptidase 9 (MMP9), and TGF-β, all factors associated with tumor progression (Figure 10). Interestedly, IFN-β and TNF-α, factors associated with anti-tumorigenesis, increased with STING particle treatment (Figure 11). Together this suggests that treatment with an encapsulated CDN can repolarize pro-tumorigenic BMDM towards an anti-tumorigenic phenotype.

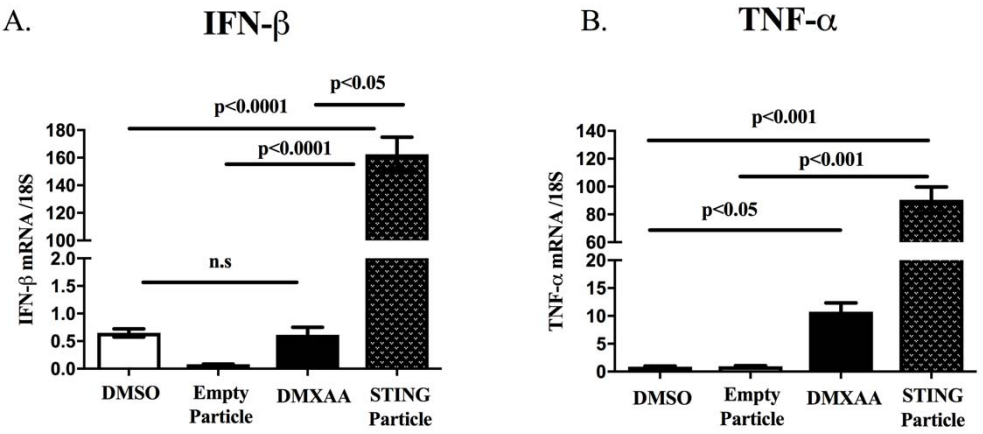

Figure 11: IL-4 stimulated BMDM treated with STING particle have an increase in expression of anti-tumorigenic factors. A. IFN-β expression is significantly increased with STING particle treatment. **B.** TNF-α expression is significantly increased with STING particle treatment. All data are presented as means ± the standard error mean (SEM). All *in vitro* experiments were done in triplicate with a minimum of three independent replicates. Data was analyzed using a one one-way ANOVA with a Tukey's post-hoc test.

Discussion

Published literature supports both pro and anti-tumorigenic activity with STING activation, but here we show that specifically activating the STING pathway in IL-4 stimulated BMDM repolarizes these cells towards an anti-tumor phenotype. Treatment with STING particle not only decreases expression of pro-tumorigenic factors, but also increases expression of factors associated with anti-tumor activity.

Macrophages, a mature myeloid cell, were chosen as the experimental target due to their phagocytic properties and their association with tumor progression. Macrophages are often found surrounding the basement membrane of a tumor and/or infiltrated within the tumor themselves [83, 166].

Several groups have targeted macrophages using an array of approaches, including but not limited to, depletion of macrophages, repolarization/re-education and interference with the CSF1/CSF1R pathway [166]. All of these studies targeting macrophages came to a similar conclusion, that targeting these cells can lead to a direct and/or indirect reduction of tumor growth and progression.

Targeting the STING pathway with nanoparticle encapsulated CDNs may provide an additional approach for macrophages repolarization. The challenge will be to take this from the *in vitro* setting, where investigators have only focused on macrophages and completely controlled the environment and adapt it to a mouse model that not only contains macrophages but many other immune cell types that will contribute to STING-dependent responses. The questions and possibilities are endless, for example, would it be beneficial to isolate pro-tumorigenic macrophages, repolarize them and then reintroduce them into a tumor-bearing host? This concept is currently being explored in immunotherapy research, where cells are extracted from individual cancer patients, reeducated and expanded *in vitro* and then reintroduced back into the same patient [167]. Another realistic possibility would be a combination treatment approach, where not only is the STING pathway activated in macrophages but checkpoint inhibitors are also introduced to stimulate T cell activity, harnessing the power of the immune system to combat cancer.

With the rapidly developing nanotechnology field, drugs and molecules that were considered undeliverable in the past are now being used successfully in mouse models and exerting unanticipated responses to tumor development. This technology will revolutionize not only how we think about targeting cancer but the way we treat it as well.

Chapter IV.

FUTURE DIRECTION AND CONCLUSIONS

Future Directions

The role of T cells in TIBD has not been fully explored, mostly because the majority of TIBD studies have utilized human xenograft models in immunocompromised mice [39, 73, 74]. Therefore, in an attempt to investigate the differences in T cell number between control and tumor-bearing mice, we took tibial bone slides from previous studies performed in immunocompetent mice and sent them to the Translational Pathology Shared Resource (TSPR) core at Vanderbilt University for CD3 staining. Figure 12 demonstrates that BALB/c mice treated with the TGF-β neutralizing antibody, 1D11, have a decreased number of CD3 positive cells as compared to the 13C4 isotype control treated mice. This decrease is seen in both tumor and non-tumor bearing mice, although only non-tumor bearing mice have a statistically significant decrease. This suggests that treatment with 1D11 can decrease the number of $CD3^+$ cells independent of tumor, and since CD3 is considered a pan T cell marker, this demonstrates that a TGF-β dependent effect on T cells in bone exists. Figure 13 is focused on the conditional knock out mouse model that contained myeloid cells that lacked TGF-βRII (TGF-βRII^{MyeKO}). In this model we observe no significant changes in $CD3^+$ cells between WT and TGF-βRII^{MyeKO} in both PBS and tumor-bearing mice, although an increase is observed in tumor-bearing mice for both WT and TGF-βRII^{MyeKO}. Perhaps the reason we observe no significant changes for this model is because the tumor was introduced intratibially, allowing the tumor to overtake the marrow space and leave little to no room for immune cells to infiltrate. This is seen by H&E staining in figure 9C where there is an overwhelming amount of tumor in the marrow space. Future experiments will have to focus on a time point that contains less tumor burden, allowing for the presence and infiltration of T and other immune cells.

Since $CD3^+$ cells were identified in BALB/c and CD3 is considered a pan T cell marker, we wanted to investigate whether we could identify what specific T subset population was changing with TGF-β inhibition.

Therefore, we performed flow cytometry on bone marrow isolated from the tibias of PBS and tumor-bearing C57BL/6 mice and stained with CD4 conjugated antibody and observed that mice treated with 1D11 had less $CD4^+$ cells than isotype control treated mice (Figure 13). This significant decrease was seen in both tumor and non-tumor bearing mice, suggesting that TGF-β inhibition with 1D11 independent of tumor can reduce the expansion of $CD4^+$ cells in bone. Publications have demonstrated that TGF-β can regulate and expand certain T cell populations, such as the $CD4^+$ T regulatory population, that can assist in tumor progression[168]. While more experiments have to be done to identify whether the T cell population that is changing with TGF-β inhibition is pro-tumorigenic, the data from CD3 staining and the CD4 flow cytometry strongly implies a role for T cells in TIBD.

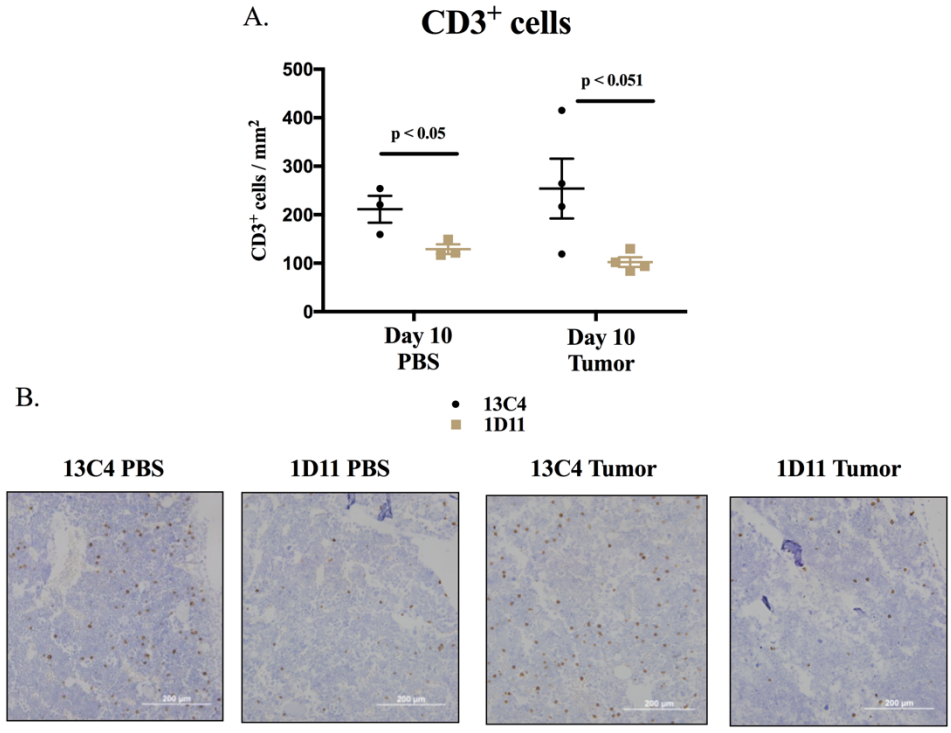

Figure 12: BALB/c mice treated with 1D11 have less $CD3^+$ cells in bone at day 10. 4T1 tumor cells/PBS was introduced intracardically seven days after 13C4/1D11 treatment began. **A.** Quantitation of immunohistochemistry (IHC) staining of CD3 in tibial bone sections. Treatment with 1D11 decreases the number the CD3 positive cells in bone. **B.** Representative images of CD3 IHC staining of PBS and tumor-bearing mice treated with 13C4 or 1D11. Quantitation performed on ImageJ software using image at 20x magnification. All data are presented as means ± the standard error mean (SEM). Data was analyzed using a one one-way ANOVA with a Tukey's post-hoc test. (3-4 mice per group). Scale, 200 μm.

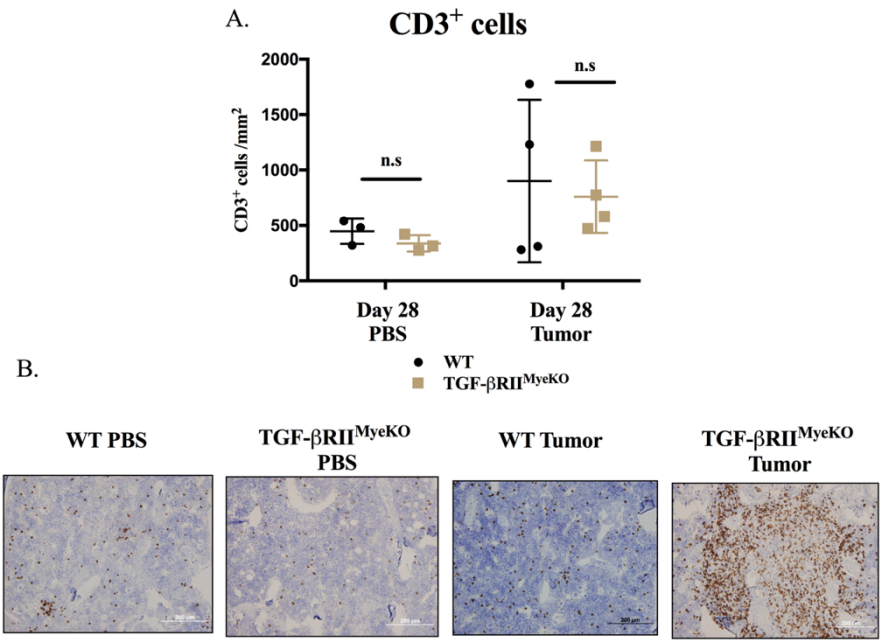

Figure 13: WT/TGF-βRII^{MyeKO} mice do not have significant differences in CD3^{+} cells in bone at day 28. Bone-derived MMTV-PyMT tumor cells/PBS were introduced intratibially at day 0. **A.** Quantitation of immunohistochemistry (IHC) staining of CD3 in tibial bone sections. WT/TGF-βRII^{MyeKO} mice do not have significant changes in CD3 positive cells in bone. **B.** Representative images of CD3 IHC staining of PBS and tumor-bearing mice. Quantitation performed on ImageJ software using image at 20x magnification. All data are presented as means ± the standard error mean (SEM). Data was analyzed using a one one-way ANOVA with a Tukey's post-hoc test. (3-4 mice per group). Scale, 200 μm.

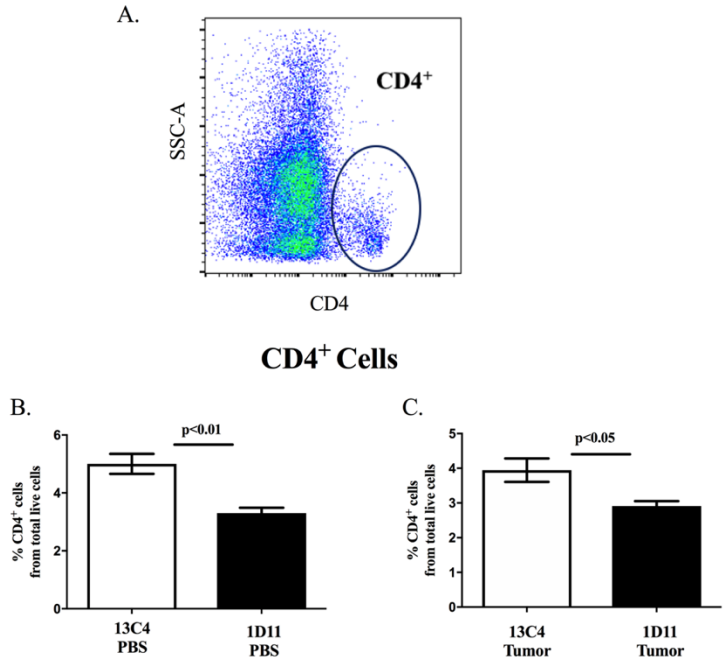

Figure 14: C57BL/6 mice treated with 1D11 have less CD4$^+$ cells in bone at day 7 by flow cytometry. A. Representative image of a bimodal CD4 positive population observed by flow cytometry. **B.** Control C57BL/6 mice treated with 1D11 have a significant decrease in CD4$^+$ cells. **C.** Tumor-bearing C57BL/6 mice treated with 1D11 have a significant decrease in CD4$^+$ cells. All data are presented as means ± the standard error mean (SEM). Data was analyzed using a standard two-tailed unpaired student's *t* test. (4-6 mice per group).

Conclusions

Patients with metastatic cancer are living longer, and while this can be attributed to many factors including new and less toxic therapeutics, longevity also increases the risk of treatment resistance and the development of new metastases. This includes the development of tumor-induced bone disease (TIBD), a complex and multifaceted illness that involves several factors that include the bone and its microenvironment. Specifically, almost 80% of patients with metastatic breast cancer have evidence of TIBD at autopsy [11]. While the bone and cancer field has primarily had a tumor-centric focus on the development and treatment of TIBD, the interest in investigating the role of osteoimmunity in the context of TIBD has gained momentum in the last decade. Osteoimmunity focuses on of the interface between the skeletal system and the immune system that includes the study of ligands, receptors, signaling molecules and transcription factors [169, 170].

While several groups including our own have demonstrated an important role for myeloid cells in the development and progression of TIBD [80-82], there are many immune progenitors residing in the bone marrow that could play an important role in the regulation of TIBD. Therefore, there needs to be a more comprehensive understanding of the cross-talk that occurs between the immune cells residing in the marrow and the tumor.

With the focus on the immune system, the question becomes, would the use of immunotherapies be beneficial on TIBD? The use of immunotherapeutics have been successful in the treatment of several different cancers [171, 172], but there are still challenges to overcome. Published literature suggests that combination therapy will be the most beneficial for the treatment of cancer, and perhaps a combination of immunotherapeutics will be the way patients are treated in the future.

REFERENCES

1. Siegel RL, Miller KD, & Jemal A (2017) Cancer statistics, 2017. *CA: A Cancer Journal for Clinicians* 67(1):7-30.
2. Narod SA & Salmena L (2011) BRCA1 and BRCA2 mutations and breast cancer. *Discovery medicine* 12(66):445-453.
3. de Ruijter TC, Veeck J, de Hoon JP, van Engeland M, & Tjan-Heijnen VC (2011) Characteristics of triple-negative breast cancer. *J Cancer Res Clin Oncol* 137(2):183-192.
4. Howlader N, *et al.* (2014) US incidence of breast cancer subtypes defined by joint hormone receptor and HER2 status. *J Natl Cancer Inst* 106(5).
5. Partridge AH, *et al.* (2016) Subtype-Dependent Relationship Between Young Age at Diagnosis and Breast Cancer Survival. *J Clin Oncol* 34(27):3308-3314.
6. Metzger-Filho O, *et al.* (2013) Patterns of Recurrence and outcome according to breast cancer subtypes in lymph node-negative disease: results from international breast cancer study group trials VIII and IX. *J Clin Oncol* 31(25):3083-3090.
7. Greene FL & Sobin LH (2008) The staging of cancer: a retrospective and prospective appraisal. *CA Cancer J Clin* 58(3):180-190.
8. Voduc KD, *et al.* (2010) Breast Cancer Subtypes and the Risk of Local and Regional Relapse. *Journal of Clinical Oncology* 28(10):1684-1691.
9. Fidler IJ (2003) The pathogenesis of cancer metastasis: the seed and soil; hypothesis revisited. *Nature Reviews Cancer* 3:453.
10. Pantel K & Brakenhoff RH (2004) Dissecting the metastatic cascade. *Nat Rev Cancer* 4(6):448-456.
11. Johnson RW, Schipani E, & Giaccia AJ (2015) HIF targets in bone remodeling and metastatic disease. *Pharmacol Ther* 150:169-177.
12. Wei S & Siegal GP (2017) Surviving at a distant site: The organotropism of metastatic breast cancer. *Semin Diagn Pathol*.
13. Coleman RE (2001) Metastatic bone disease: clinical features, pathophysiology and treatment strategies. *Cancer Treatment Reviews* 27(3):165-176.
14. Kang Y, *et al.* (2003) A multigenic program mediating breast cancer metastasis to bone. *Cancer Cell* 3(6):537-549.
15. Bartsch R & Bergen E (2017) ASCO 2017: highlights in breast cancer. *Memo* 10(4):228-232.
16. Slamon DJ, *et al.* (2001) Use of Chemotherapy plus a Monoclonal Antibody against HER2 for Metastatic Breast Cancer That Overexpresses HER2. *New England Journal of Medicine* 344(11):783-792.
17. Gradishar WJ, *et al.* (2017) NCCN Guidelines Insights: Breast Cancer, Version 1.2017. *Journal of the National Comprehensive Cancer Network* 15(4):433-451.
18. Geyer CE, *et al.* (2006) Lapatinib plus Capecitabine for HER2-Positive Advanced Breast Cancer. *New England Journal of Medicine* 355(26):2733-2743.
19. Baselga J, *et al.* (2012) Everolimus in Postmenopausal Hormone-Receptor–Positive Advanced Breast Cancer. *New England Journal of Medicine* 366(6):520-529.
20. Finn RS, *et al.* (2016) Palbociclib and Letrozole in Advanced Breast Cancer. *New England Journal of Medicine* 375(20):1925-1936.
21. Fong PC, *et al.* (2009) Inhibition of Poly(ADP-Ribose) Polymerase in Tumors from BRCA Mutation Carriers. *New England Journal of Medicine* 361(2):123-134.

22. Raggatt LJ & Partridge NC (2010) Cellular and molecular mechanisms of bone remodeling. *J Biol Chem* 285(33):25103-25108.
23. Boyce BF, Yoneda T, Lowe C, Soriano P, & Mundy GR (1992) Requirement of pp60c-src expression for osteoclasts to form ruffled borders and resorb bone in mice. *J Clin Invest* 90(4):1622-1627.
24. Grafe I*, et al.* (2017) TGF-beta Family Signaling in Mesenchymal Differentiation. *Cold Spring Harb Perspect Biol*.
25. Huang W, Yang S, Shao J, & Li YP (2007) Signaling and transcriptional regulation in osteoblast commitment and differentiation. *Frontiers in bioscience : a journal and virtual library* 12:3068-3092.
26. Komori T (2010) Regulation of osteoblast differentiation by Runx2. *Advances in experimental medicine and biology* 658:43-49.
27. Nakashima K*, et al.* (2002) The novel zinc finger-containing transcription factor osterix is required for osteoblast differentiation and bone formation. *Cell* 108(1):17-29.
28. Bonewald LF (2011) The amazing osteocyte. *Journal of bone and mineral research : the official journal of the American Society for Bone and Mineral Research* 26(2):229-238.
29. Nakashima T*, et al.* (2011) Evidence for osteocyte regulation of bone homeostasis through RANKL expression. *Nature medicine* 17(10):1231-1234.
30. Komori T (2013) Functions of the osteocyte network in the regulation of bone mass. *Cell and tissue research* 352(2):191-198.
31. Sims NA & Vrahnas C (2014) Regulation of cortical and trabecular bone mass by communication between osteoblasts, osteocytes and osteoclasts. *Archives of Biochemistry and Biophysics* 561:22-28.
32. Takayanagi H (2007) Osteoimmunology: shared mechanisms and crosstalk between the immune and bone systems. *Nature reviews. Immunology* 7(4):292-304.
33. Teitelbaum SL (2000) Bone resorption by osteoclasts. *Science (New York, N.Y.)* 289(5484):1504-1508.
34. Fox SW & Lovibond AC (2005) Current insights into the role of transforming growth factor-beta in bone resorption. *Mol Cell Endocrinol* 243(1-2):19-26.
35. Burgess TL*, et al.* (1999) The ligand for osteoprotegerin (OPGL) directly activates mature osteoclasts. *The Journal of cell biology* 145(3):527-538.
36. Kakonen SM & Mundy GR (2003) Mechanisms of osteolytic bone metastases in breast carcinoma. *Cancer* 97(3 Suppl):834-839.
37. Mavrogenis AF*, et al.* (2016) Modern Palliative Treatments for Metastatic Bone Disease: Awareness of Advantages, Disadvantages, and Guidance. *The Clinical journal of pain* 32(4):337-350.
38. Mundy GR (1997) Mechanisms of bone metastasis. *Cancer* 80(8 Suppl):1546-1556.
39. Sterling JA, Edwards JR, Martin TJ, & Mundy GR (2011) Advances in the biology of bone metastasis: how the skeleton affects tumor behavior. *Bone* 48(1):6-15.
40. Juarez P & Guise TA (2011) TGF-beta in cancer and bone: implications for treatment of bone metastases. *Bone* 48(1):23-29.
41. Page JM*, et al.* (2015) Matrix rigidity regulates the transition of tumor cells to a bone-destructive phenotype through integrin beta3 and TGF-beta receptor type II. *Biomaterials* 64:33-44.
42. Siegel PM & Massague J (2003) Cytostatic and apoptotic actions of TGF-beta in homeostasis and cancer. *Nat Rev Cancer* 3(11):807-821.

43. Kulkarni AB, *et al.* (1993) Transforming growth factor beta 1 null mutation in mice causes excessive inflammatory response and early death. *Proceedings of the National Academy of Sciences* 90(2):770-774.
44. Derynck R & Zhang YE (2003) Smad-dependent and Smad-independent pathways in TGF-beta family signalling. *Nature* 425(6958):577-584.
45. Morikawa M, Derynck R, & Miyazono K (2016) TGF-beta and the TGF-beta Family: Context-Dependent Roles in Cell and Tissue Physiology. *Cold Spring Harb Perspect Biol* 8(5).
46. Chen TL & Bates RL (1993) Recombinant human transforming growth factor beta 1 modulates bone remodeling in a mineralizing bone organ culture. *Journal of bone and mineral research : the official journal of the American Society for Bone and Mineral Research* 8(4):423-434.
47. Breen EC, *et al.* (1994) TGF beta alters growth and differentiation related gene expression in proliferating osteoblasts in vitro, preventing development of the mature bone phenotype. *Journal of cellular physiology* 160(2):323-335.
48. Harris SE, *et al.* (1994) Effects of transforming growth factor beta on bone nodule formation and expression of bone morphogenetic protein 2, osteocalcin, osteopontin, alkaline phosphatase, and type I collagen mRNA in long-term cultures of fetal rat calvarial osteoblasts. *Journal of bone and mineral research : the official journal of the American Society for Bone and Mineral Research* 9(6):855-863.
49. Janssens K, ten Dijke P, Janssens S, & Van Hul W (2005) Transforming growth factor-beta1 to the bone. *Endocrine reviews* 26(6):743-774.
50. Kim KK, *et al.* (2006) Repetitive exposure to TGF-beta suppresses TGF-beta type I receptor expression by differentiated osteoblasts. *Gene* 379:175-184.
51. Geiser AG, *et al.* (1998) Decreased bone mass and bone elasticity in mice lacking the transforming growth factor-beta1 gene. *Bone* 23(2):87-93.
52. Filvaroff E, *et al.* (1999) Inhibition of TGF-beta receptor signaling in osteoblasts leads to decreased bone remodeling and increased trabecular bone mass. *Development (Cambridge, England)* 126(19):4267-4279.
53. Ohishi M, *et al.* (2005) Suppressors of cytokine signaling-1 and -3 regulate osteoclastogenesis in the presence of inflammatory cytokines. *Journal of immunology (Baltimore, Md. : 1950)* 174(5):3024-3031.
54. Hayashi T, Kaneda T, Toyama Y, Kumegawa M, & Hakeda Y (2002) Regulation of receptor activator of NF-kappa B ligand-induced osteoclastogenesis by endogenous interferon-beta (INF-beta) and suppressors of cytokine signaling (SOCS). The possible counteracting role of SOCSs- in IFN-beta-inhibited osteoclast formation. *J Biol Chem* 277(31):27880-27886.
55. Lovibond AC, Haque SJ, Chambers TJ, & Fox SW (2003) TGF-beta-induced SOCS3 expression augments TNF-alpha-induced osteoclast formation. *Biochem Biophys Res Commun* 309(4):762-767.
56. Fox SW, Haque SJ, Lovibond AC, & Chambers TJ (2003) The possible role of TGF-beta-induced suppressors of cytokine signaling expression in osteoclast/macrophage lineage commitment in vitro. *Journal of immunology (Baltimore, Md. : 1950)* 170(7):3679-3687.

57. Murakami T, *et al.* (1998) Transforming growth factor-beta1 increases mRNA levels of osteoclastogenesis inhibitory factor in osteoblastic/stromal cells and inhibits the survival of murine osteoclast-like cells. *Biochem Biophys Res Commun* 252(3):747-752.
58. Thirunavukkarasu K, *et al.* (2001) Stimulation of osteoprotegerin (OPG) gene expression by transforming growth factor-beta (TGF-beta). Mapping of the OPG promoter region that mediates TGF-beta effects. *J Biol Chem* 276(39):36241-36250.
59. Quinn JM, *et al.* (2001) Transforming growth factor beta affects osteoclast differentiation via direct and indirect actions. *Journal of bone and mineral research : the official journal of the American Society for Bone and Mineral Research* 16(10):1787-1794.
60. Takai H, *et al.* (1998) Transforming growth factor-beta stimulates the production of osteoprotegerin/osteoclastogenesis inhibitory factor by bone marrow stromal cells. *J Biol Chem* 273(42):27091-27096.
61. Levy L & Hill CS (2006) Alterations in components of the TGF-beta superfamily signaling pathways in human cancer. *Cytokine Growth Factor Rev* 17(1-2):41-58.
62. Bierie B & Moses HL (2006) Tumour microenvironment: TGFbeta: the molecular Jekyll and Hyde of cancer. *Nat Rev Cancer* 6(7):506-520.
63. Pickup M, Novitskiy S, & Moses HL (2013) The roles of TGFbeta in the tumour microenvironment. *Nat Rev Cancer* 13(11):788-799.
64. Mima K, *et al.* (2013) Epithelial-mesenchymal transition expression profiles as a prognostic factor for disease-free survival in hepatocellular carcinoma: Clinical significance of transforming growth factor-beta signaling. *Oncology letters* 5(1):149-154.
65. Forrester E, *et al.* (2005) Effect of conditional knockout of the type II TGF-beta receptor gene in mammary epithelia on mammary gland development and polyomavirus middle T antigen induced tumor formation and metastasis. *Cancer research* 65(6):2296-2302.
66. Cheng N, *et al.* (2005) Loss of TGF-beta type II receptor in fibroblasts promotes mammary carcinoma growth and invasion through upregulation of TGF-alpha-, MSP- and HGF-mediated signaling networks. *Oncogene* 24(32):5053-5068.
67. Novitskiy SV, *et al.* (2012) Deletion of TGF-beta signaling in myeloid cells enhances their anti-tumorigenic properties. *Journal of leukocyte biology* 92(3):641-651.
68. Mohan S & Baylink DJ (1991) Bone growth factors. *Clinical orthopaedics and related research* (263):30-48.
69. Kakonen SM, *et al.* (2002) Transforming growth factor-beta stimulates parathyroid hormone-related protein and osteolytic metastases via Smad and mitogen-activated protein kinase signaling pathways. *J Biol Chem* 277(27):24571-24578.
70. Guise TA, *et al.* (1996) Evidence for a causal role of parathyroid hormone-related protein in the pathogenesis of human breast cancer-mediated osteolysis. *J Clin Invest* 98(7):1544-1549.
71. Henderson MA, *et al.* (2006) Parathyroid hormone-related protein localization in breast cancers predict improved prognosis. *Cancer research* 66(4):2250-2256.
72. Thomas RJ, *et al.* (1999) Breast cancer cells interact with osteoblasts to support osteoclast formation. *Endocrinology* 140(10):4451-4458.
73. Buenrostro D, Mulcrone PL, Owens P, & Sterling JA (2016) The Bone Microenvironment: a Fertile Soil for Tumor Growth. *Curr Osteoporos Rep* 14(4):151-158.
74. Buenrostro D, Park SI, & Sterling JA (2014) Dissecting the role of bone marrow stromal cells on bone metastases. *Biomed Res Int* 2014:875305.

75. Marvel D & Gabrilovich DI (2015) Myeloid-derived suppressor cells in the tumor microenvironment: expect the unexpected. *J Clin Invest* 125(9):3356-3364.
76. Bronte V*, et al.* (2016) Recommendations for myeloid-derived suppressor cell nomenclature and characterization standards. *Nat Commun* 7:12150.
77. Youn JI, Nagaraj S, Collazo M, & Gabrilovich DI (2008) Subsets of myeloid-derived suppressor cells in tumor-bearing mice. *Journal of immunology (Baltimore, Md. : 1950)* 181(8):5791-5802.
78. Movahedi K*, et al.* (2008) Identification of discrete tumor-induced myeloid-derived suppressor cell subpopulations with distinct T cell-suppressive activity. *Blood* 111(8):4233-4244.
79. Srivastava MK, Sinha P, Clements VK, Rodriguez P, & Ostrand-Rosenberg S (2010) Myeloid-derived suppressor cells inhibit T-cell activation by depleting cystine and cysteine. *Cancer research* 70(1):68-77.
80. Park SI*, et al.* (2013) Parathyroid hormone-related protein drives a CD11b+Gr1+ cell-mediated positive feedback loop to support prostate cancer growth. *Cancer research* 73(22):6574-6583.
81. Danilin S*, et al.* (2012) Myeloid-derived suppressor cells expand during breast cancer progression and promote tumor-induced bone destruction. *Oncoimmunology* 1(9):1484-1494.
82. Sawant A*, et al.* (2013) Myeloid-derived suppressor cells function as novel osteoclast progenitors enhancing bone loss in breast cancer. *Cancer research* 73(2):672-682.
83. Lewis CE & Pollard JW (2006) Distinct role of macrophages in different tumor microenvironments. *Cancer research* 66(2):605-612.
84. Pollard JW (2008) Macrophages define the invasive microenvironment in breast cancer. *Journal of leukocyte biology* 84(3):623-630.
85. Coussens LM & Werb Z (2002) Inflammation and cancer. *Nature* 420(6917):860-867.
86. Biswas SK*, et al.* (2006) A distinct and unique transcriptional program expressed by tumor-associated macrophages (defective NF-kappaB and enhanced IRF-3/STAT1 activation). *Blood* 107(5):2112-2122.
87. Qian BZ & Pollard JW (2010) Macrophage diversity enhances tumor progression and metastasis. *Cell* 141(1):39-51.
88. Chang MK*, et al.* (2008) Osteal tissue macrophages are intercalated throughout human and mouse bone lining tissues and regulate osteoblast function in vitro and in vivo. *Journal of immunology (Baltimore, Md. : 1950)* 181(2):1232-1244.
89. Winkler IG*, et al.* (2010) Bone marrow macrophages maintain hematopoietic stem cell (HSC) niches and their depletion mobilizes HSCs. *Blood* 116(23):4815-4828.
90. Alexander KA*, et al.* (2011) Osteal macrophages promote in vivo intramembranous bone healing in a mouse tibial injury model. *Journal of bone and mineral research : the official journal of the American Society for Bone and Mineral Research* 26(7):1517-1532.
91. Zitvogel L & Kroemer G (2015) Cancer: Antibodies regulate antitumour immunity. *Nature* 521(7550):35-37.
92. Thomas DA & Massague J (2005) TGF-beta directly targets cytotoxic T cell functions during tumor evasion of immune surveillance. *Cancer Cell* 8(5):369-380.
93. Shevach EM (2009) Mechanisms of foxp3+ T regulatory cell-mediated suppression. *Immunity* 30(5):636-645.

94. Rajewsky K (1996) Clonal selection and learning in the antibody system. *Nature* 381(6585):751-758.
95. Balkwill F, Montfort A, & Capasso M (2013) B regulatory cells in cancer. *Trends Immunol* 34(4):169-173.
96. Zhang K, *et al.* (2011) CD8+ T cells regulate bone tumor burden independent of osteoclast resorption. *Cancer research* 71(14):4799-4808.
97. Monteiro AC, *et al.* (2013) T cells induce pre-metastatic osteolytic disease and help bone metastases establishment in a mouse model of metastatic breast cancer. *PloS one* 8(7):e68171.
98. Siegel RL, Miller KD, & Jemal A (2016) Cancer statistics, 2016. *CA: A Cancer Journal for Clinicians* 66(1):7-30.
99. Biswas S, *et al.* (2011) Anti-Transforming Growth Factor ß Antibody Treatment Rescues Bone Loss and Prevents Breast Cancer Metastasis to Bone. *PLoS ONE* 6(11):e27090.
100. Yin JJ, *et al.* (1999) TGF-β signaling blockade inhibits PTHrP secretion by breast cancer cells and bone metastases development. *The Journal of Clinical Investigation* 103(2):197-206.
101. Mohammad KS, *et al.* (2011) TGF-beta-RI kinase inhibitor SD-208 reduces the development and progression of melanoma bone metastases. *Cancer research* 71(1):175-184.
102. Nyman JS, *et al.* (2016) Combined treatment with a transforming growth factor beta inhibitor (1D11) and bortezomib improves bone architecture in a mouse model of myeloma-induced bone disease. *Bone* 91:81-91.
103. Juárez P, *et al.* (2012) Halofuginone Inhibits the Establishment and Progression of Melanoma Bone Metastases. *Cancer research* 72(23):6247-6256.
104. Korpal M, *et al.* (2009) Imaging transforming growth factor-[beta] signaling dynamics and therapeutic response in breast cancer bone metastasis. *Nat Med* 15(8):960-966.
105. Cook LM, *et al.* (2016) Predictive computational modeling to define effective treatment strategies for bone metastatic prostate cancer. 6:29384.
106. Zhuang J, *et al.* (2012) Osteoclasts in multiple myeloma are derived from Gr-1+CD11b+myeloid-derived suppressor cells. *PLoS One* 7(11):e48871.
107. Gabrilovich DI, Ostrand-Rosenberg S, & Bronte V (2012) Coordinated regulation of myeloid cells by tumours. *Nature reviews. Immunology* 12(4):253-268.
108. Pang Y, *et al.* (2013) TGF-beta signaling in myeloid cells is required for tumor metastasis. *Cancer discovery* 3(8):936-951.
109. Meng X, *et al.* (2016) Myeloid-specific TGF-beta signaling in bone promotes basic-FGF and breast cancer bone metastasis. *Oncogene* 35(18):2370-2378.
110. Yang L, *et al.* (2004) Expansion of myeloid immune suppressor Gr+CD11b+ cells in tumor-bearing host directly promotes tumor angiogenesis. *Cancer Cell* 6(4):409-421.
111. Wyckoff J, *et al.* (2004) A Paracrine Loop between Tumor Cells and Macrophages Is Required for Tumor Cell Migration in Mammary Tumors. *Cancer research* 64(19):7022-7029.
112. Ryzhov SV, *et al.* (2014) Role of TGF-β Signaling in Generation of CD39⁺CD73⁺ Myeloid Cells in Tumors. *The Journal of Immunology* 193(6):3155-3164.

113. D'Amico L, *et al.* (2016) Dickkopf-related protein 1 (Dkk1) regulates the accumulation and function of myeloid derived suppressor cells in cancer. *The Journal of experimental medicine* 213(5):827-840.
114. Johnson RW, *et al.* (2011) TGF-beta promotion of Gli2-induced expression of parathyroid hormone-related protein, an important osteolytic factor in bone metastasis, is independent of canonical Hedgehog signaling. *Cancer research* 71(3):822-831.
115. Bierie B, *et al.* (Abrogation of TGF-β signaling enhances chemokine production and correlates with prognosis in human breast cancer. *The Journal of Clinical Investigation* 119(6):1571-1582.
116. Yang L, *et al.* (2008) Abrogation of TGFβ Signaling in Mammary Carcinomas Recruits Gr-1+CD11b+ Myeloid Cells that Promote Metastasis. *Cancer Cell* 13(1):23-35.
117. Chytil A, Magnuson MA, Wright CVE, & Moses HL (2002) Conditional inactivation of the TGF-β type II receptor using Cre:Lox. *genesis* 32(2):73-75.
118. Yang J, *et al.* (2014) Myeloid IKKβ Promotes Antitumor Immunity by Modulating CCL11 and the Innate Immune Response. *Cancer research* 74(24):7274-7284.
119. Forrester E, *et al.* (2005) Effect of Conditional Knockout of the Type II TGF-β Receptor Gene in Mammary Epithelia on Mammary Gland Development and Polyomavirus Middle T Antigen Induced Tumor Formation and Metastasis. *Cancer research* 65(6):2296-2302.
120. Campbell JP, Merkel AR, Masood-Campbell SK, Elefteriou F, & Sterling JA (2012) Models of Bone Metastasis. (67):e4260.
121. Hardbower DM, *et al.* (EGFR regulates macrophage activation and function in bacterial infection. *The Journal of Clinical Investigation* 126(9):3296-3312.
122. Mulcrone PL, *et al.* (2017) Skeletal Colonization by Breast Cancer Cells Is Stimulated by an Osteoblast and beta2AR-Dependent Neo-Angiogenic Switch. *Journal of bone and mineral research : the official journal of the American Society for Bone and Mineral Research* 32(7):1442-1454.
123. Gong D, *et al.* (2012) TGFbeta signaling plays a critical role in promoting alternative macrophage activation. *BMC immunology* 13:31.
124. Boutard V, *et al.* (1995) Transforming growth factor-beta stimulates arginase activity in macrophages. Implications for the regulation of macrophage cytotoxicity. *The Journal of Immunology* 155(4):2077-2084.
125. Udagawa N, *et al.* (1990) Origin of osteoclasts: mature monocytes and macrophages are capable of differentiating into osteoclasts under a suitable microenvironment prepared by bone marrow-derived stromal cells. *Proceedings of the National Academy of Sciences of the United States of America* 87(18):7260-7264.
126. Edwards JR, *et al.* (2010) Inhibition of TGF-beta signaling by 1D11 antibody treatment increases bone mass and quality in vivo. *Journal of bone and mineral research : the official journal of the American Society for Bone and Mineral Research* 25(11):2419-2426.
127. Gabrilovich DI & Nagaraj S (2009) Myeloid-derived suppressor cells as regulators of the immune system. *Nature reviews. Immunology* 9(3):162-174.
128. Hanahan D & Weinberg RA (2011) Hallmarks of cancer: the next generation. *Cell* 144(5):646-674.

129. Kawano M, *et al.* (2015) The significance of G-CSF expression and myeloid-derived suppressor cells in the chemoresistance of uterine cervical cancer. *Scientific reports* 5:18217.
130. Shojaei F, *et al.* (2009) G-CSF-initiated myeloid cell mobilization and angiogenesis mediate tumor refractoriness to anti-VEGF therapy in mouse models. *Proceedings of the National Academy of Sciences of the United States of America* 106(16):6742-6747.
131. Hollmen M, *et al.* (2016) G-CSF regulates macrophage phenotype and associates with poor overall survival in human triple-negative breast cancer. *Oncoimmunology* 5(3):e1115177.
132. Delitto D, *et al.* (2015) The inflammatory milieu within the pancreatic cancer microenvironment correlates with clinicopathologic parameters, chemoresistance and survival. *BMC cancer* 15:783.
133. Kim HK, De La Luz Sierra M, Williams CK, Gulino AV, & Tosato G (2006) G-CSF down-regulation of CXCR4 expression identified as a mechanism for mobilization of myeloid cells. *Blood* 108(3):812-820.
134. Sasaki S, *et al.* (2016) Essential roles of the interaction between cancer cell-derived chemokine, CCL4, and intra-bone CCR5-expressing fibroblasts in breast cancer bone metastasis. *Cancer Letters* 378(1):23-32.
135. Allan EH, *et al.* (1990) Osteoblasts display receptors for and responses to leukemia-inhibitory factor. *Journal of Cellular Physiology* 145(1):110-119.
136. Grimaud E, *et al.* (2002) Leukaemia Inhibitory Factor (Lif) Is Expressed in Hypertrophic Chondrocytes and Vascular Sprouts during Osteogenesis. *Cytokine* 20(5):224-230.
137. Li X, *et al.* (2014) LIF promotes tumorigenesis and metastasis of breast cancer through the AKT-mTOR pathway. *Oncotarget* 5(3):788-801.
138. Douglas AM, *et al.* (1997) Expression and function of members of the cytokine receptor superfamily on breast cancer cells. *Oncogene* 14(6):661-669.
139. Maes C (2013) Role and regulation of vascularization processes in endochondral bones. *Calcified tissue international* 92(4):307-323.
140. Morris JC, *et al.* (2014) Phase I Study of GC1008 (Fresolimumab): A Human Anti-Transforming Growth Factor-Beta (TGFβ) Monoclonal Antibody in Patients with Advanced Malignant Melanoma or Renal Cell Carcinoma. *PLOS ONE* 9(3):e90353.
141. den Hollander MW, *et al.* (2015) TGF-beta Antibody Uptake in Recurrent High-Grade Glioma Imaged with 89Zr-Fresolimumab PET. *Journal of nuclear medicine : official publication, Society of Nuclear Medicine* 56(9):1310-1314.
142. de Gramont A, Faivre S, & Raymond E (2017) Novel TGF-beta inhibitors ready for prime time in onco-immunology. *Oncoimmunology* 6(1):e1257453.
143. Chen X, *et al.* (2014) Effective chemoimmunotherapy with anti-TGFbeta antibody and cyclophosphamide in a mouse model of breast cancer. *PLoS One* 9(1):e85398.
144. Tabe Y, *et al.* (2013) TGF-beta-Neutralizing Antibody 1D11 Enhances Cytarabine-Induced Apoptosis in AML Cells in the Bone Marrow Microenvironment. *PLoS One* 8(6):e62785.
145. Liu J, *et al.* (2012) TGF-β blockade improves the distribution and efficacy of therapeutics in breast carcinoma by normalizing the tumor stroma. *Proceedings of the National Academy of Sciences* 109(41):16618-16623.

146. Bouquet F, *et al.* (2011) TGFβ1 Inhibition Increases the Radiosensitivity of Breast Cancer Cells In Vitro and Promotes Tumor Control by Radiation In Vivo. *Clinical Cancer Research* 17(21):6754-6765.
147. Burdette DL & Vance RE (2013) STING and the innate immune response to nucleic acids in the cytosol. *Nat Immunol* 14(1):19-26.
148. Ng KW, Marshall EA, Bell JC, & Lam WL (2018) cGAS-STING and Cancer: Dichotomous Roles in Tumor Immunity and Development. *Trends Immunol* 39(1):44-54.
149. Barber GN (2011) Innate immune DNA sensing pathways: STING, AIMII and the regulation of interferon production and inflammatory responses. *Curr Opin Immunol* 23(1):10-20.
150. Barber GN (2015) STING: infection, inflammation and cancer. *Nature reviews. Immunology* 15(12):760-770.
151. Nowarski R, Gagliani N, Huber S, & Flavell RA (2013) Innate immune cells in inflammation and cancer. *Cancer immunology research* 1(2):77-84.
152. White MJ, *et al.* (2014) Apoptotic caspases suppress mtDNA-induced STING-mediated type I IFN production. *Cell* 159(7):1549-1562.
153. Swann JB, *et al.* (2008) Demonstration of inflammation-induced cancer and cancer immunoediting during primary tumorigenesis. *Proceedings of the National Academy of Sciences of the United States of America* 105(2):652-656.
154. Ahn J, *et al.* (2014) Inflammation-driven carcinogenesis is mediated through STING. *Nat Commun* 5:5166.
155. Salcedo R, Cataisson C, Hasan U, Yuspa SH, & Trinchieri G (2013) MyD88 and its divergent toll in carcinogenesis. *Trends Immunol* 34(8):379-389.
156. Ahn J, Konno H, & Barber GN (2015) Diverse roles of STING-dependent signaling on the development of cancer. *Oncogene* 34(41):5302-5308.
157. Zhu Q, *et al.* (2014) Cutting edge: STING mediates protection against colorectal tumorigenesis by governing the magnitude of intestinal inflammation. *Journal of immunology (Baltimore, Md. : 1950)* 193(10):4779-4782.
158. Gajewski TF, Schreiber H, & Fu YX (2013) Innate and adaptive immune cells in the tumor microenvironment. *Nat Immunol* 14(10):1014-1022.
159. Woo SR, *et al.* (2014) STING-dependent cytosolic DNA sensing mediates innate immune recognition of immunogenic tumors. *Immunity* 41(5):830-842.
160. Deng L, *et al.* (2014) STING-Dependent Cytosolic DNA Sensing Promotes Radiation-Induced Type I Interferon-Dependent Antitumor Immunity in Immunogenic Tumors. *Immunity* 41(5):843-852.
161. Roberts ZJ, *et al.* (2007) The chemotherapeutic agent DMXAA potently and specifically activates the TBK1-IRF-3 signaling axis. *The Journal of experimental medicine* 204(7):1559-1569.
162. Corrales L, *et al.* (2015) Direct Activation of STING in the Tumor Microenvironment Leads to Potent and Systemic Tumor Regression and Immunity. *Cell reports* 11(7):1018-1030.
163. Downey CM, Aghaei M, Schwendener RA, & Jirik FR (2014) DMXAA causes tumor site-specific vascular disruption in murine non-small cell lung cancer, and like the endogenous non-canonical cyclic dinucleotide STING agonist, 2'3'-cGAMP, induces M2 macrophage repolarization. *PloS one* 9(6):e99988.

164. Wilson JT*, et al.* (2015) Enhancement of MHC-I antigen presentation via architectural control of pH-responsive, endosomolytic polymer nanoparticles. *The AAPS journal* 17(2):358-369.
165. Connelly L, Jacobs AT, Palacios-Callender M, Moncada S, & Hobbs AJ (2003) Macrophage endothelial nitric-oxide synthase autoregulates cellular activation and pro-inflammatory protein expression. *J Biol Chem* 278(29):26480-26487.
166. Coussens LM, Zitvogel L, & Palucka AK (2013) Neutralizing tumor-promoting chronic inflammation: a magic bullet? *Science (New York, N.Y.)* 339(6117):286-291.
167. Schmitt TM, Stromnes IM, Chapuis AG, & Greenberg PD (2015) New Strategies in Engineering T-cell Receptor Gene-Modified T cells to More Effectively Target Malignancies. *Clinical cancer research : an official journal of the American Association for Cancer Research* 21(23):5191-5197.
168. Wan YY & Flavell RA (2007) Regulatory T cells, transforming growth factor-beta, and immune suppression. *Proceedings of the American Thoracic Society* 4(3):271-276.
169. Lorenzo J, Horowitz M, & Choi Y (2008) Osteoimmunology: interactions of the bone and immune system. *Endocrine reviews* 29(4):403-440.
170. Arron JR & Choi Y (2000) Bone versus immune system. *Nature* 408(6812):535-536.
171. Anderson KG, Stromnes IM, & Greenberg PD (2017) Obstacles Posed by the Tumor Microenvironment to T cell Activity: A Case for Synergistic Therapies. *Cancer Cell* 31(3):311-325.
172. Chapuis AG*, et al.* (2017) Tracking the Fate and Origin of Clinically Relevant Adoptively Transferred CD8(+) T Cells In Vivo. *Science immunology* 2(8).